Ann. Rev. Nucl. Sci. 1976. 26 : 239–317

THE VARIABLE MOMENT OF INERTIA (VMI) MODEL AND THEORIES OF NUCLEAR COLLECTIVE MOTION

*5575

Gertrude Scharff-Goldhaber and Carl B. Dover
Brookhaven National Laboratory,[1] Upton, New York 11973

Alan L. Goodman[2]
Carnegie-Mellon University, Pittsburgh, Pennsylvania 15213

CONTENTS

[1] Work supported by the US Energy Research and Development Administration.
[2] Work supported by the National Science Foundation. Present address : Tulane University, New Orleans, Louisiana 70118.

Foreword

From the discovery of the atomic nucleus in 1911 arose a remarkably successful (though even now incomplete) theory of atomic structure, in which the nucleus was at first treated as a point. With the discovery of the neutron in 1932 began a slow evolution of a class of models for nuclear structure, now known as "microscopic theories." In such models the nucleus is treated as a collection of A bodies, Z protons, and $N = A - Z$ neutrons interacting with each other through instantaneous two-body potentials. That these are only approximate models, rather than fundamental theories, becomes clearer with time, as the importance of relativistic effects, meson degrees of freedom, and internal nucleon structure is recognized.

Even without these difficulties, the A-body problem is so formidable that "realistic" calculations for $A > 3$ are simplified versions of a fully microscopic theory, in which one truncates the number of degrees of freedom and often makes use of phenomenologically determined parameters. It cannot be denied that much has been

learned, especially about some specific aspects of nuclear structure and the response of the nucleus to external probes, but it is obvious that nuclear theory has not achieved a completeness approaching that of atomic physics and quantum electrodynamics. Therefore it is valuable to study in a phenomenological way nuclear processes that may correspond to excitation of only one or a few degrees of freedom. Understanding of these degrees of freedom and the reasons for their dominance permits development of our intuition about a unique physical object, the quantum droplet.

For such studies the natural sequence might be to examine first the systematics of ground-state properties, and then go on to look for patterns in spectra of low-lying excited states, which could be related to the most "macroscopic" aspects of the nuclear droplet. The recognition of patterns in the ground-state bands of nuclei with even Z and N was slow, and only recently has been quantified in terms of simple and surprisingly accurate empirical rules. These rules indicate that nuclei with widely differing ground-state structure respond in similar ways when they acquire a small amount of energy—they rotate. However, the effect of the rotational motion seems to be different for different ground-state structure; highly deformed, stable nuclei simply rotate, so that the moment of inertia is almost independent of angular velocity. Unstable and less deformed nuclei show a tendency to become more deformed as they rotate faster.

The studies leading to these conclusions depend heavily on information about both excitation energies and electric quadrupole moments. The interplay between the results of these empirical studies and the formulation of various nuclear models is briefly sketched in the historical introduction presented in Section 1. In Section 2 the phenomenological variable moment of inertia (VMI) model and its ramifications are discussed. Section 3 deals with the relation of moments of inertia to transition quadrupole moments and presents two simple models, and Section 4 discusses the nature of transitions from the "VMI phase." Sections 5–8 give a comprehensive survey of theoretical approaches which, while still unable to derive quantitatively the VMI rule, have overcome various limitations arising from previous model assumptions. At the end, we present our conclusions and outline areas requiring further research.

1 *Historical Introduction*

1.1 ATOMIC HYPERFINE STRUCTURE AND NUCLEAR QUADRUPOLE MOMENTS When Wolfgang Pauli (1) interpreted Nagaoka's discovery of hyperfine structure in the spectra of Hg atoms as being caused by the angular momentum or spin of the atomic nucleus, he pointed out that the electric quadrupole moments of Hg nuclei appear to be considerably smaller than one might expect ($Q \ll Zed^2$; $d = A^{1/3}$ 10^{-13} cm), implying a high degree of spherical symmetry. He expressed the hope that the study of atomic hyperfine structure might eventually provide important insight into the detailed structure of the nucleus, which he referred to as "das Kerngebäude." Almost twelve years passed until this challenge was taken up by Casimir (2), who evolved a theory of the effect of the nuclear electric quadrupole moment on hyperfine structure. From the measurements by Schüler & Schmidt (3),

Casimir was able to deduce very large quadrupole moments for three nuclei in the rare earth region, namely ^{151}Eu (1.5b), ^{153}Eu (3.2b), and ^{175}Lu ($\sim$6.3b).

1.2 PACKING FRACTION, THE CHARGED LIQUID DROP, AND EARLY CLUES TO NUCLEAR SHELL STRUCTURE A very important clue to nuclear structure had meanwhile evolved from a quite different experimental approach. In the late 1920s Aston's pioneering mass spectroscopic results had become extensive enough to allow the conclusion that the packing fraction, which is a measure of the mean binding energy per nucleon, has an almost constant value except for the lightest nuclei. This suggested that forces between nucleons are qualitatively similar to the forces between identical atoms, which Heitler & London (4) had been able to ascribe to the short-range quantum mechanical exchange force between electrons. On this basis Gamow (5) proposed a quite remarkable liquid drop model of the nucleus, consisting mainly of α particles, and held together by surface tension.

Deviations from constancy of the packing fraction for certain mass and charge values, on the other hand, led Stefan Mayer to point out "that the packing fraction seems to show a *periodic* behavior which is related to the well-known periods in the natural classification of the elements" (6). This was clearly an invitation to invent the nuclear shell model!

With the discovery of the neutron and the introduction of the concepts of isotopic spin and charge independence of the strong nucleon-nucleon forces, it became possible to define nuclear models with some precision. Weizsäcker (7) proposed an approximate semiempirical formula for the nuclear ground-state binding energy, which is presented here in the form stated by Bohr & Mottelson (8):

$$B = b_{\text{vol}} A - b_{\text{surf}} A^{2/3} - \frac{1}{2} b_{\text{sym}} \frac{(N-Z)^2}{A} - \frac{3}{5} \frac{Z^2 e^2}{5R_c}, \qquad 1.1.$$

where the first term denotes the volume energy. b_{vol} gives the binding energy per nucleon for infinite nuclear matter (9).[3] The second term corresponds to the surface energy E_s, the third term to the symmetry energy, and the fourth term to the Coulomb energy E_c. Here

$$b_{\text{vol}} \approx 16 \text{ MeV}, \qquad b_{\text{sym}} \approx 50 \text{ MeV},$$

$$b_{\text{surf}} \approx 17 \text{ MeV}, \qquad R_c = \gamma_0 A^{1/3} \approx 1.24 A^{1/3} \text{ fm}.$$

Simultaneously, early versions of the shell model were based on the regularities discovered in relative and absolute isotopic abundances, which gave further evidence on "magic numbers," and the systematics of ground-state spins and magnetic moments of light nuclei. Difficulties were encountered, however, in deducing the larger magic numbers from a plausible coupling scheme (11).

1.3 SEARCH FOR ROTATIONAL BANDS Thibaud (12) in 1930 had suggested that rotations of nuclei may reveal themselves in the fine structure of α spectra. Teller &

[3] Unfortunately, recent variational methods for the theoretical calculation of this energy have suggested new uncertainties about the reliability of microscopic theory in its current form (10).

Wheeler (13), following this suggestion, carried out a search for rotational bands in alpha- and beta-ray spectra, in the hope of being able to determine nuclear moments of inertia. Their search was unsuccessful, partly because it concentrated mainly on the spectrum of ^{208}Pb, now known to be a doubly magic nucleus, and partly because the nuclear spectroscopy of the second nucleus investigated, ^{238}U, was still quite incomplete. It is worth mentioning, however, that the authors of this paper expected a spin sequence $J = 1, 2, 3, 4, \ldots$, even parity, as in a polar molecule. They predicted energy levels of 3.3, 10, 20, ... keV according to the equation

$$E_J = \frac{\hbar^2}{2} \frac{J(J+1)}{\mathcal{I}}, \qquad 1.2.$$

with $\mathcal{I}$ being the rigid moment of inertia of a sphere with uniform mass distribution and $r_0 = 2 \times 10^{-13}$ cm.

1.4 SLOW NEUTRON CAPTURE, FISSION, AND DYNAMICS OF THE LIQUID DROP Meanwhile, Niels Bohr (14) had suggested an interpretation of the newly discovered resonance capture of slow neutrons in nuclei in terms of nuclear oscillations very similar to the oscillations of a liquid drop that had been described in detail by Rayleigh. The same model turned out to be a fruitful starting point for the description of fission (15). Frenkel (16), on the basis of similar considerations, arrived at a precise criterion for the occurrence of spontaneous fission:

$$E_c/E_s > 2, \qquad 1.3.$$

where E_c and E_s denote the fourth and second terms in Equation 1.1. Frenkel also surmised that under certain conditions the most stable shape of a nucleus may be deformed. Jensen (17), in his Nobel Prize lecture in 1963, related that to Niels Bohr, the "hot" liquid drop model, which was so successful in the interpretation of compound nucleus formation, seemed incompatible with shell structure. Because of this, and the intervening war, shell model investigations that had been vigorously pursued in the early 1930s were more or less shelved.

1.5 THE INDIVIDUAL PARTICLE SHELL-MODEL Finally, after the war, the independent particle shell-model could not be refuted any longer, once the difficulties concerning the interpretation of the magic numbers for the somewhat heavier nuclei were resolved by the hypothesis of strong spin-orbit coupling (18). Briefly, this model, for an odd-A nucleus, consists of a spherically symmetric, central potential in whose field the single odd nucleon moves. Both neutrons and protons independently are predicted to fill shells with the magic numbers 2, 8, 20, 28, 50, 82, and 126. From this model followed not only the systematics of binding energies, relative and absolute abundances and ground-state spins (19), and magnetic moments, but also the sequence of spins and magnetic moments of excited states in odd-A nuclei.

1.6 RELATION BETWEEN ENERGY AND TRANSITION RATE FOR SINGLE PARTICLE TRANSITION Weisskopf computed the rate T for a single particle transition from

an initial state J' to a final state J. For an electric quadrupole transition, the γ transition rate for a single proton is

$$T_\gamma[(\text{sec})^{-1}] = 7.23 \times 10^7 A^{4/3} E_\gamma^5(\text{MeV}) = 2.45 \times 10^{60} B(E2)_{\text{sp}}(\text{cm}^4) E_\gamma^5(\text{MeV}), \quad 1.4.$$

where $T_\gamma = [\tau(\text{sec})]^{-1}[1+\alpha]^{-1}$, τ denotes the mean lifetime, E is the transition energy (in MeV), α the total internal conversion coefficient, and $B(E2)_{\text{sp}}$ (in cm^{-4}) denotes the reduced single-particle transition rate (a "Weisskopf unit").

1.7 ODD-A QUADRUPOLE MOMENTS, ENHANCED $E2$ TRANSITIONS IN EVEN-EVEN NUCLEI, AND ROTATIONAL BANDS. THE BOHR-MOTTELSON COLLECTIVE MODEL AND THE EXPANSION OF ROTATIONAL ENERGIES IN TERMS OF $J(J+1)$. The shell model stimulated new interest in the systematic study of electric quadrupole moments of ground states of odd-A nuclei. An earlier result had given an interesting clue: in 1940 Schmidt (20) reported a systematic deviation, as a function of Z, of nuclear quadrupole moments from values expected for a sphere, and pointed out that minima of this function occurred near the "magic numbers" $Z = 50$ and 82. Several authors (21) presented compilations of Q vs the number of the odd nucleons. The results showed a strong dependence of the magnitude and sign of the quadrupole moment on shell structure. The quadrupole moment was found to become larger away from closed shells and to attain negative values just after a shell was filled. This clearly implied a deformation of the nucleus between closed shells. Townes, Foley & Low (22), from a more detailed analysis of the data, then concluded that protons and neutrons tend to be "oriented or polarized to allow maximum overlap between proton and neutron distributions." This result was explained by Rainwater (23), who showed that once a slight deformation exists due to the presence of several nucleons beyond a closed shell, the addition of more extra-core nucleons will lead to increasing spheroidal distortion, assuming the volume remains constant. He thus put Frenkel's hypothesis (16) on a more solid basis. A. Bohr went on to develop the theory of the quantization of angular momentum in the field of a nucleus with spheroidal symmetry, independent of the origin of deformation (24). He pointed out that since in a spheroidal potential the degeneracy in the magnetic quantum number will be removed, the energies of the m substates will vary as functions of the axially symmetric deformation. Later, Nilsson (25) calculated these functions $E(K\pi N n_z \Lambda)$ using a harmonic oscillator potential, both for positive (prolate) and negative (oblate) deformations. Carefully revised on the basis of empirical data over the years, such "Nilsson diagrams" have become an essential tool in nuclear physics.

Bohr explained the absence of low-lying rotational levels arrived at by Teller & Wheeler (13) by assuming that the nucleus does not rotate like a rigid structure: "It seems quite possible that a rotation of the nucleus involves the motion of only a fraction of the nuclear particles, due to an incomplete rigidity of the nuclear structure, or due to exchange effects of the type considered by Teller & Wheeler."

The successes of the shell model directed the interest of nuclear physicists toward the study of excited states of odd-A nuclei, which in a very short period gave

abundant proof of the simplicity and predictive power of the shell model. The classification of isomeric transitions by Goldhaber & Sunyar (26) provided valuable tests for the new individual particle theory of electromagnetic transition rates. In most cases the observed rates were lower. There were, however, some surprising exceptions. While even-even nuclei were generally thought to be rather featureless structures that simply provided a spherical potential for the odd nucleon, there were among the isomeric transitions studied a small number of low-energy ($\sim 80 \rightarrow$ 100 keV) electric quadrupole ($E2$) transitions in even-even rare-earth nuclei that had transition rates two orders of magnitude higher than expected. The authors attributed this "enhancement" to the cooperative nature of these transitions. They pointed out that they occurred exactly in a region where the largest quadrupole moments in odd-A nuclei had been observed, indicating that both phenomena must have the same origin. Further, a survey of the spin-parity of first excited states in even-even nuclei showed that they are predominantly $2+$. The implications of this empirical rule were considered in detail from a theoretical point of view by A. Bohr (27).

The low-lying $2+$ states in rare earth even-even nuclei depopulated by enhanced $E2$ ($2+ \rightarrow 0+$) transitions, were recognized by Bohr & Mottelson (28) as the missing lowest levels of rotational bands expected from Equation 1.2. They were soon able to carry their analysis further (29). In a review of isomeric transitions (30), they found that the four γ rays following the 5.5-hr transition in ^{180}Hf reported by Burson et al (31) obeyed almost precisely the $J(J+1)$ rule for a cascade $0+ \leftarrow 2+ \leftarrow 4+ \leftarrow 6+ \leftarrow 8+$. A coincidence measurement (32) proved that indeed all four γ's are in cascade, and an angular correlation measurement (33) showed that they are all $E2$ transitions. Further supporting the evidence for rotational bands (29) were 3 triple cascades, in ^{176}Hf, and in two actinide nuclei, ^{226}Ra and ^{228}Th. Although in some of these nuclei the $J(J+1)$ rule was more or less violated, the authors believed that it should suffice to add a correction term

$$\Delta E_J = -BJ^2(J+1)^2, \qquad 1.5.$$

of the type known from the theory of molecular spectra, attributed to rotation-vibration interaction. It therefore became customary to list $\mathcal{I}$ and B as the parameters characterizing a rotational band.

The properties of rotational bands strengthened Bohr & Mottelson's conviction that a deformed nucleus has cylindrical symmetry, so that the component K of the total angular momentum along the axis of symmetry is a good quantum number. The deformation parameter β provides a measure of the departure from spherical symmetry. The deformed nucleus was assumed to be an essentially incompressible spheroid of constant density, in which neutrons and protons are uniformly distributed (34). In addition to rotation, two types of quadrupole vibrations of considerably higher frequency than that of the rotations ($\hbar\omega \approx 1$ MeV) were thought to be most prominent: beta vibrations around the equilibrium deformation, for which $K = 0$, and for which the spin sequence of the superimposed rotational band is 0, 2, 4, . . . , even parity, and the asymmetry producing gamma vibrations, with $K = 2$ and spin sequence 2, 3, 4, 5, . . . , even parity. (The asymmetry parameter

γ is an angular coordinate. For $\gamma = 0$ or π the deformation is symmetric about the axis of symmetry, and of prolate and oblate shape, respectively. For $\gamma = 30°$, the asymmetry is at a maximum.)

1.8 RELATION BETWEEN MOMENT OF INERTIA AND TRANSITION QUADRUPOLE MOMENT: THE HYDRODYNAMICAL MODEL LEADS TO DISCREPANCY The hydrodynamical expression proposed for the nuclear moment of inertia defined by Equation 1.2 was the irrotational one (34):

$$\mathcal{I} = \frac{9}{8\pi} AMR_0^2\beta^2, \qquad 1.6$$

where β is the deformation parameter, M the nucleon mass, and R_0 the nuclear radius. The intrinsic quadrupole moment Q_0, which is related to the reduced transition probability $B(E2)$ by

$$Q_0^2 = \frac{16\pi}{5} B(E2)(0 \rightarrow 2), \qquad 1.7$$

is given by

$$Q_0 = 3/(5\pi)^{1/2} ZR_0^2\beta. \qquad 1.8$$

By eliminating β from Equations 1.6 and 1.8, one obtains

$$\mathcal{I} = \frac{5M}{8} \frac{A}{Z^2R_0^2} Q_0^2 = \frac{5M}{8R_0^2} \frac{A^{1/3}}{Z^2} Q_0^2. \qquad 1.9$$

However, this equation led to a discrepancy.

A detailed analysis by Sunyar (35) of the measured energies and lifetimes of $2+$ states in even-even nuclei ranging from ^{152}Sm to ^{198}Hg resulted in the conclusion that the moments of inertia deduced from E_2 values are 4 to 5 times larger than the irrotational values. This is 2 to 3 times smaller than $\mathcal{I}_{\text{rigid}}$. The problem of the origin of the nuclear moment of inertia, to which we soon return, is the main concern of this review.

1.9 FIRST $2+$ STATE ENERGIES IN EVEN-EVEN NUCLEI: ENERGY GAP AND PAIRING FORCE Soon after the discovery of enhanced $E2$ transitions of $80 \rightarrow 100$ keV to the ground states of even-even nuclei in the rare-earth region, there started a largely model-independent phenomenological study of level schemes of all known even-even nuclei, both stable and radioactive. The motivation was the expectation that this procedure might yield some insight into the structure of the even-even core of an odd-A nucleus, which had so far been considered only as the source of the potential in which the odd nucleon moves. This study was based partly on literature reviews and partly on experiments performed with this objective in mind. It went through several stages, which are described below.

The questions asked were: what are the properties of excited states of even-even nuclei, their spins and parities, energies, lifetimes, and electromagnetic moments? What symmetry properties do they reveal? How do they vary with

neutron and proton number? Can analytic expressions be found that describe the level energies as functions of other level properties such as the angular momentum?

The first stage consisted of a review (36) of the spins, parities, and energies of the three lowest states in even-even nuclei. In contrast to the variety of the spin-

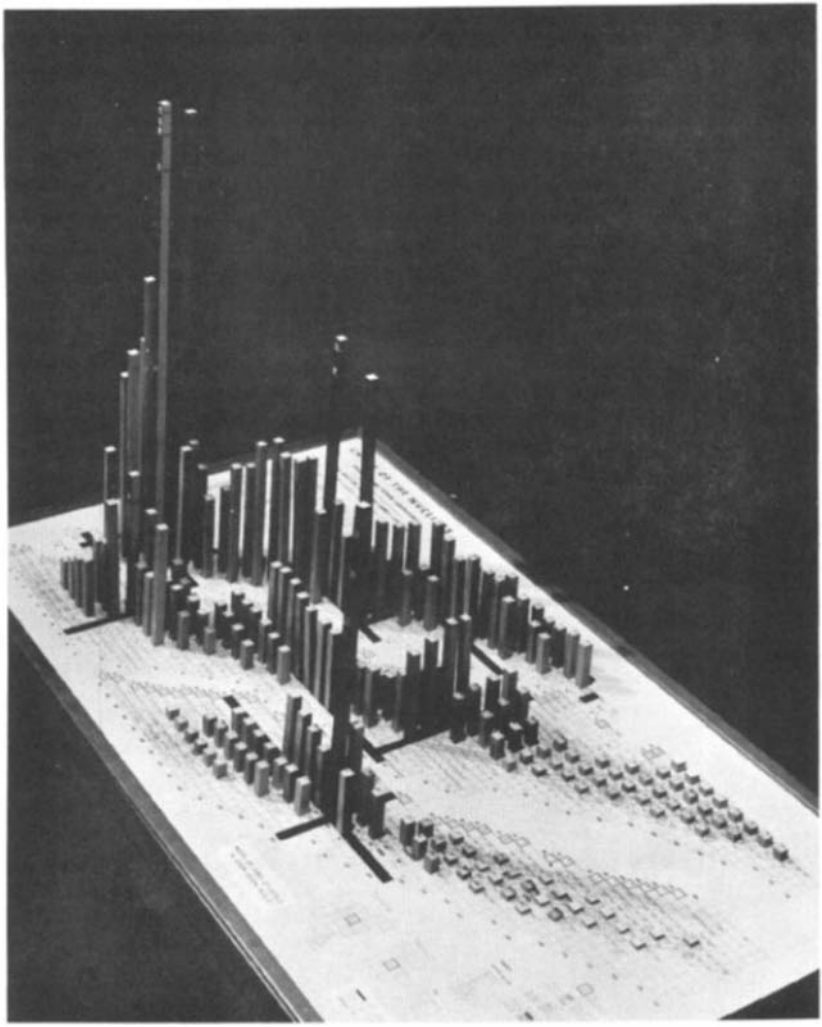

Figure 1 Three-dimensional model of the energies of the first 2+ states of even-even nuclei vs proton and neutron numbers. Magic numbers are indicated by heavy bars in the $Z-N$ plane. The model shows that the excitation energies are very large at magic numbers, but fall off steeply and attain the smallest values midway between magic numbers. The lowest energies are attained in the larger shells (rare earths and actinides).

parities of levels in odd-A nuclei, it was found that even-even nuclei show astonishingly regular features: without exception the ground states were found to be $0+$, the first excited states, with very few exceptions,[4] were $2+$, and the overwhelming majority of second excited states were either $4+$, $2+$, or $0+$. These findings were in agreement both with the collective model (27) and the extended shell model (37), which had evolved simultaneously.

The excitation energy of the first excited $(2+)$ state reflects the nuclear shell structure in great detail (Figure 1). From the highest values at doubly magic numbers [$\sim$20 MeV at ^{4}He (not shown), $\sim$6 MeV at ^{16}O] it decreases first rapidly, then more gradually to reach the lowest value approximately midway between the closed neutron and proton shells. The lowest values, $\sim$40 keV, are attained for the heaviest nuclei known (e.g. ^{250}Cf).[5] An unsuccessful attempt was made to represent the energy of the first $2+$ state as a function that is separable into a neutron and proton part. This failure implied that neutron-proton interactions contribute to the $2+$ energy.

The fact that the spacing between the ground-state (g.s.) and the first excited state near magic numbers is approximately an order of magnitude larger than in odd-A nuclei, instead of being equal or even smaller, presented a puzzle. Also, no "intrinsic" states, i.e. states due to the promotion of one or two nucleons to a higher orbit at energies $\lesssim$1 MeV are populated in even-even nuclei: this "energy gap" was attributed (39) to the effect of "residual" forces acting between nucleons, i.e. forces not included in the average single-particle potential. It was concluded that in addition to the force that tends to deform the nucleus, there must be a force between like particles that tends to preserve the spherical shape. Also, such a force must be responsible for the reduction of the moment of inertia compared with the rigid-body value, since the Inglis cranking model (40), assuming *non-interacting* particles contained in a rotating external potential, yields $\mathcal{I} = 0$ for closed-shell nuclei, and $\mathcal{I} = \mathcal{I}_{\text{rigid}}$ for nuclei with any number of nucleons beyond

[4] The exceptions to the $2+$ rule for the first excited state now known are the following:

Nucleus	$I\pi$	E
^{4}He	$0+$	20.2
^{14}O	$(1-)$	5.17
^{14}C	$1-$	6.0932
^{16}O	$0+$	6.052
^{40}Ca	$0+$	3.348
^{72}Ge	$0+$	0.690
^{90}Zr	$0+$	1.75
^{98}Mo	$0+$	0.7349
^{208}Pb	$3-$	2.6145

[5] The shell dependence of the quadrupole excitations is in sharp contrast with the behavior of the giant electric dipole vibrations, which are ascribed to vibrations of protons against neutrons and whose energy, in first approximation, depends only on the mass of the nucleus (38).

closed shells.[6] A force fulfilling these requirements is the pairing force. First, Bohr & Mottelson (42) suggested "a greatly simplified model, in which the whole effect of nucleons outside of closed shells is represented by two interacting nucleons in p-states." As interaction (pairing-force) parameter between the nucleons they chose $v = U/\hbar\omega$, where U is the energy difference between the $J = 0$ and $J = 2$ states of the two nucleons and $\hbar\omega$ the configuration spacing. They were able to fit approximately the empirical $\mathcal{I}$ values [taken to be $(\hbar^2/2E_2)$] as a function of β [as deduced from $B(E2)$] by setting $v = 1/3$. The nuclei included in this survey ranged from $^{150}Nd_{90}$ to $^{188}Os_{112}$, with β ranging from 0.2 to 0.45.

1.10 ANALOGY WITH A SUPERCONDUCTOR: PAIRING-PLUS-QUADRUPOLE MODEL AND MOMENT OF INERTIA An important step forward was made in 1958. Bardeen, Cooper & Schrieffer, and, independently, Bogoliubov had succeeded in explaining superconductivity on the assumption that a weak attractive force exists between two electrons. Following this, Bohr, Mottelson & Pines (43) pointed out that the mathematical approach developed for the understanding of superconductivity might be applied to the "pairing force" in nuclei, while nuclear deformation might be ascribed to a quadrupole-quadrupole interaction between two nucleons. Following their suggestion, Belyaev developed a theory based on the "pairing-plus-quadrupole (PPQ) force." Griffin & Rich (44) and Nilsson & Prior (45) applied the same theory to the problem of the moment of inertia and arrived at fairly satisfactory values for a few nuclei in the rare earth and actinide regions.

Mottelson & Valatin (46) carried the analogy with a superconductor one step further. They argued that just as superconductivity vanishes when an external magnetic field has reached a critical magnitude, so the energy gap vanishes at a critical angular velocity ω_c due to the action of the Coriolis forces.[7] At that point the nuclear moment of inertia will abruptly approach the rigid-body value $\mathcal{I}_{\text{rigid}}$. They stated that the critical angular momentum J_c is given by the equation $J_c = \omega_c \mathcal{I}_{\text{rigid}}$ and estimated that $J_c \simeq 12$ in the rare-earth region and $J_c \simeq 18$ in the actinide region. A search for this effect was thought to be valuable to test the description of the pairing correlations in nuclei. As we show in Section 4 and later sections, an effect of this kind was indeed later discovered, and the estimates for J_c were in remarkably good agreement with observation. However, the phenomena observed above J_c are more complex than Mottelson & Valatin had foreseen.

In Section 2 a phenomenological approach to the problem of the moment of inertia, applicable not only to strongly deformed but to all nonmagic nuclei is discussed.

1.11 FIRST 2+ STATE ENERGY TREATED AS A SCALE FACTOR: THE VIBRATIONAL MODEL The second stage in the phenomenological study occurred long before

[6] A lucid presentation of the cranking model approach is included in Sorensen's review article entitled "Nuclear Moment of Inertia at High Spin" (41).

[7] The role of the Coriolis force was first discussed by Bohr (27).

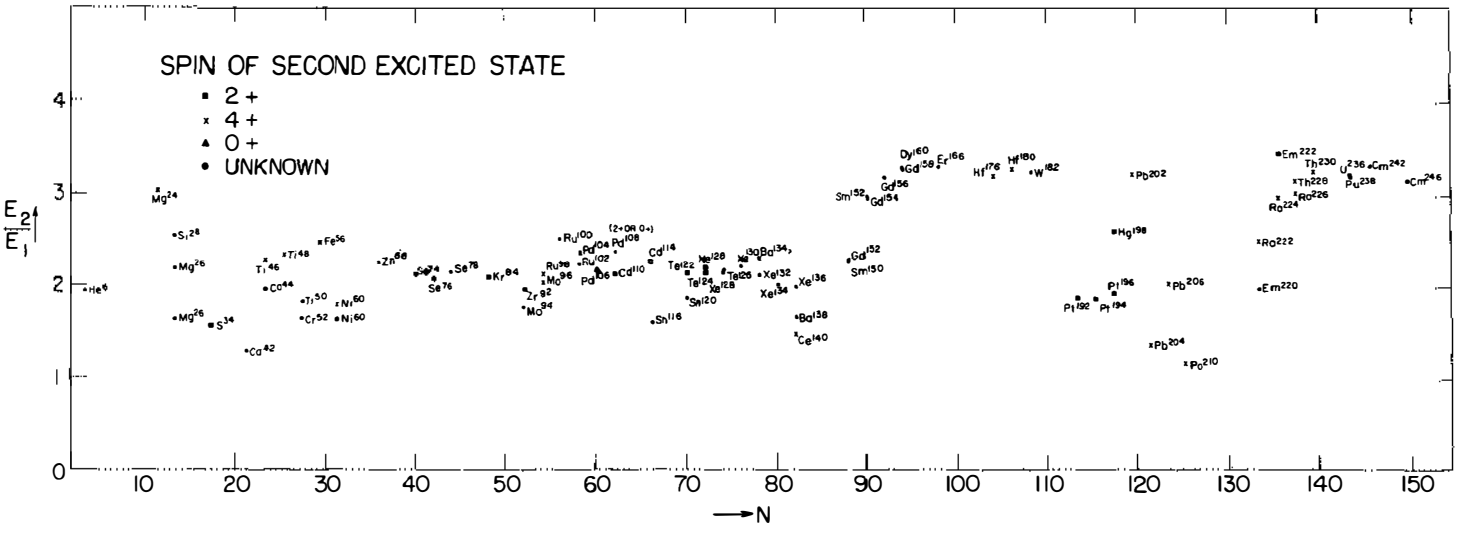

Figure 2 Ratios of E_2/E_1 as function of neutron number N. The character of the first excited state is 2+ in all cases. The character of the second excited state is denoted by triangles for 0^+, squares for 2^+, crosses for 4^+, and dots for states of unknown spin (unless given in parentheses). An abrupt increase occurs between 88 and 90 neutrons. Low values occur at magic numbers 50 and 82. The figure appeared in (47). The character of the second excited state in all nuclei included with $N \geqq 90$ was later found to be 4+.

the pairing-plus-quadrupole model was conceived. It was concerned with the variation of the energy (E_2) of the second excited state (47), established to be in general either 2+, 0+, or 4+. The excitation energy E_1 of the first 2+ state was taken as a scale factor. As we have seen, E_1 depends not only on the nuclear volume, but reflects details of the shell structure, including neutron-proton interactions. Figures 2 and 3, reproduced from the original paper, demonstrate that the ratios, E_2/E_1, both as functions of N and of the energy E_1, form definite patterns: they can be divided into a rotational group for which $E_2/E_1 \simeq 3.33$ and into a second group, for which $E_2/E_1 \simeq 2.2$, referred to as vibrational or near-harmonic. This fact, together with previously established rules for the transition rates between levels of the vibrational group, suggested as a model a spherical nucleus whose surface is capable of undergoing one, two, or more phonon excitations of the quadrupole type; hence the first excited state is 2+, the second a 0+, 2+, 4+ triplet, etc. For the "ideal" vibrator, $E_2/E_1 = 2$, and $[B(E2)(2 \rightarrow 1)]/[B(E2)(1 \rightarrow 0)] = 2$. By a shell-model calculation involving four nucleons above a closed shell core, it could be shown that the degeneracy of the triplet state is lifted and the ratio is increased from 2 to ~ 2.2. An abrupt transition from the vibrational to the rotational pattern is observed between 88 and 90 neutrons, both for Sm ($Z = 62$) and Gd ($Z = 64$). This appears to be due to the fact that the $h_{11/2}$ shell "breaks up" as a function of deformation (48). A similar abrupt change takes place in the actinide region, in this case between 86 and 88 protons (49). The vibrational model is still widely used for the analysis of level schemes, although we now know

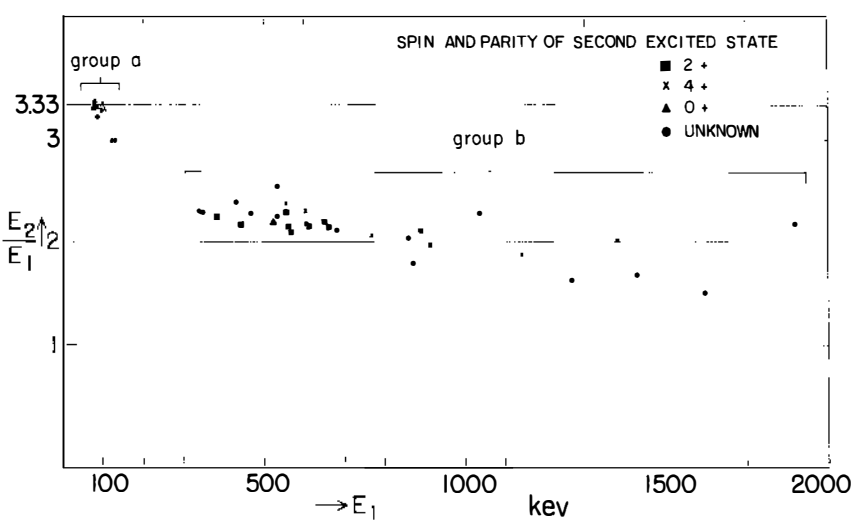

Figure 3 Ratios of E_2/E_1 as function of E_1 for $36 < N < 108$. The same symbols are used as in Figure 2. A gap in the energy E_1 is seen between the high (i.e. rotational) values and the low (vibrational) values. At the highest energies the ratio decreases below the vibrational value. Figure taken from (47).

that it is oversimplified, since already the 2+ state deviates from the spherica shape (see Section 1.13). On the strength of the same empirical evidence, an alter native model was proposed by Wilets & Jean (50), namely that of a "γ-unstable' nucleus. The empirical evidence on level energies then presented was recentl confirmed (51), on the basis of the much more numerous data accumulatec meanwhile.

1.12 "TRANSITIONAL" LEVEL SCHEMES IN EVEN-EVEN Os NUCLEI AND MALLMANN CURVES The abruptness in the transitions between the vibrational and rotationa regions suggested the possibility that there might be no intermediate solution, i.e that either the forces that bring about the spherical shape take over, or, if severa nucleon pairs of both kinds are present, the aligning forces will give the nucleus an appreciable deformation. An "intermediate coupling" calculation to answer this problem seemed out of the question. However, a survey of the energies of 2+ states as a function of N and Z suggested (Figure 4) that on the high-A side of the rare-earth region a much more gradual transition occurs than between 88 and 90 neutrons. In particular, the Os ($Z = 76$) nuclei seemed suitable for systematic study via the positron and K-capture decay of the odd-odd Ir ($Z = 77$) nuclei. A series of experiments was undertaken at BNL, which led to a surprising result (52): a gradual transition from the rotational to the vibrational level pattern occurred with increasing neutron number. Indeed, a cascade 0+, 2+, 4+, 6+, 8+ was found in a nucleus that had an almost equidistant level pattern, namely ^{190}Os. Such a cascade is now referred to as a ground-state band. During the succeeding years a number

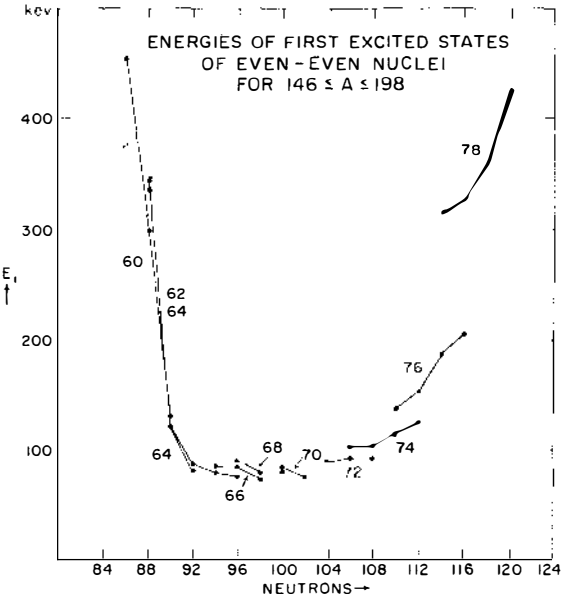

Figure 4 Excitation energies of the first 2+ state for the rare-earths region. The energies in Os ($Z = 76$) nuclei partly bridge the gap occurring between 88 and 90 neutrons.

of experimental studies of the decay schemes of odd-odd Ir nuclei were carried out (53–55). The results confirmed and greatly extended the early conclusions. Results from several other laboratories, notably at Berkeley (56), further expanded the knowledge of the striking regularities in the excitation patterns of "transitional nuclei." Figure 5 presents a survey of Os level schemes compiled several years ago.

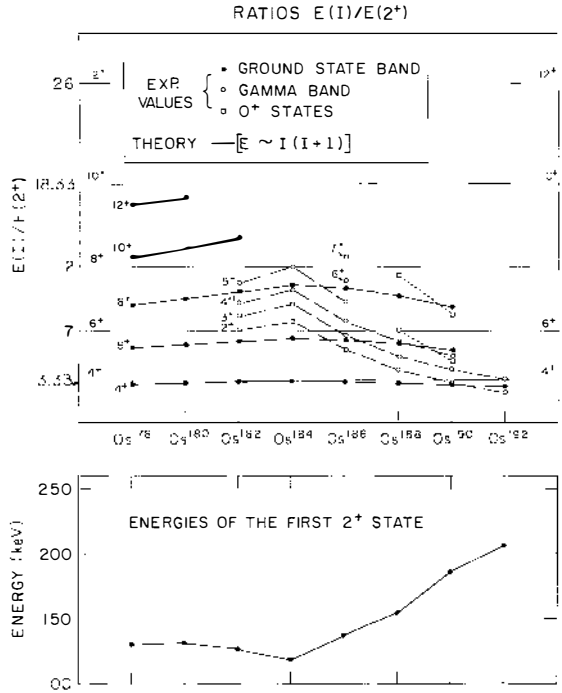

Figure 5 Ratios of energies E_J of excited states in even-even Os nuclei to E_2 (energy of first 2+ state). In the lower part of the figure the energies of 2+ states in Os nuclei with $102 \leqq N \leqq 116$ are shown. The upper part presents the ratios E_J/E_2 for ground-state bands, denoted by solid circles. These may be compared with the horizontal lines indicating the "perfect rotor" values $J(J+1)$. From the peak values at ^{184}Os, the most neutron-deficient stable isotope of Os (with only 0.018% relative abundance) for which E_2 is at a minimum, the ratios fall off slowly both toward the neutron-deficient side and toward the heavier isotopes. The open circles denote ratios of states in the gamma band. In ^{184}Os the 2′+ ground state of the ($K = 2$) gamma band (2+, 3+, 4+, 5+) lies above the 6+ state of the ground-state band. An analogous band was populated in ^{182}Os, which exhibits only a slight drop in the ratios. On the neutron-rich side, however, the ratios for the ($K = 2$) bands, while preserving the same spin sequence and general appearance, fall rapidly to lower values so that in ^{192}Os the 2′+ state lies just below the 4+ ($K = 0$) state. The ratios R_4 and $R_{2'}$ strongly resemble the corresponding ratios known from two-phonon states of "vibrators." (Two sets of O+ states are known in ^{188}Os and ^{190}Os. By extrapolating the ratios for the lower set to ^{192}Os, the approximate value expected for the O+ member of the triplet results. However, no such O+ state is known in ^{192}Os.) Thus the Os level schemes represent an almost complete transition from rotor (^{184}Os) to vibrator (^{192}Os).

The lower part of the figure presents the energies of the first 2+ states in even-even Os nuclei vs N, and the upper part the ratios E_J/E_2, $K = 0$ (ground-state bands) and E'_J/E_2, $K = 2$ (now referred to as "quasi-gamma bands") vs N, and also a few ratios for excited 0+ states. It is seen that the ground-state band ratios decrease slowly from almost rotational values (indicated by horizontal lines) at ^{184}Os toward the vibrational ones at ^{192}Os. They also decrease toward the neutron-deficient side, where the isotopes become more and more beta-unstable. The ratios for the "quasi-gamma bands" decrease precipitously as the neutron number increases. One interesting feature, not apparent in Figure 5, is the odd-even staggering, particularly well displayed by the quasi-gamma band in ^{186}Os (55).

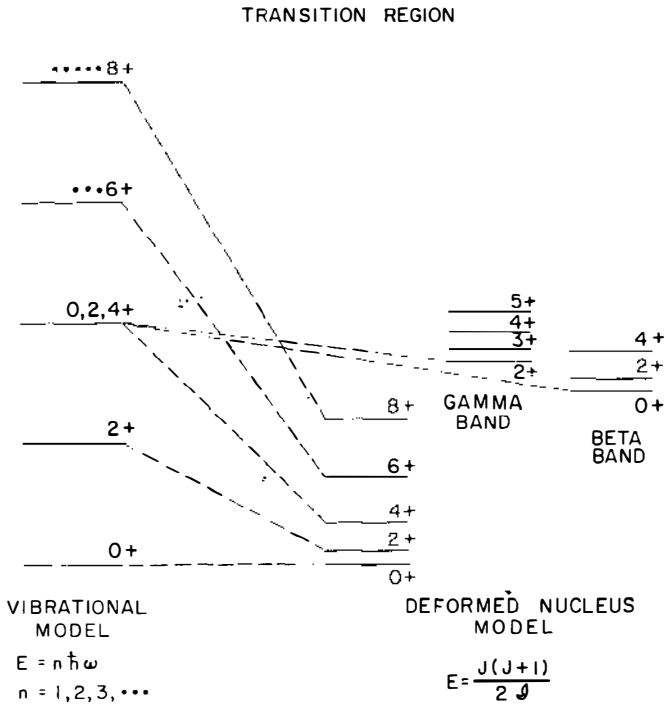

Figure 6 Schematic level schemes of spherical and deformed nuclei. At the right, the ground-state, gamma- and beta-bands of a "good rotor" are indicated. Their components along the symmetry axis are $K = 0$, 2, and 0, respectively. At the left the first three levels predicted for vibrational nuclei are shown. The 0, 2, 4 triplet, here shown as degenerate, is thought to be split by coupling one or two nucleon pairs to the spherical core. The dashed lines indicate the gradual transitions observed in the level schemes of Os nuclei from the states of the two-phonon triplet to the 4+ state of the ground-state band and the 2+ and 0+ ground states of the gamma- and beta-bands. The Mallmann curves (Figure 7) imply the scaling property of the lines connecting the one, two, ... phonon levels with highest spin with the levels of the ground-state band of the good rotor.

The conclusions from this empirical study are summarized in schematic form in Figure 6. The states of the rotational band go over into the highest spin states of the vibrational multiplets, whereas the 2+ ground state of the γ band goes over into the 2+ state of the vibrational two-phonon triplet, and the 0+ ground state of the β band into the 0+ triplet state. In the intervening years, in addition to ground-state bands, "quasi-gamma" and "quasi-beta" bands have been populated in many even-even nuclei. A valuable tabulation of these bands has been provided by Sakai (57).

About two years after the first report on the Os level schemes, Mallmann (58) made an important contribution. Impressed by the similarity of the curves E_J/E_2 vs N for $J = 4, 6, 8$ in the Os nuclei, he plotted the ratios E_6/E_2 and E_8/E_2 vs E_4/E_2 for all known rotational bands, bands for transitional nuclei (Os), and a few other ground-state bands. The latter pertained to nuclei with lower E_4/E_2 values, some of them being singly magic (Figure 7). It turned out that these ratios formed two "universal" curves, i.e. the energies in ground-state bands seemed to "scale!" No existing nuclear theory explained this puzzling fact. Mallmann showed further that the expansion in $J(J+1)$ (Equation 1.5) diverges quite badly already very close to the rotational region (*dashed curves*).

Meanwhile, the detailed analysis of the Os level schemes (55) showed that the ground-state bands, but not the quasi-gamma bands, were in rather good agreement with an axially asymmetric rotor model suggested by Davydov & Filipov (59). The axial asymmetry, according to this interpretation, increased from 16° to 25° between ^{186}Os and ^{192}Os. The fit was not much improved by the inclusion of the interaction of β-vibrational motion with the rotational motion according to Davydov & Chaban (60).

Baranger, who had become intrigued by the interesting regularities and symmetry properties displayed by the even-even Os nuclei, devised a microscopic Hartree-Fock-Bogoliubov theory to explain this behavior (61) (see Section 8). In collaboration with Kumar (62), he analyzed the degree of validity of this method, and was able to give a fairly detailed account of energies and electromagnetic moments of excited states and the transition probabilities between these states. However, the "scaling" behavior did not follow from this theory.

1.13 ELECTRIC QUADRUPOLE MOMENTS OF 2+ STATES IN SPHERICAL NUCLEI AND ENERGIES OF EXTENDED GROUND STATE BANDS IMPLY INCREASE OF MOMENT OF INERTIA WITH ANGULAR MOMENTUM Following a suggestion of Breit, electric quadrupole moments of 2+ states of several nuclei whose level schemes correspond to the vibrational pattern (Section 1) were determined by means of the "reorientation effect" (63) and found to be rather large. Although the accuracy of determination of static quadrupole moments is not as good (~30–100%) as that for transition quadrupole moments (~2–10%), the main result was beyond doubt: the vibrational model had to be modified.

A more recent compilation by Christy & Häusser (64) is based on several different methods of determining electric quadrupole moments of 2+ states. The comparison with the transition quadrupole moments shows close correlation in

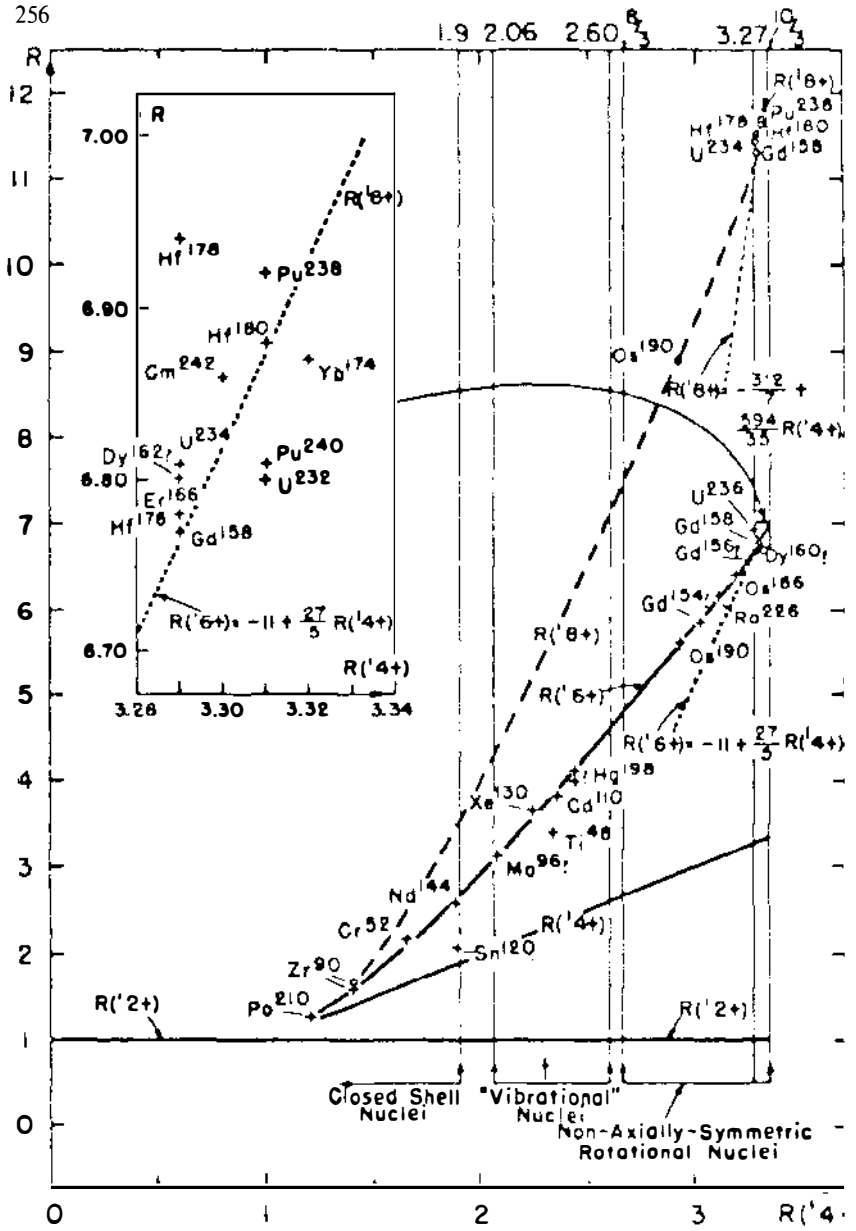

Figure 7 Empirical ratios $E_6/E_2[R('6+)]$ and $E_8/E_2[R('8+)]$ as functions of E_4/E_2. The points lie on two "universal curves." The two-term expansion in $J(J+1)$ (*dotted lines*) is shown to diverge from these curves already close to the rotational limit. Later results showed that the curves do not continue to $E_4/E_2 = 1$, but stop at ~ 1.8 (see Figure 16). The figure is reproduced from (58).

general. The general behavior of $Q(0+ \rightarrow 2+)$ values is discussed in detail in Sections 3.1 and 3.2.

A new chapter for the exploration of nuclear structure opened when Morinaga & Gugelot (65) devised a method for populating ground-state bands in even-even nuclei by means of $(\alpha, 2n)$ and $(\alpha, 4n)$ reactions. This approach permitted the study of these bands to higher J values than the observation of the decay of natural or artificial radioactive isotopes. The latter is limited to $J \lesssim J'+1$, where J' denotes the spin of the parent nucleus. The new method made use of the high energy and angular momentum imparted to the nucleus by the incoming particle. Soon afterwards it was extended to heavier ions, which permitted the study of even higher angular momenta in the product nucleus, and increased the range of these product nuclei to more unstable species at the neutron-deficient side of the valley of stability (66). Moreover, the study of nuclei undergoing spontaneous fission, in particular of ^{252}Cf (67), and of spallation or fission products obtained by bombardment with very high energy particles, in particular protons, extended the range to the neutron-rich side of the valley of stability. In this way g.s. bands up to $J = 22$ were populated. More recently, Coulomb excitation experiments succeeded in populating very high spin states, e.g. by bombarding ^{238}U with Kr and Xe ions, a 3067.2-keV $(22+)$ state was populated in ^{238}U (68). In all these cases the energy spacings at higher J are smaller than required by the $J(J+1)$ rule. The bands could not generally be fitted by adding a term to the energy quadratic or cubic in $J(J+1)$. Morinaga (69) was the first to suggest that the decrease in spacing was due to an increase in the moment of inertia $\mathcal{I}$. He proposed the term *softness* for the percentage increase of $\mathcal{I}$ per unit change of J, $\Delta\mathcal{I}/\mathcal{I}\Delta J$ and discussed the form of the dependence of this quantity on J as a function of N and Z.

1.14 BETA-STRETCHING MODEL AND SELF-CONSISTENT FOURTH-ORDER CRANKING MODEL FIT BANDS IN STRONGLY DEFORMED NUCLEI An attempt to give a physical explanation for the increase in $\mathcal{I}$ was made by Diamond, Stephens & Swiatecki (70). They suggested a semiclassical model based on "the idea of a spinning nucleus being stretched out under the influence of the centrifugal force," the so-called beta-stretching model. Here the energy is given by

$$E_J(\beta) = \tfrac{1}{2}C(\beta_J - \beta_0)^2 + \frac{J(J+1)}{2\mathcal{I}(\beta)}, \qquad 1.10.$$

where $\mathcal{I}$ is the moment of inertia in terms of $\hbar^2$. The first term represents a kind of rotational Hooke's Law. The equilibrium condition

$$\partial E_J/\partial\beta = 0 \qquad 1.11.$$

fixes the value of β_J, if $\mathcal{I}(\beta)$ is a known function. β_0 denotes the g.s. deformation parameter, and C the stiffness parameter. The authors assumed that the relation $\mathcal{I} \propto \beta^2$ holds. Their comparison of Equation 1.10 with g.s. bands in strongly deformed, neutron-deficient nuclei showed good agreement in general.

An important advance was made by Harris (71), who first proposed a consistent expansion of the energy and moment of inertia in powers of ω^2, as an alternative to the $J(J+1)$ expansion of Bohr & Mottelson. He found excellent agreement

with the energies in g.s. bands of deformed nuclei. His formalism is a generalization of the Inglis cranking model. As a special case, the Harris model with two parameters may be written

$$[J(J+1)]^{1/2} = \omega(\mathscr{I}_0 + \omega^2/2C), \tag{1.12.}$$

$$E = \frac{1}{2}\left(\mathscr{I}_0 + \frac{3\omega^2}{4C}\right)\omega^2. \tag{1.13.}$$

Elimination of ω leads to an expression for the level energy E in terms of the two parameters $\mathscr{I}_0$ and C.

2 *The VMI Model*

2.1 AN ANALYTICAL EXPRESSION FOR THE MALLMANN CURVES IN TERMS OF AN EFFECTIVE VARIABLE MOMENT OF INERTIA Although the energies $E_J(N, Z)$ of states in the g.s. bands of even-even nuclei could not be given in analytical form (Section 1), the time seemed ripe to attempt a derivation of Mallmann's "universal curves" for E_J/E_2 in closed form. As we have seen in Section 1, in such an expression E_2 would have the role of a scale factor. The plan was to include, in addition to strongly deformed nuclei, the transitional, vibrational, and perhaps even magic nuclei (see Figure 7). In searching for such an expression the following considerations were taken into account:

1. The expansion of g.s. band energies in terms of $J(J+1)$ diverges (58) from the observed behavior already close to the "adiabatic limit" (34) ($R_4 = 10/3$).
2. The "moment of inertia" $\mathscr{I}$ deduced from energy spacings in ground-state bands increases steadily with increasing J (69).
3. The static quadrupole moments found in "spherical" nuclei for $2+$ states show that these nuclei must also have nonvanishing moments of inertia in the $2+$ state.
4. The energies of g.s. bands in even-even Os nuclei, which vary so regularly with neutron number (Figure 5), are best described by assuming that these nuclei have appreciable axial asymmetry. Nevertheless, they are in agreement with the Mallmann scaling law. Thus the analytical expression should not necessarily require axial symmetry.
5. Since the scaling law depends on only two quantities, E_2 and E_4, it should be possible to find a two-parameter expression for the curves E_J/E_2 as a function of E_4/E_2.[8]

The β-stretching formalism (70) appeared to be a promising starting point. However, it presupposes axial symmetry and requires knowledge of the dependence of the moment of inertia on the deformation parameter β. In order to meet these objections, β was replaced (72) by a general variable t, which might include the effects not only of deformation, but also of the effective pairing forces (see also

[8] This approach then seemed to violate two "basic" assumptions of the collective model (34): weak rotation-vibration mixing, and axial symmetry. However, in retrospect these assumptions had no general basis in nuclear dynamics.

Section 5). Least-squares fits to the data were attempted using the relation $\mathscr{I} = \text{const}\ t^n$ with $n = 1, 2, 3$. For g.s. bands ranging from $3.33 \geqq E_4/E_2 \geqq 2.34$, the best fits were obtained for $n = 1$. Hence, t may be replaced by the effective moment of inertia (73). The level energy is thus given by

$$E_J(\mathscr{I}) = \tfrac{1}{2}C(\mathscr{I} - \mathscr{I}_0)^2 + \tfrac{1}{2}[J(J+1)]/\mathscr{I}. \qquad 2.1.$$

The equilibrium condition

$$\partial E(\mathscr{I})/\partial \mathscr{I} = 0 \qquad 2.2.$$

determines the moment of inertia $\mathscr{I}_J$ (given in units of $\hbar^2$). Equations 2.1 and 2.2 are referred to as the variable moment of inertia (VMI) model.

The parameters C and $\mathscr{I}_0$ are the stiffness parameter and g.s. moment of inertia (for $\mathscr{I}_0 > 0$), respectively. From Equations 2.1 and 2.2 one obtains

$$\mathscr{I}_J^3 - \mathscr{I}_0 \mathscr{I}_J^2 = [J(J+1)]/2C. \qquad 2.3.$$

This equation has one real root for any finite positive value of $\mathscr{I}_0$ and C. A least-squares fitting procedure was applied to all measured values E_J in a given band. However, confidence in the VMI model was considerably strengthened when it was found that fitting the two lowest-level energies (E_2, E_4) alone also permits a good fit to higher levels.

2.2 RANGE OF VALIDITY OF THE MODEL In (73) a softness parameter σ was introduced, which measures the relative initial variation of $\mathscr{I}$ with respect to J. This quantity, which is somewhat analogous to the "initial susceptibility" in ferromagnetism, is obtained from Equation 2.3 as

$$\sigma \equiv [\mathscr{I}^{-1}\, \mathrm{d}\mathscr{I}/\mathrm{d}J]_{J=0} = 1/2C\mathscr{I}_0^3. \qquad 2.4.$$

If one defines $r_J = \mathscr{I}_J/\mathscr{I}_0$ and divides Equation 2.3 by $\mathscr{I}_0^3$, one obtains

$$r_J^3 - r_J^2 = \sigma J(J+1). \qquad 2.5.$$

In the "adiabatic limit," i.e. for a perfect rotor, $\sigma = 0$, and hence $r_J = 1$. $R_J = E_J/E_2$ then becomes

$$R_J(\sigma = 0) = \tfrac{1}{6}J(J+1). \qquad 2.6.$$

On the other hand, as $\sigma \to \infty$

$$R_J(\sigma \to \infty) = [\tfrac{1}{6}J(J+1)]^{2/3}. \qquad 2.7.$$

In (73) this was taken as the lower limit of validity of the VMI model. From Equation 2.7 one deduces for this limit $R_4 = 2.23$. Figure 8 presents σ as a function of R_4 for the interval $2.23 \leqq R_4 \leqq \frac{10}{3}$. $\mathscr{I}_0$ vanishes at $R_4 = 2.23$.

2.3 PHYSICAL MEANING OF PARAMETERS Table 1 of (73) presents experimental values for $E_J(J = 0, 2, 4, \ldots)$ for 88 bands ranging from $A = 108$ to 248, which are compared with the energy values deduced from the VMI law by least-squares fitting. These bands span the range of R_4 from 2.3 to 3.33. For each nucleus the quantities

C, $\mathcal{I}_0$, σ, and $\mathcal{I}_J$ are listed. Figure 9 presents a projective view of $\mathcal{I}_0$ vs N and Z. It is seen that the nuclei nearest closed neutron shells have the smallest $\mathcal{I}_0$ values. As more neutrons and protons are added to closed shells, $\mathcal{I}_0$ rises first steeply and rather smoothly, then less steeply and reaches a peak value approximately at the center of the rectangle defined by $82 \leqq N \leqq 126$ and $50 \ll Z \leqq 82$.

There is, however, no complete particle-hole symmetry in $\mathcal{I}_0$. $\mathcal{I}_0$ does not fall off as steeply on approaching the closed shell at $N = 126$ as it rises above $N = 82$. A behavior of $\mathcal{I}_0$ similar to that in Pt is observed in the Hg ($Z = 80$) isotopes, whose g.s. bands have been studied only recently (74).

The rise in $\mathcal{I}_0$ with increasing number of extra-shell nucleons is further observed for the region $50 \leqq N \leqq 82$, $50 \ll Z \ll 82$, and for $N > 126$, $Z > 82$. It is clear from Figure 9 that the magnitude of $\mathcal{I}_0$ not only reflects the number of extra-shell nucleons, but also the polarization these bring about in the core. The maximum values of $\mathcal{I}_0$, for nuclei ranging from ^{12}C to the actinides, are roughly proportional to $A^{5/3}$.

In Figure 10, the stiffness parameter C is plotted vs A. This graph contains more up-to-date values and includes bands of spherical nuclei as defined in Section 1.

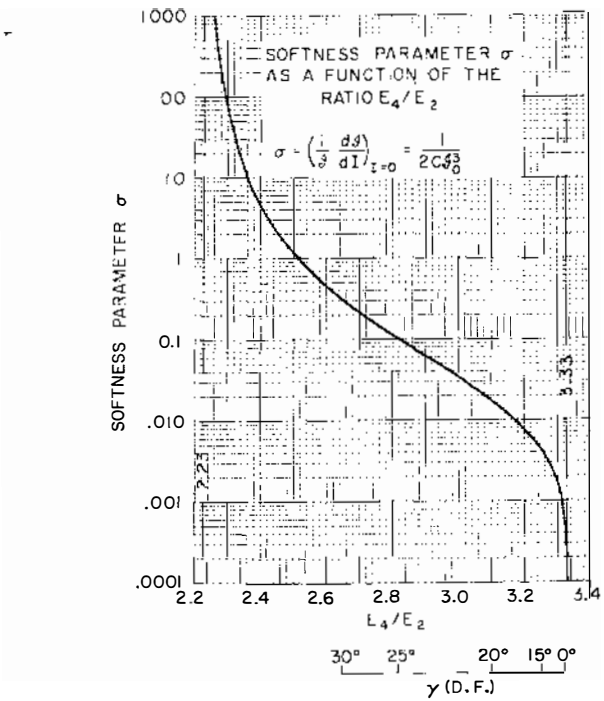

Figure 8 Softness parameter σ plotted vs R_4. (The angular momentum is denoted here by I.) Also shown are the corresponding values of the parameter γ according to the asymmetric model of Davydov & Filippov (59). [This figure was first published in (73).]

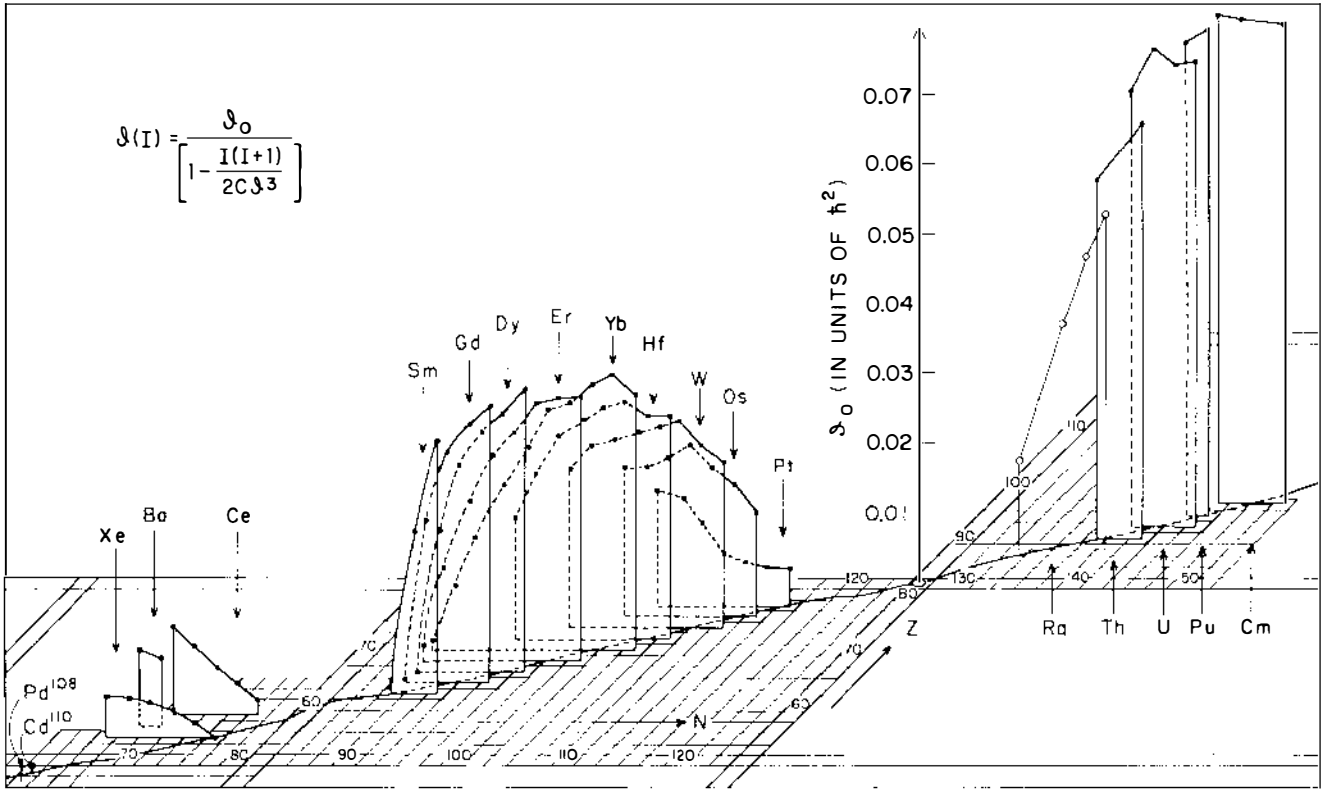

Figure 9 Three-dimensional diagram of $\mathcal{J}_0$ (computed from equations 2.1 and 2.3) vs N and Z. [This figure was first published in (73).]

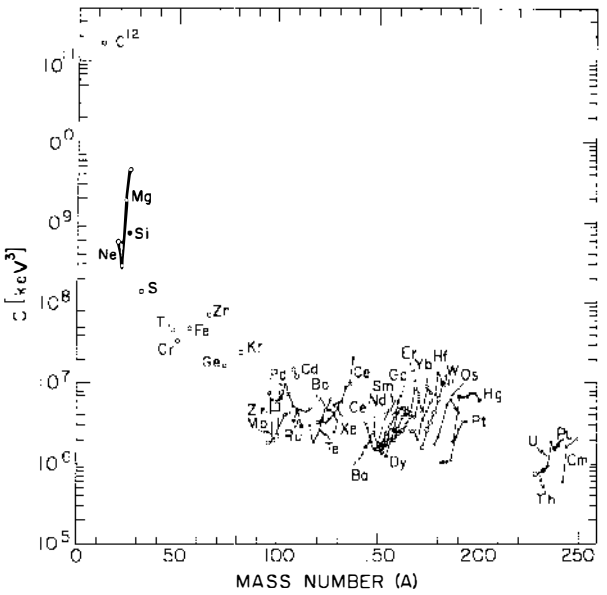

Figure 10 Stiffness parameter C as a function of A. Points for isotopes of the same element are connected by solid lines, which peak at the most stable nuclei.

The stiffness parameter decreases by approximately five orders of magnitude between the nucleus ^{12}C and the heaviest actinides, which, interestingly enough, decay spontaneously. The points for isotopes of the same element are connected by solid lines. For each element one observes a rise of C as the most stable isotope is approached, beyond which point a decrease occurs. It is of interest to note that for the region $82 \ll N \leqq 126$, $50 \leqq Z \ll 82$, the highest C value occurs for ^{180}Hf. As was mentioned in Section 1.7, this is the nucleus in which the first rotational band was discovered, and which showed very little deviation from $J(J+1)$. In the actinide region, one observes a correlation (75) between the maximum value of C for a given element and the longest spontaneous fission half-life.

2.4 EQUIVALENCE OF VMI MODEL WITH HARRIS'S CRANKING MODEL In (73) the equivalence of the VMI model with Harris's fourth-order cranking model is proven. This complete equivalence is best understood if we write the two sets of equations in the form given below.

$$\text{I.} \begin{cases} E = \mathbf{J}^2/2\mathscr{I} + C(\mathscr{I}-\mathscr{I}_0)^2/2, \\ \left(\dfrac{\partial E}{\partial \mathscr{I}}\right)_J = 0, \end{cases} \tag{2.8.}$$

$$\text{II.} \begin{cases} \dfrac{\mathrm{d}E}{\mathrm{d}\mathbf{J}} = \omega, \\ \text{with} \quad \mathbf{J}^2 = (\mathscr{I}\omega)^2 = J(J+1), \\ \text{and} \quad \mathscr{I} = \mathscr{I}_0 + \omega^2/2C. \end{cases} \tag{2.9.}$$

I) is here analogous to the Newtonian version, and (II), to the Hamilton's equation expression of the same physical model.

2.5 EXTENSION OF VMI MODEL TO NEGATIVE VALUES OF $\mathcal{I}_0$ An extension of the VMI model toward magic nuclei, in the spirit of the "Mallmann curves" (Figure 7), was arrived at (76) on the following grounds: inspection of Figure 9 reveals that $\mathcal{I}_0$ decreases steeply as the magic numbers are approached (e.g. in the rare-earth region as the neutron number decreases toward lower values), and tends to become negative before the magic number (e.g. $N = 82$) is reached. Also, R_J ratios for a number of ground-state bands with $R_4 < 2.23$ had just become available and could be compared with computed values. In general the agreement was found to be good (although not as precise as for higher R_4 values), and the parameters were shown to be physically meaningful. A definite contrast between the computed curves and the original Mallmann curves was found. While the latter (based on very scanty data) continued smoothly toward $R_4 = 1$, the "extension" stops at $R_4 = 1.82$. The solution of the problem is indicated in Figure 11, which presents the left side of Equation 2.5 as a function of $r = \mathcal{I}/\mathcal{I}_0$. The branch on the right corresponds to deformed nuclei for which $\mathcal{I}_0$, and therefore r, is positive; the left, negative, branch corresponds to nuclei for which $\mathcal{I}_0$ is negative. The right side of the equation corresponds to a set of horizontal lines for every value of σ. For the

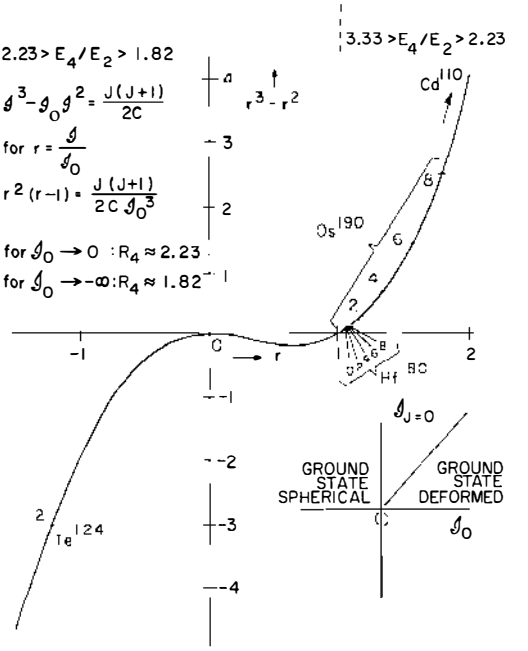

Figure 11 Left side of cubic equation $(r^3 - r^2)$ as function of $r(= \mathcal{I}/\mathcal{I}_0)$. The negative branch pertains to the extension of the VMI model. The inset at the lower right portrays the relation between ground state moment of inertia $\mathcal{I}_{J=0}$ and $\mathcal{I}_0$.

deformed branch, for $J = 0$, one obtains $r = 1$, i.e. $\mathcal{I} = \mathcal{I}_0$. For the spherical branch, however, $r_{J=0} = 0$ and hence $\mathcal{I}_{J=0} = 0$. The relation between the ground-state moment of inertia $\mathcal{I}_{J=0}$ and $\mathcal{I}_0$ is shown in the inset in the right lower part of the figure. The solution for the 2+ state of a nucleus (^{124}Te) with a spherical ground state is indicated on the left branch. On the right branch, r_J values for a good rotor (^{180}Hf) and a soft rotor (^{190}Os) are shown. No solution exists for $0 < r < 1$. This part of the cubic curve resembles the "Maxwell instability" in the van der Waals equation. Mariscotti (77) attempted to fit bands of closed shell nuclei, using two different roots of the cubic equation for the description of a single band with the transition from one root to the other between the ground state and the first excited state. In this treatment the angular momentum and the angular velocity assigned to the 2+ state have opposite sign, i.e. $\mathcal{I}(2)$ is negative.

We can now compare the increase of the moment of inertia for a "spherical" nucleus with increasing J, with that of deformed nuclei (Figure 12). One finds that for well-deformed, stable nuclei, e.g. for ^{180}Hf, $\mathcal{I}$ is almost constant as J increases. For nuclei with the *most* deformed ground states, namely those occurring approximately halfway between proton and neutron shells, one finds $\mathcal{I}_0 \propto A^{5/3}$. This relation does not hold, however, for the transition nuclei, as is immediately evident from the coincidence of the curves for ^{120}Xe ($Z = 54$, i.e. four protons beyond the closed shell) and ^{194}Pt ($Z = 78$, four proton holes). For these nuclei the moments of inertia increase steeply from their value at $J = 0$. The most dramatic relative increase of $\mathcal{I}$ with J, however, is found in nuclei with very small positive or with negative values of $\mathcal{I}_0$, e.g. ^{110}Cd and ^{120}Te ($R_4 = 1.99$).[9] The realization that nuclei with $R_4 \sim 2.23$ are extremely "soft" (73) removes the difficulties encountered by the simplest form of vibrational model (47) (which assumes a spherical equilibrium shape for all J), such as the appreciable static quadrupole moments of 2^+ states, (Section 1.13) and the smooth variation of Q_{02} (see Section 3) and of ratios of $B(E2)$'s in the transition from spherical to rotational. As was pointed out above, the parameter C, which determines the steepness of the "potential" $\frac{1}{2}C(\mathcal{I}-\mathcal{I}_0)^2$, is largest, in a given element, for the most stable nuclei. Even for stable isotopes, C takes on smaller values for Xe and Pt, which have relatively low-lying intrinsic odd-parity states, and also for the heavy elements, which have large symmetry energies.

2.6 LOWER LIMIT OF VALIDITY OF EXTENDED VMI MODEL This limit was deduced as follows: Equation 2.5 may be written in the form:

$$r^2(r-1) = -X, \qquad 2.10.$$

[9] For nuclei with $R_4 < 2.23$, the definition (2.4) of the softness parameter is not valid.

$\longrightarrow$

Figure 12 Using Equations 2.1 and 2.3, moments of inertia $\mathcal{I}(J)$ have been computed by least-squares fitting of the energies of ground-state-band levels. Some representative examples of rotational bands (^{180}Hf, ^{170}Hf, ^{238}U, ^{242}Cm, ^{248}Cm); bands in transition nuclei (^{120}Xe, ^{194}Pt); and "vibrational" bands (^{110}Cd, ^{120}Te) are shown. Values for the stiffness parameter C in units of 10^6 keV^3 are given in parentheses. This figure was first published in (76).

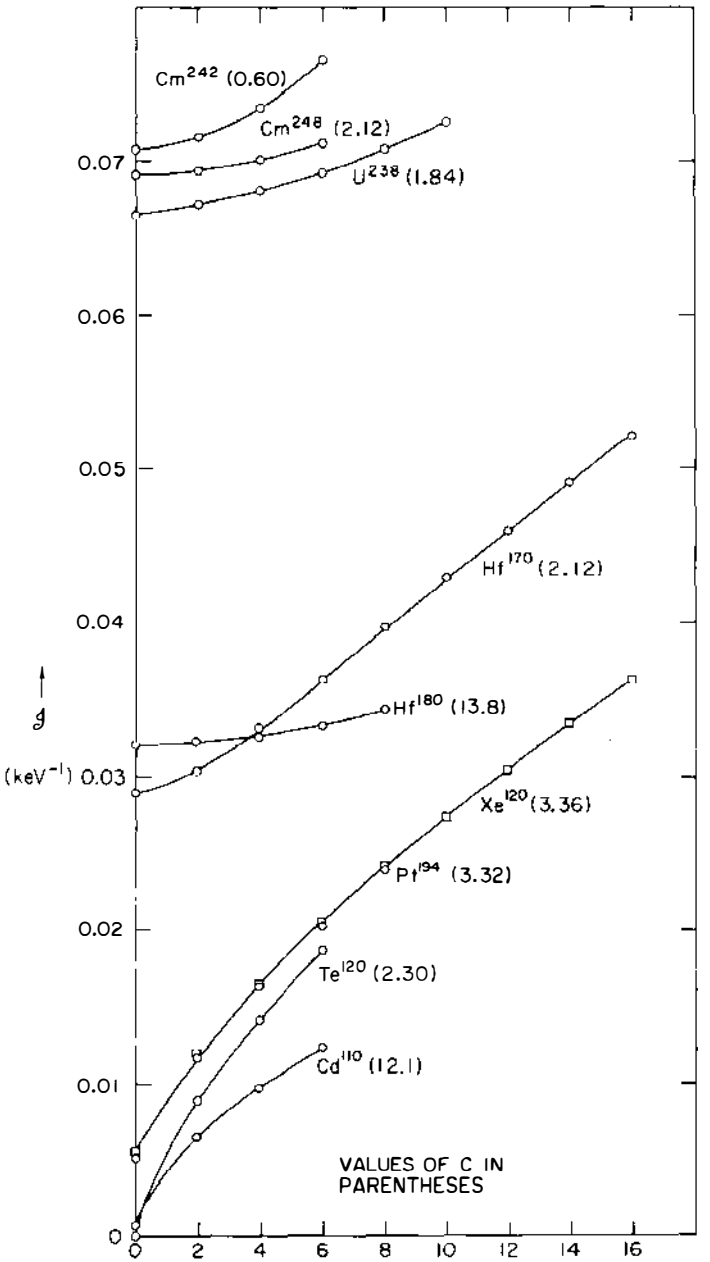

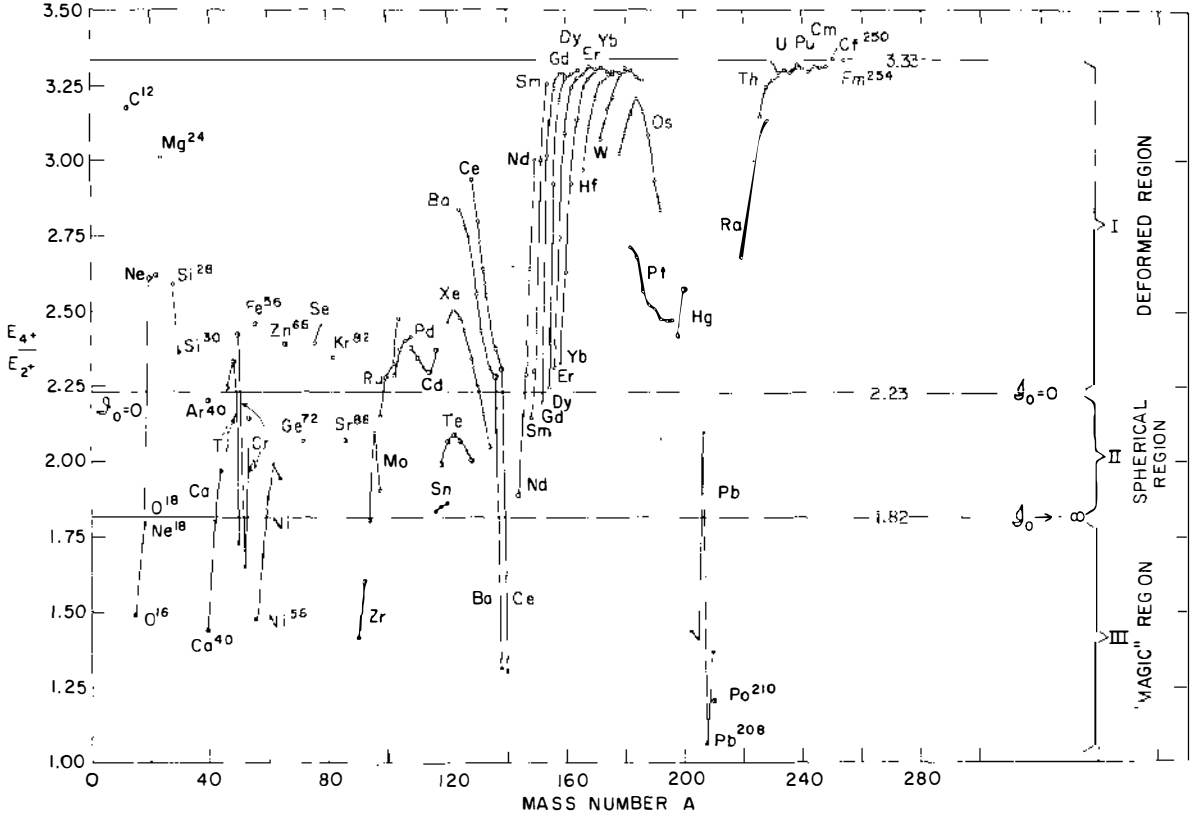

Figure 13 Empirical values of E_4/E_2 as a function of A. Points for isotopes of the same element are connected by solid lines. The horizontal line at 3.33 indicates the perfect rotor limit. The line at 2.23 divides the deformed from the spherical region. At this value the

with

$$r = \mathcal{I}/\mathcal{I}_0;\ X = |J(J+1)/2C\mathcal{I}_0^3|.$$

For $r \neq 0$ one can write $r = 1 - X/r^2$ and find graphic solutions for r by plotting each side of the equation separately. For all $X > 0$ there is one real negative root that goes smoothly from $r \approx -(X)^{1/3}$ to $r \approx -(X)^{1/2}$ as X goes from large to small values. For this region one finds $\mathcal{I}_{J=0} = 0$ and therefore, according to Equation 2.1, $E_0 = \frac{1}{2}C\mathcal{I}_0^2$.[10] The limiting value for R_4 is again 2.23 as $\mathcal{I}_0 \to 0$. For large negative $\mathcal{I}_0$ one obtains $R_4 \to (20/6)^{1/2} = 1.82$.

Figure 13 presents the ratio R_4 as a function of A. The interval $2.23 < R_4 < 3.33$ is denoted as the deformed region, the interval $1.82 < R_4 < 2.23$ as the spherical region, and the interval $1 < R_4 < 1.82$, which contains only singly and doubly magic nuclei, as the magic region. In the deformed region the ground-state moment of inertia is $\mathcal{I}_{J=0} = \mathcal{I}_0$, while in the spherical region, as mentioned above, $\mathcal{I}_{J=0}$ vanishes. This means that as $\mathcal{I}_0$ changes sign, $\partial\mathcal{I}_{J=0}/\partial\mathcal{I}_0$ has a discontinuity, which is reminiscent of a second-order phase transition. Negative values for $\mathcal{I}_0$ require the introduction of a new physical concept into the model. This is the notion of "increased resistance to departure from spherical symmetry:" The larger the negative value of $\mathcal{I}_0$, the more firmly the nucleus resists cranking.

2.7 COMPARISON OF EXTENSION OF VMI MODEL WITH EMPIRICAL VALUES In Figure 14 the established experimental values for R_6 and R_8 are plotted against R_4. Included are all cases with $R_4 < 2.23$ in which γ-ray cascades had been observed, including ^{50}Ti, ^{52}Cr, and ^{90}Zr, whose levels are known from studies of radioactive decay. The solid curves extend the predictions of the VMI model to the spherical region. The experimental points lie along two branches: The first or VMI branch extends leftward from the deformed region. *The points on this branch are well fitted by the extended VMI model and terminate precisely at $R_4 = 1.8$, the natural limit of the model.* The nuclei on this branch in the spherical region are never more than four nucleons from singly magic. The second or magic branch extends to the right from $R_4 = 1$ and consists entirely of doubly and singly magic nuclei for $R_4 < 1.82$.

2.8 THE VMI PHASE Figure 15 presents R_J ratios vs R_4 for the whole region of validity of the VMI model, and for magic nuclei. The solid lines are computed from Equations 2.1 and 2.3. Ratios for light nuclei are indicated by bold symbols. Although they deviate more from the solid lines than the ratios for heavier ($A \gtrsim 90$) nuclei, they exhibit the same general behavior. This figure was prepared in 1972. In the meantime, ground-state bands have been populated to $J = 22$, and perhaps 24 (in ^{238}U). At high-J states deviations from the VMI ratios have been observed, usually in the direction of smaller energy spacings, i.e. larger moments of inertia. While in some of the ground-state bands the deviations set in gradually, in others they occur abruptly. In the latter case they recalled the "phase transitions" predicted by Mottelson & Valatin (46) at J_c, the "critical angular momentum," at which the

[10] Thieberger (78) proposed an ingenious hydrodynamic analog of the extended VMI model, which explains the meaning of this threshold energy in classical terms.

pairing energy for neutrons or protons suddenly decreases to a low value. Although strictly speaking the concept of phase transition is only applicable to a many-body system. one may define the region in the R_J–R_4 plane below J_c and between $R_4 = 1.82$ and 3.33 as the "VMI phase." J_c is highest at the highest R_4 values and decreases fairly gradually toward $R_4 = 1.82$.

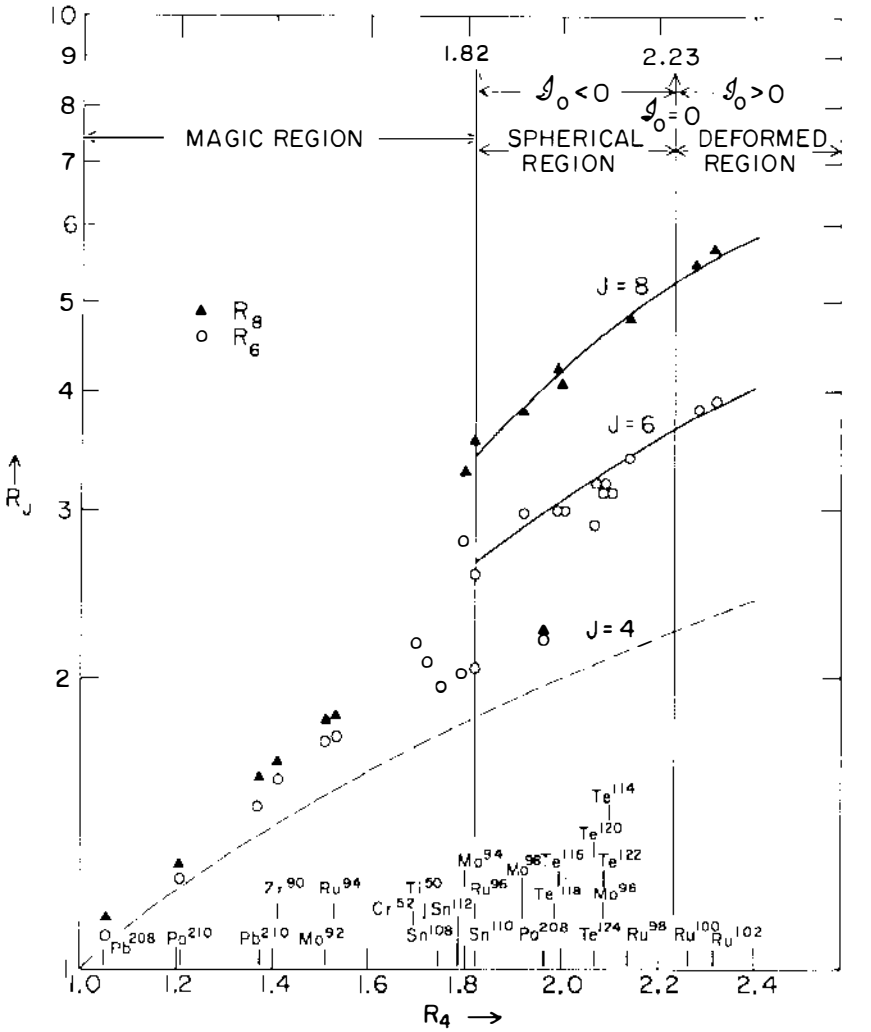

Figure 14 Ratios E_6/E_2 and E_8/E_2 (logarithmic scale) as functions of E_4/E_2 for the magic and spherical regions. The solid curves are computed from Equations 2.1 and 2.3. The dashed line indicates R_4. Only the beginning of the deformed region is shown. In the magic zone the R_4, R_6, and R_8 values are almost degenerate. In ^{208}Po ($R_4 = 1.96$), backbending occurs already above the 4+ state (see Section 4). This figure was reproduced from (76).

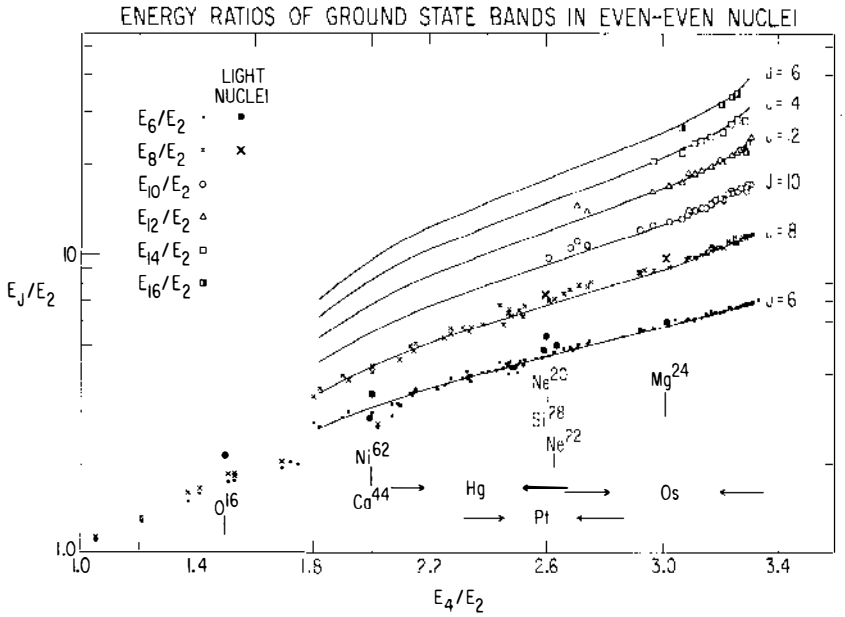

Figure 15 Energy ratios E_J/E_2 plotted vs E_4/E_2 for the whole range of validity of the VMI model: $1.82 \leqq E_4/E_2 \leqq 3.33$. Near the rotational limit, good agreement with the model predictions (*solid curves*) is found in many cases up to $J = 14$ or 16. For lower R_4 values deviations occur at lower J values. The range of isotopes of the transition elements Os and Pt are indicated by arrows. The Hg isotopes range from slightly deformed to spherical. Light isotopes are indicated by bold symbols. At the left ($E_4/E_2 < 1.82$), the almost degenerate 6+ and 8+ states of a number of singly or doubly magic nuclei are shown.

2.9 PROTON PARTICLE-HOLE ASYMMETRY IN R_4 AND DEVIATIONS FROM THE VMI MODEL

A striking asymmetry with respect to the $Z = 50$ shell has long been noticed (73), as seen in Figure 13. The R_4 values for the Cd ($Z = 48$) isotopes are above the line separating the deformed from the spherical region, while the values for the Te ($Z = 52$) isotopes lie below. Figure 16 presents more recent data of E_2 and R_4 for the isotopes of the elements $Z = 46$ (Pd), 48 (Cd), 50 (Sn), 52 (Te), and 54 (Xe), as functions of N. The E_2 and R_4 values for Pd and Xe are very similar, but the asymmetry between the two-proton (Te) and two-proton hole nuclei (Cd) appear here to be even more dramatic (79). The non-magic nucleus ^{132}Te ($N = 80$) even violates the rule that only magic nuclei have $R_4 < 1.82$. In Figure 17, the R_6 and R_8 values for Cd and Te are compared with the VMI predictions. A deviation increasing with N is seen for the neutron-rich Te nuclei. This indicates that the phase transition occurs in these nuclei already between $J = 4$ and $J = 6$. The asymmetry has been tentatively attributed to a good overlap between the extra-shell proton pair and an $h_{11/2}$ neutron pair missing from the same major shell ($50 \rightarrow 82$). The deviation of the R_6 and R_8 values in ^{208}Po (Figure 14) appears to be caused by a similar effect.

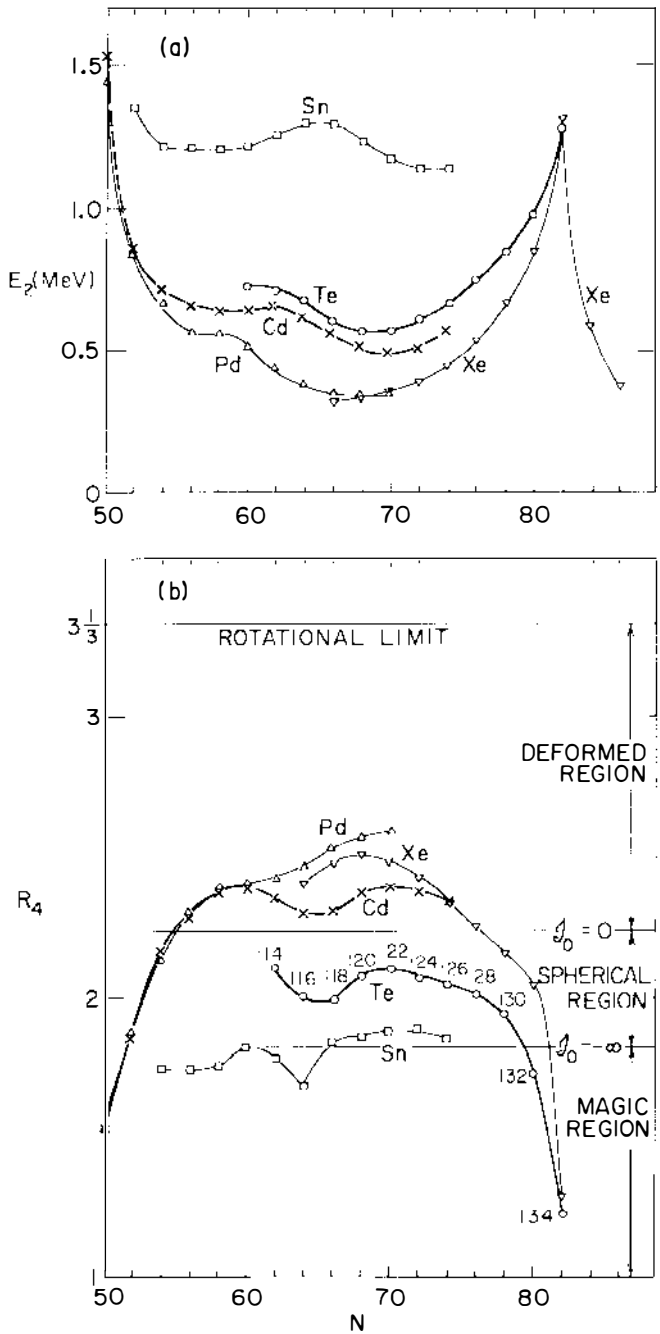

Figure 16 E_2 and R_4 values for $Z = 46$ (Pd), 48 (Cd), 50 (Sn), 52 (Te), and 54 (Xe) are plotted vs N in the top and bottom part of the figure, respectively (see text).

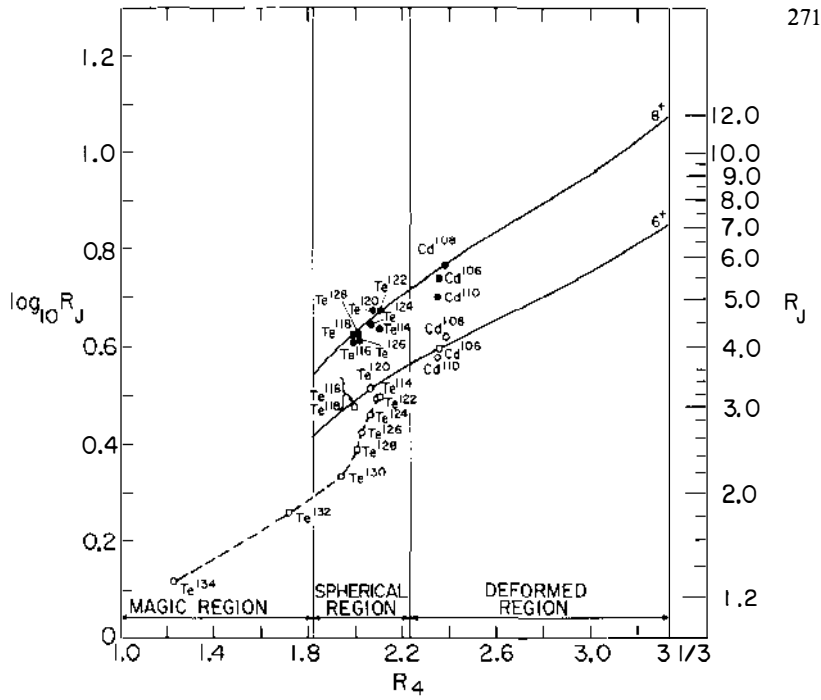

Figure 17 Log plot of R_J vs R_4. The R_J values for the neutron-rich Te nuclei deviate increasingly from the model predictions as $N = 82$ is approached i.e. backbending occurs already above the 4+ state.

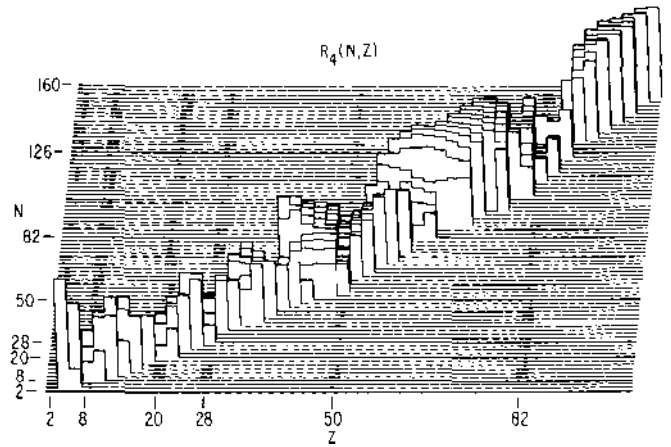

Figure 18 Three-dimensional presentation of R_4 vs N and Z. Magic numbers are indicated by heavier lines. Here R_4 ratios take on minimum values. The abrupt transition from spherical to rotational between 88 and 90 neutrons for $Z = 60$, 62, and 64 is clearly seen. For lower and higher Z values the transition is more gradual. (G.S.G. is indebted to I. K. Kopp for his assistance in the preparation of this figure.)

An interaction of neutrons and protons appears to be also responsible for the change from vibrational to rotational spectra in the rare-earth region. The three-dimensional presentation (Figure 18) of R_4 versus the number of neutrons and protons shows that the previously noted abruptness of the transition in equilibrium shape between 88 and 90 neutrons depends sensitively on the proton number. The transition becomes more gradual on the proton-deficient and proton-rich side of the valley of stability.

2.10 CORRESPONDENCE BETWEEN MODEL PARAMETERS C, $\mathcal{I}_0$, AND h, AND THE ENERGIES E_2 AND E_4 Figure 19 presents the relationship of the VMI model parameters and the energies E_2 and E_4. For a unified treatment of the VMI phase, it is advantageous to replace the softness parameter σ, which has a pole at $R_4 = 2.23$ (see Figure 8), by the "hardness parameter"

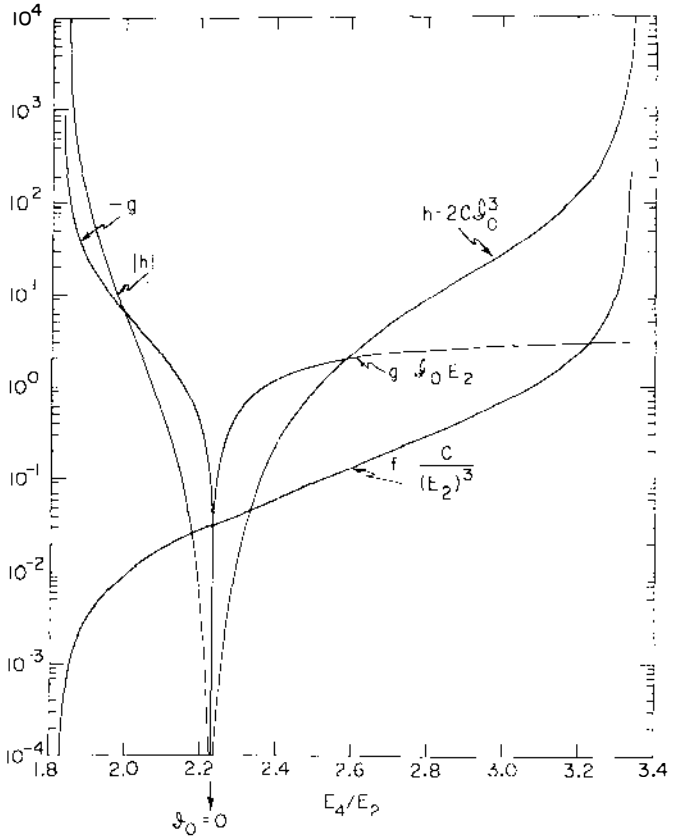

Figure 19 The functions $f = C/(E_2)^3$, $g = \mathcal{I}_0 E_2$, and $h = |2C\mathcal{I}_0^3|$ are plotted vs E_4/E_2. A plot of this type allows the determination of VMI energy values for $J > 4$ using Eq. 2.1. $\mathcal{I}_J$ values can be determined using Figure 11 and the value for h from this figure.

$$h = 1/\sigma = |2C\mathcal{I}_0^3|. \qquad 2.11.$$

For $\mathcal{I}_0 < 0$, the original definition given in Equation 2.4 does not hold; nevertheless the parameter provides a useful measure of the increasing resistance to departure from spherical symmetry as $\mathcal{I}_0$ approaches $-\infty$.

We note that starting from the rotational limit the function $g = \mathcal{I}_0 E_2$ falls off quite slowly until it approaches the spherical limit at 2.23. This behavior is responsible for the stability of $\mathcal{I}_0$ discussed in Section 7. The function $f = C/(E_2)^3$, on the other hand, varies by many orders of magnitude in the same region. The effect on the stiffness parameter C of this variation is partly compensated by the variation of $(E_2)^3$ in the opposite direction. Near the rotational limit, the variation of C is relatively unimportant, since there the contribution of the term $C/2(\mathcal{I} - \mathcal{I}_0)^2$ to the energy is very small. However, at lower R_4 values, a relatively small lack in precision of the measured energies can alter the value of C appreciably. Approximate graphical solutions of the VMI parameters for a given ground-state band can be obtained from Figure 19. With the value of $\sigma = 1/h$ so determined, $\mathcal{I}_J$ values may be deduced from Figure 11.

2.11 VMI FITS OF $K = 2$ BANDS IN EVEN-EVEN NUCLEI AND OF GROUND-STATE BANDS IN ODD-ODD NUCLEI Table 1 lists VMI parameters for $K = 2$ and ground-state bands in a deformed nucleus (^{166}Er) and a transitional nucleus (^{186}Os). For ^{166}Er the two sets of parameters are very similar; the $K = 2$ band is slightly more deformed and less soft. For this nucleus the excitation energy of the ground state of the $K = 2$ band $[E(2'+)]$ is 785.9 keV. The band in ^{186}Os, with $E(2'+) =$ 767.5 keV, could not be fitted well because of the odd-even staggering mentioned in Section 1.12. It is, however, less deformed and softer than the ground-state band.

Further compared in Table 1 are ground-state bands in two odd-odd nuclei, one well-deformed (^{164}Ho), and one transitional (^{194}Ir), with the ground-state bands

Table 1 Parameters of $K = 2$ bands of even-even nuclei and ground-state (g.s.) bands of odd-odd nuclei compared with those of ground-state bands of appropriate even-even nuclei. (This table is a reproduction of Table III in reference 73.)

Nucleus		$\mathcal{I}_0$	σ
$_{68}Er^{166}$	g.s.	0.0369	0.0024
	$K = 2$	0.0402	0.0021
$_{76}Os^{186}$	g.s.	0.0215	0.0082
	$K = 2$	0.0176	0.037
$_{67}Ho^{164}$		0.0539	0.000001
$_{66}Dy^{162}$		0.0369	0.0019
$_{77}Ir^{194}$		0.0200	0.071
$_{76}Os^{192}$		0.0124	0.091

of their even-even cores. It had previously been shown (80) that the moment of inertia of an odd-odd nucleus, which always appreciably exceeds that of the even-even core, is in agreement with the assumption that the experimentally determined contributions of the odd proton and that of the odd neutron may simply be added to the moment of inertia of the even-even core to obtain the moment of inertia of the odd-odd nucleus. It is seen from Table 1 that the deformed odd-odd nucleus ^{164}Ho is an almost perfect rotor, and that also the transitional nucleus ^{194}Ir is more deformed and less soft than ^{192}Os.

2.12 MODIFICATIONS OF THE VMI FORMALISM, HIGHER-ORDER CORRECTIONS, AND THEORETICAL JUSTIFICATIONS Since the VMI model had been shown to fit ground-state bands of a wide range of even-even nuclei, numerous attempts have been made to improve the fits even further, either by using different expressions or higher terms in the angular velocity expansion. Among the latter the lucid and thorough study by Saethre et al (81) stands out. It is dealt with in detail in Sections 5 and 7. Also, both macroscopic and microscopic models have been

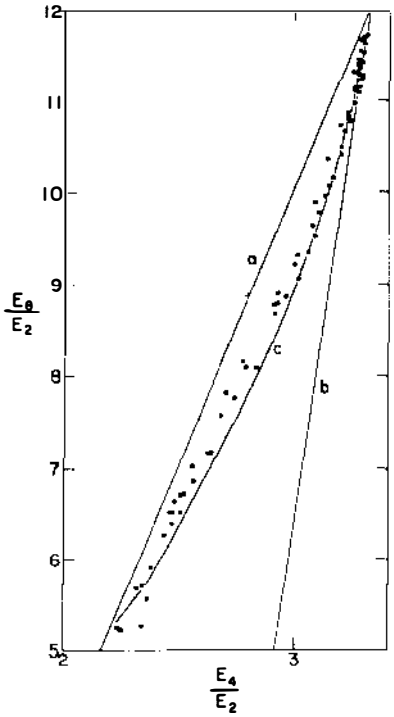

Figure 20 E_8/E_2 is plotted vs E_4/E_2. The solid curves correspond to predictions from (*a*) the Ejiri formula $E_J = \frac{1}{8}J(J-2)E_4/E_2 - \frac{1}{4}J(J-4)$, which is identical with the prediction from the anharmonic vibrational model; (*b*) the Bohr-Mottelson two-term expansion in $J(J+1)$; and (*c*) the VMI model. The figure is reproduced from (83).

proposed in order to explain the observed regularities (Sections 6–8). We wish to discuss here only two energy expressions frequently used by experimentalists for the analysis of their data. The first one is the expansion of E in terms of $J(J+1)$. The second one is a phenomenological expression suggested by Ejiri et al (82), which has the form

$$E_J = aJ + k[J(J+1)]. \qquad 2.12.$$

From Equation 2.12 one obtains the ratios R_J in terms of R_4:

$$R_J = \tfrac{1}{8}J(J-2)R_4 - \tfrac{1}{4}J(J-4). \qquad 2.13.$$

Das, Dreizler & Klein (83), who attempted to fit bands in the "spherical" region by means of an anharmonic vibrational model, arrived at an expression similar to Equation 2.12, except for an additional cubic term in J. These authors then compared three model predictions for R_6 and R_8 as functions of R_4 with the experimental values. Figure 20 presents these comparisons for R_8. Curve a corresponds to Equation 2.13, curve b to the two-term expansion in $J(J+1)$, and curve c to the VMI model. It is evident that b diverges close to the rotational region, as Mallmann had already pointed out, and that c gives a better overall fit for the whole region than curve a, except for $R_4 \approx 2$, where curves a and c give equally good fits.

The Ejiri formalism continues smoothly toward $R_4 = 1$. In the interval between $R_4 = 2$ and $R_4 = 1.5$ the higher states ($J \geqq 6$) go below the 4+ state; at $R_4 = 1.33$ they become degenerate with the 2+ state; finally, as $R_4 \to 1$, they approach $E = 0$. This inverted order of states has not been observed.

2.13 RELATIONSBETWEEN $E_{2'}/E_2$, $B(E2)(2' \to 2)/B(E2)(2 \to 0)$, AND R_4 For the ideal vibrational nucleus, the enhancement of the transition from the two-phonon state to the one-phonon state is predicted to be twice that from the one-phonon state to the ground state. However, most measured ratios were found to be somewhat smaller than two. The VMI model makes it possible to study the ratio of reduced transition probabilities as a function of the softness parameter σ. First studied (73) was the ratio $[B(E2)(2' \to 2)]/[B(E2)(2 \to 0)]$, which provides a measure of the coupling between the quasi-γ band and the ground-state band. Since σ is a monotonic function of R_4 (Figure 8), the ratio of reduced transition probabilities has been correlated with R_4, (Figure 11, *bottom*). The top part of Figure 21 presents, on a logarithmic scale, the ratio between the ground-state energy E_2' of the quasi-γ band and the energy E_2. This ratio, of the order of 10 at the rotational limit, rapidly decreases and soon approaches the value ~ 2, which corresponds to the ideal vibrator. In the bottom part, the open circles at $R_4 = 10/3$ and 2 indicate the theoretical predictions ($\ll 1$ and 2) for the rotational and vibrational limits. Starting from the rotational limit, the experimental points lie on a straight line corresponding to the equation:

$$\frac{B(E2)(2' \to 2)}{B(E2)(2 \to 0)} = 5 - \frac{3}{2}R_4. \qquad 2.14.$$

Near the vibrational limit, the statistical errors of the experimental points are

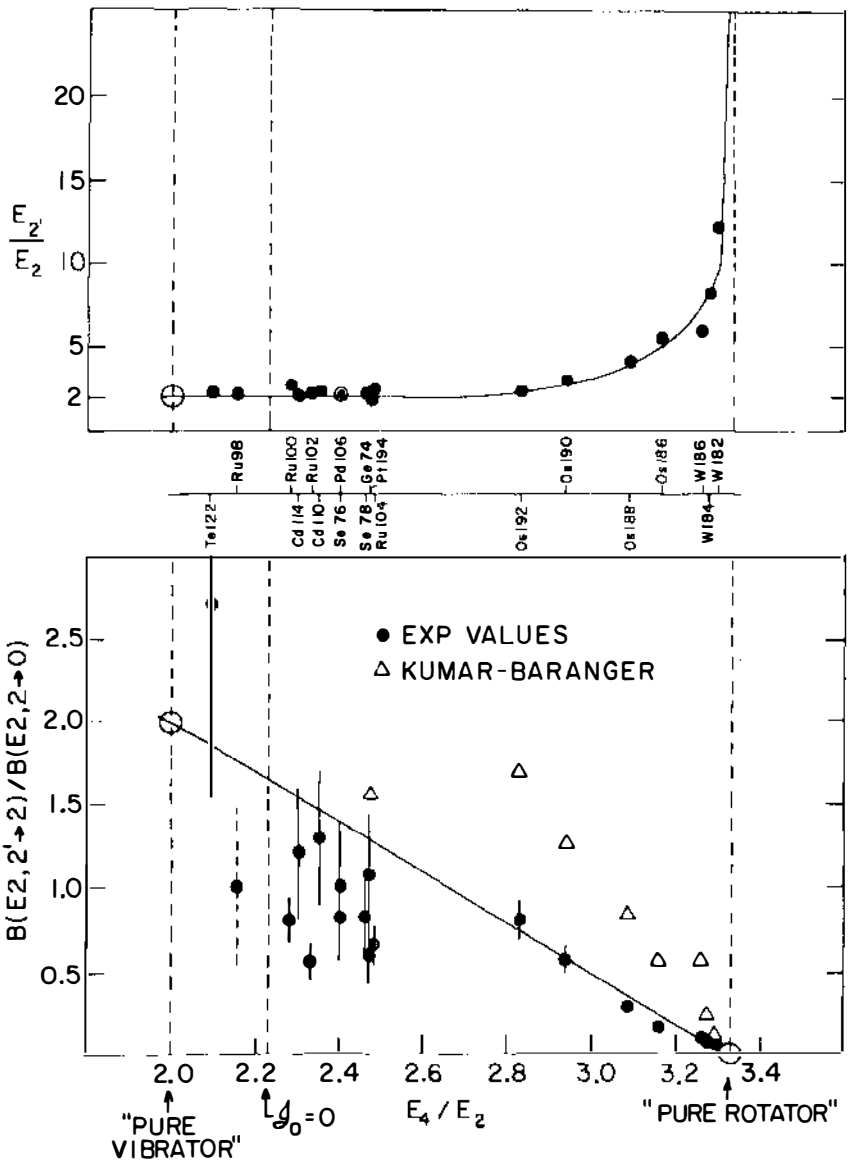

Figure 21 This figure displays the coupling strength of the quasi-gamma band to the ground-state band vs E_4/E_2. The top part shows a logarithmic plot of the ratio of the energy $E_{2'}$ (ground state of the quasi-gamma band) to E_2. In the bottom part the ratio of the $B(E2)$ values for the transitions $2' \rightarrow 2$ to $2 \rightarrow 0$ are presented. The straight line connects the limiting values 2 for $E_4/E_2 = 2$ and $\ll 1$ for $E_4/E_2 = 3.33$. The triangles give Kumar & Baranger's theoretical predictions. This figure is reproduced from (73).

considerably larger. However, with one exception (^{122}Te), there appears to be a tendency for the ratios to fall below the straight line. The regularity exhibited by the experimental points contrasts with the values predicted by the pairing-plus-quadrupole model indicated by triangles. Further experimental and theoretical investigation of the relation of the enhancement ratios, including also the 0+ and 4+ states of the two-phonon triplet, would be of great value.

3 *Relation Between Moment of Inertia and Transition Quadrupole Moment*

3.1 DEPENDENCE OF RELATION BETWEEN $\mathcal{I}$ AND Q ON A AND Z In Section 1.8 we have seen that the hydrodynamical model predicted a relation between these two quantities of the form

$$\mathcal{I} \propto Q_0^2 A^{1/3}/Z^2. \tag{3.1}$$

Here $\mathcal{I}$, in units of $\hbar^2$, was taken to be $\mathcal{I} = 3/E_2$. The mass range covered by Sunyar (35) was not extensive enough to allow any definite conclusion on the validity of the A dependence. Grodzins (84) later compared the A and Z dependence of $E_2 \times B(E2)$ for a much larger range of even-even nuclei, namely $12 \leqq A \leqq 240$, with empirical data and found a deviation of the A dependence from the hydrodynamical prediction. He proposed for all but a few exceptions adjacent to doubly magic nuclei, the formula

$$1/E_2 \propto B(E2)A/Z^2, \tag{3.2}$$

whereas, as he pointed out, the A and Z dependence predicted by the hydrodynamical model (Equation 3.1) as well as by the asymmetric nucleus model (59) and also by the vibrational model (47), is $A^{1/3}/Z^2$. However, for the latter the constant of proportionality is almost three times larger than for a deformed nucleus. Thus an abrupt change would have been expected to occur between 88 and 90 neutrons, but none was found.

3.2 DEPENDENCE OF $\mathcal{I}$ ON Q IN THE VMI MODEL The VMI model attributes a moment of inertia $\mathcal{I}(J)$ to each state of the ground-state band. We define an "average" moment of inertia $\mathcal{I}_{02} = \frac{1}{2}[\mathcal{I}(0)+\mathcal{I}(2)]$, which may be related to the transition quadrupole moment $Q_{02} = [(16\pi/5)B(E2)(0 \rightarrow 2)]^{1/2}$ for all non-magic even-even nuclei. [It should be kept in mind that in contrast to the previous approaches where $\mathcal{I} \propto 1/E_2$, both $\mathcal{I}(0)$ and $\mathcal{I}(2)$ are deduced from the spectrum of the ground-state band, i.e. from E_2 *and* E_4.]

A study (73) covering the range $120 < A < 186$ resulted in the relation

$$\mathcal{I}_{02} = Q_{02}^2/k^2, \tag{3.3}$$

where $k = (39.4 \pm 2.6) \times 10^{-24}$ cm^2 keV$^{1/2}$ is *independent* of A.

After the extension of the VMI model to negative values of $\mathcal{I}_0$, it was possible to correlate data for nuclei with spherical ground states as well as for deformed nuclei. Moreover, light nuclei were included in the survey, which covered a range $12 \leqq A \leqq 252$.

Figure 22 shows a log-log plot of $\mathcal{I}_{02}$ vs Q_{02} (85, 86), based on recent literature values. It is at once apparent that a strong correlation between the two quantities exists over the whole range of transition quadrupole moments. Closer analysis reveals a strong dependence on shell structure, as is shown presently. (Figure 23 is identical to Figure 22, with the exception of the nuclear symbols.) The plot resembles a sea horse, consisting of three distinct parts:

1. In the "tail," where the $(Q, \mathcal{I})$ values are very small and the points refer to nuclei that possess only one or two neutron or proton pairs (particles or holes) beyond a closed shell. These are either light deformed nuclei or heavier "spherical" nuclei. In this region $\mathcal{I}$ is approximately proportional to Q.
2. The "main body" corresponds to larger $(Q, \mathcal{I})$ values, pertaining to nuclei with several neutron and proton pairs beyond closed shells, i.e. nuclei in the transition and strongly deformed regions. Here $\mathcal{I}$ is proportional to Q^2, as was stated above.

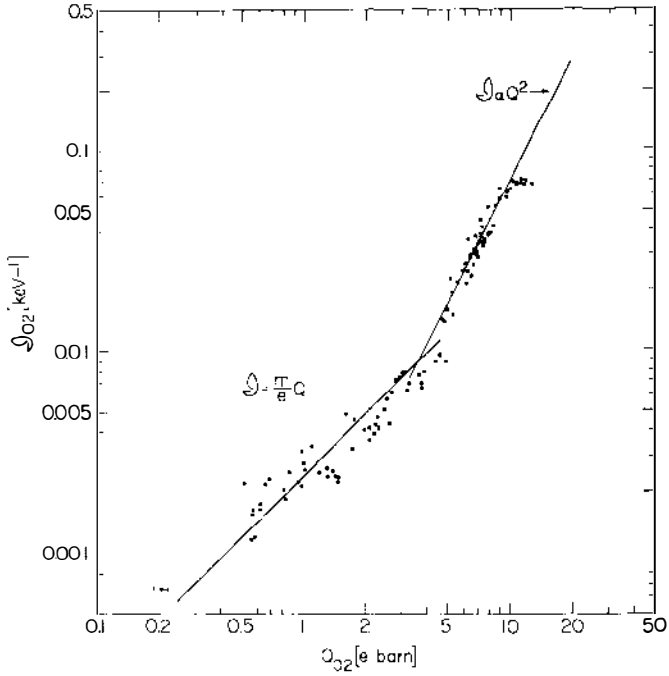

Figure 22 Log-log plot of the average moment of inertia $\mathcal{I}_{02} = [\mathcal{I}(0)+\mathcal{I}(2)]/^2$ vs the transition quadrupole moment Q_{02}. A linear part and a quadratic part can be clearly distinguished. The horizontal part for the highest $\mathcal{I}-Q$ values refer to spontaneously fissioning actinides. The linear part is interpreted by the alpha-particle dumbbell model, the quadratic part by a macroscopic two-fluid model.

3. The "head" consists of the very largest $(Q, \mathcal{I})$ values found for the heaviest actinides $[U(A \geqq 234), \mathrm{Pu}, \mathrm{Cm}, \mathrm{Cf}]$ (87). Here $\mathcal{I}$ is roughly constant, while Q continues to increase. All nuclei in this region fission spontaneously.

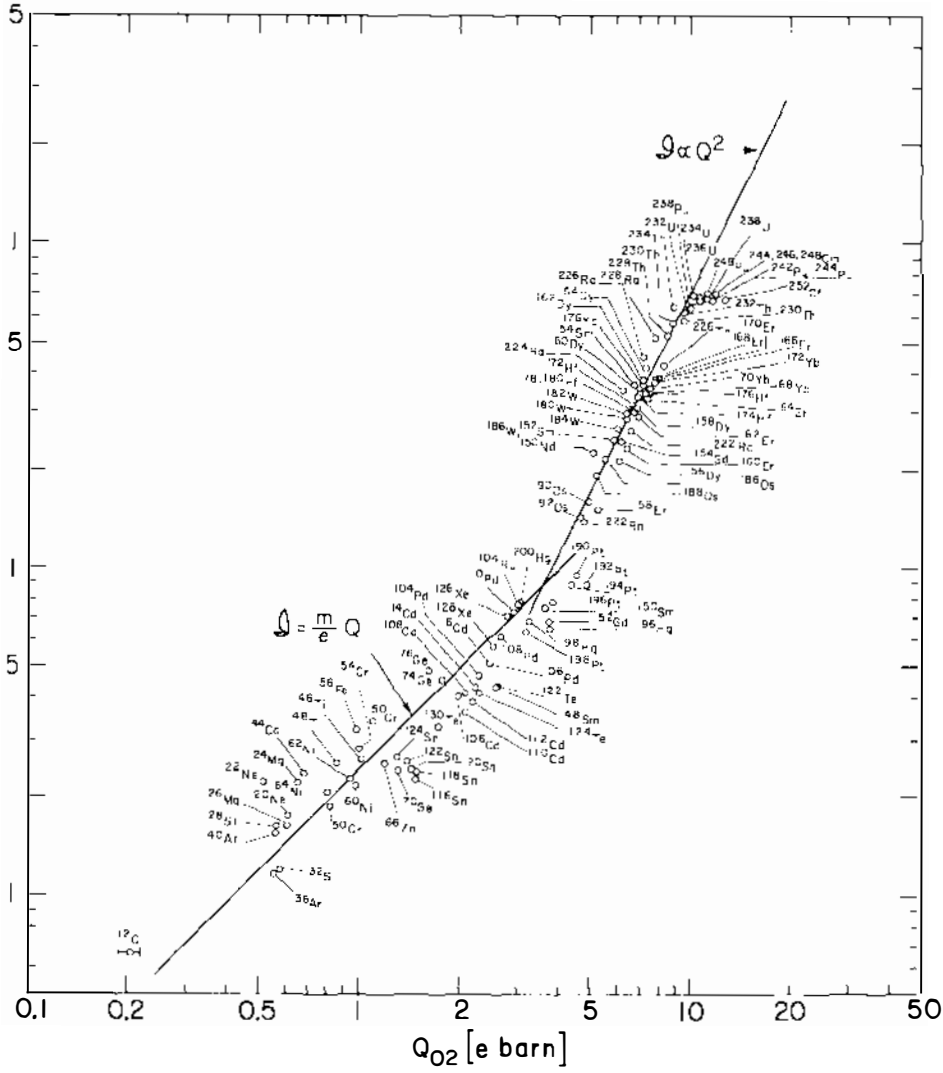

Figure 23 Same as Figure 22, with nuclear symbols added. The linear part consists of nuclei with one or two extra-shell nucleon pairs of one kind. It includes both light deformed nuclei and heavier spherical nuclei. The quadratic part corresponds to the deformed nuclei in the rare-earth and actinide regions.

3.3 THE ALPHA-PARTICLE DUMBBELL MODEL The straight line traced through the *tail* (Figure 23) is given by a dumbbell model.

$$\begin{aligned} \mathcal{I} &= 2M_\alpha R^2 \approx 2.4 \times 10^{-4} A^{2/3}\ (\text{keV})^{-1}, \\ Q &= 4\, e_\alpha R^2 \approx 9.6 \times 10^{-2}\, A^{2/3}\ (e\ 10^{-24}\ \text{cm}^2), \\ R &= 1.1\, A^{1/3}\ \text{fm}, \\ Q/\mathcal{I} &= 415\ (e\ 10^{-24}\ \text{cm}^2\ \text{keV}). \end{aligned} \qquad 3.4$$

In this expression R is the half-density radius of the nucleus. The naive picture is one of two alpha particles connected by a massless rod, whose length is equal to the nuclear half-density diameter.

3.4 MACROSCOPIC TWO-FLUID MODEL FOR DEFORMED NUCLEI The $\mathcal{I} \propto Q^2$ rule which covers a wide range of deformations, has so far not found a microscopic explanation. However, one possible derivation of the rule follows from a macroscopic two-fluid model, based on the assumption that a nucleus governed by this rule is deformed into a spheroid characterized by a single significant deformation parameter ε. We assume that the spheroidal nuclear potential acts as a "bucket;" rotating the bucket causes some of the material to be dragged along, while part of the material is in a superfluid state (due to the pairing force), and therefore is not dragged along.

We assume that at every point in the nucleus the local mass density ρ is the sum of the superfluid mass density, which does not participate in the rotation, and an inertial density ρ_{in}, which does participate as in normal rigid rotation. The ratio $f = \rho_{\text{in}}/\rho$ is assumed to be a constant, independent of position in the nucleus. This constant is determined according to the relation

$$f = \xi \int \mathrm{d}^3 r [\rho(\mathbf{r}) - \bar{\rho}(\mathbf{r})]^2/\rho(0); \qquad 3.5$$

where ξ is a dimensionless constant determined by fitting with experiment $\bar{\rho}(r) = (1/2\pi) \int \mathrm{d}\varphi \rho(r)$, and the azimuthal integration over φ is about the axis of rotation of the nuclear spheroid perpendicular to the axis of symmetry. It is at once evident that $\mathcal{I} = f \mathcal{I}_{\text{rigid}}$ and that the fraction f vanishes if the deformation vanishes. Since we have $f \propto \varepsilon^2$ to first order, we get $\mathcal{I} \propto Q^2$ if we assume that $Q \propto \varepsilon$.

It was assumed that the neutrons and protons are both distributed according to the same deformed Woods-Saxon function

$$\rho(\mathbf{r}) = \rho_0 / \{1 + \exp[r - R(1 + \varepsilon P_2(\cos\Theta)]/a\}, \qquad 3.6$$

with $\int \mathrm{d}^3 r \rho(r) = A$, and $a = 0.5$ fm.

In Figure 24 the experimental results for $\mathcal{I}$ vs Q^2 (*open circles*) are compared with the model predictions (*solid circles*). Excellent agreement is obtained with $\xi = \frac{1}{20}$, *independent* of A, up to and including ^{232}U.

3.5 DEVIATION FROM THE TWO-FLUID MODEL PREDICTION FOR SPONTANEOUSLY FISSIONING ACTINIDES The sudden deviation for the heaviest actinides is not explained by the model. One would have expected the $\mathcal{I}$ vs Q^2 curve to fall below

the model predictions as $\mathcal{I}$ approached the rigid-body value, which is a natural limit, but the actual departure is much more striking than such considerations would suggest. Several possible causes for the departure come to mind. The large hexadecapole moments occurring in this region (87), the near degeneracy of prolate and oblate valence-shell orbits (which might be responsible for the constancy of the 2+ state and 4+ state energies of the heaviest actinide nuclei) (88, 89), or the possibility that due to the Coulomb repulsion the protons might be slightly more concentrated near the poles of these most elongated nuclei than the neutrons.

3.6 THE $\mathcal{I}$ VS Q RELATION FOR HIGHER TRANSITIONS A study of the $\mathcal{I}$ vs Q relation for higher transitions in the band would be desirable. Here $Q_{J\to J+2}$ is related to $B(E2)(J \to J+2)$ by

$$Q^2_{J\to J+2} = \frac{32\pi(2J+3)(2J+5)}{15(J+1)(J+2)(2J+1)} B(E2)(J \to J+2). \qquad 3.7.$$

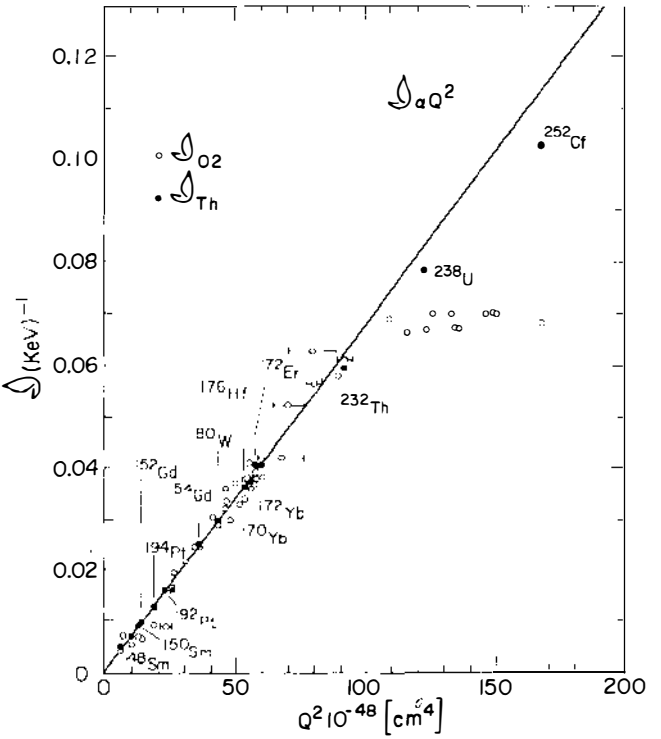

Figure 24 Linear plot of $\mathcal{I}_{02}$ vs Q^2_{02}. Predictions from the two-fluid model are shown by solid circles, empirical values by open circles. The straight line corresponds to $\mathcal{I}_{02} = (1/k^2)Q^2_{02}$. The Q^2_{02} values for the heaviest actinide nuclei increase by almost 50%, while the $\mathcal{I}_{02}$ values remain approximately constant.

For strongly deformed nuclei a preliminary survey shows that the $\mathcal{I} \propto Q^2$ relation still holds for $2+ \rightarrow 4+$ transitions. For the $4+ \rightarrow 6+$ transitions one finds that the empirical $\mathcal{I}$ values fall above the predicted ones by $\sim 10\%$, for $6+ \rightarrow 8+$ transitions by $\sim 20\%$. For transitional nuclei this lag appears to become more pronounced. Very few $B(E2)$ values are so far known for $(2+ \rightarrow 4+)$ transitions in the vibrational region.

4 *Transitions from the VMI Phase*

4.1 THE $\mathcal{I}$ VS ω^2 PLOT According to Equation 2.9,

$$\mathcal{I} = \mathcal{I}_0 + \omega^2/2C. \qquad 4.1.$$

Measured transition energies within a ground-state band presented in this form yield a very sensitive criterion for deviations from the Harris-VMI model predictions. (For convenience Equation 4.1 is multiplied by 2.) For a transition $J \rightarrow J-2$ the ordinate is given by

$$2\mathcal{I} = \frac{\Delta(J(J+1))_{J \rightarrow J-2}}{\Delta E_{J \rightarrow J-2}} = \frac{4J-2}{\Delta E_{J \rightarrow J-2}} \qquad 4.2.$$

and the abscissa by

$$\omega^2 = \left[\frac{\Delta E_{J \rightarrow J-2}}{[J(J+1)]^{1/2} - [(J-2)(J-1)]^{1/2}} \right]^2. \qquad 4.3.$$

According to Equations 4.2 and 4.3, the initial part of the curve consists of an almost straight line, which usually curves slightly upward. Were the quantities plotted differentials instead of energy differences, the line would be perfectly straight. The intercept at $\omega^2 = 0$ is $2\mathcal{I}_0$ and the initial slope is $1/C$.

4.2 PHASE TRANSITIONS IN DEFORMED AND SPHERICAL NUCLEI By the use of heavier ions as bombarding particles, ground-state bands have been populated during recent years to very high J states. The results have been compiled in various articles and reviews (41, 66, 81). The most extensive compilation (66) ranges from ^{72}Se to ^{242}Pu. It includes near-magic, vibrational, and strongly deformed nuclei. As the magic-number limit is approached, the slope becomes increasingly steeper. The shapes of the $\mathcal{I}$ vs ω^2 curves after deviation from VMI are varied: besides "backbending," i.e. a triple-valued curve in ω^2, a more gradual increase, with ultimate flattening or even downbending has been observed. In Figure 25 we compare an $\mathcal{I}$ vs ω^2 plot for the deformed nucleus ^{158}Dy determined by Thieberger et al (90) up to $J = 22$, with an $\mathcal{I}$ vs ω^2 plot for the "vibrational" nucleus ^{104}Pd, whose ground-state band was populated by Cochavi et al (91) up to $J = 14$. For ^{158}Dy, $J_c = 14$, while for ^{104}Pd $J_c = 6$ or 8. However, the ω^2 value at which backbending takes place is higher for ^{104}Pd. For this nucleus, double backbending is observed. A systematic study of neutron-deficient even-even Pd nuclei (^{104}Pd$\rightarrow^{98}$Pd) revealed a bewildering number of cascades besides the ground-state band (92), especially in ^{102}Pd and ^{100}Pd. These cascades are frequently interconnected and they all terminate in states $J \geqq 2$ of the ground-state band. Among these cascades

quasi-rotational bands, of both odd and even parity, have been established. Iachello, partly in collaboration with Arima (93), has developed an interacting boson model, whose predictions were compared with results for these and other vibrational nuclei. Quadrupole and octopole bosons were considered.

While a number of features in the observed level schemes are in agreement with the model predictions, e.g. the general features of the odd-parity bands, it is too early to judge whether coupling of quasi-particles to quadrupole bosons do not yield equally good or better agreement. As is shown in Sections 6 and 7, the interactions between bands strongly affect the backbending behavior of the ground-state band.

4.3 HEURISTIC VALUE OF THE VMI MODEL FOR THE SPHERICAL REGION In Section 2.9 we discussed a deviation from VMI predictions occurring in the neutron-rich Te nuclei, which implies $J_c = 4$. This phenomenon was attributed to strong overlap of a proton pair with a neutron pair, i.e. α clustering.

In Figure 14, which presents R_J vs R_4 values for $1.82 < R_4 \leqq 2.23$, more scatter of the empirical values is observed than for the deformed region (Figure 15). In

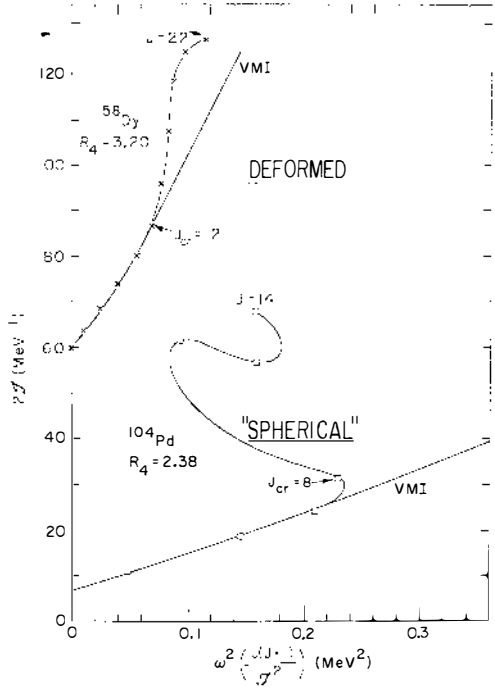

Figure 25 Comparison between an $\mathcal{I}$ vs ω^2 plot for a neutron-deficient rotor (^{158}Dy); [E_2 = 98.94 keV; C = 2.64 (10^6 keV^3)] with that of a "vibrator" (^{104}Pd): [E_2 = 555.8 keV; C = 10.23 (10^6 keV^3)]. The VMI predictions are shown by solid lines. For the rotor J_c = 12, while for the vibrator J_c = 6 or 8.

the case of the Te nuclei (not included in Figure 14), instead of the scatter, one finds with increasing N an increasing but regular deviation from the R_6 curve (Figure 17). It appears that as more nuclei in this region are studied, regularities in the deviations from the VMI model are observed. This kind of "fine structure" may also be connected with α clustering. This, in turn, appears to throw an interesting light on the relation between $\mathcal{I}_{02}$ and Q_{02} found for the spherical region (Section 3.3), which agrees so well with a naive alpha dumbbell model plus a superfluid core.

4.4 VMI BEHAVIOR OF QUASI-ROTATIONAL BANDS IN ODD-A NUCLEI In this review we have limited our attention to the structure of even-even nuclei. However, it is worth mentioning that excellent fits were obtained for quasi-rotational bands in odd-A nuclei, based on the assumption that the even-even core obeys the VMI law. Such calculations were carried out both for spheroidal (94) and for triaxial (95) nuclei.

5 *Phenomenological Generalizations of the VMI Model for the Low-Spin Region*

In the previous sections, the phenomenological basis for the VMI model has been reviewed. The success of the model led to a number of attempts to improve upon it phenomenologically or to provide it with a microscopic derivation. In this section, we discuss the VMI model in terms of a more general treatment of the low-spin region. We reserve for Section 6 a treatment of models for both the low-spin and backbending regions and defer the discussion of microscopic models to Sections 7 and 8.

As remarked by Harris and others (71, 96, 97), the energy E must satisfy the classical self-consistency condition

$$\frac{\partial E}{\partial \omega} = \omega \frac{\partial \langle J_x \rangle}{\partial \omega}, \qquad 5.1.$$

where x is the axis of rotation perpendicular to the symmetry axis. In analogy to the variational solution of the "cranking" problem, we now assume that E is a function of $\langle J_x \rangle$ and a generalized set of "stretching variables" x_i ($i = 1$ to N). The quantities x_i can be taken to represent quadrupole deformations of the nucleus, neutron and proton pairing parameters, etc. We now require that E be a minimum with respect to variations of x_i at fixed $\langle J_x \rangle$, i.e. $(\partial E/\partial x_i)_{\langle J_x \rangle} = 0$. If we now *define* the moment of inertia $\mathcal{I}(x_i)$ as $\langle J_x \rangle/\omega$, we can use Equation 5.1 and the above minimum condition to obtain (97)

$$\left(\frac{\partial E}{\partial \langle J_x \rangle}\right)_{x_i} = \langle J_x \rangle / \mathcal{I}(x_i). \qquad 5.2.$$

Integrating Equation 5.2 and taking $\langle J_x \rangle = [J(J+1)]^{1/2}$, we find that E must always have the general form

$$E = \frac{J(J+1)}{2\mathcal{I}(x_i)} + f(x_i), \qquad 5.3.$$

where $f(x_i)$ is an arbitrary "potential function" (98). Further dynamical input is now necessary to specify the dependence of f on the variables x_i.

In microscopic theories (see Sections 1 and 8), deviations in energy from the rigid rotor formula arise mainly from Coriolis anti-pairing of neutrons and protons, centrifugal stretching (near transition nuclei), and higher-order corrections to the cranking model (99, 100). To the extent that these different effects can be decoupled and treated in the harmonic approximation, the problem reduces to a standard normal-mode problem with N modes, for which

$$f(x_i) = \frac{1}{2}\sum_{i=1}^{N} C_i(x_i - x_{i0})^2, \qquad 5.4.$$

where x_{i0} is the equilibrium value of the variable x_i. The calculation of the coefficients C_i in a microscopic theory is the subject of Section 7. In this section, we are content to use the *form* (Equation 5.4) suggested by microscopic theories as a vehicle for developing a set of phenomenological models, the VMI model being among them.

It was shown by Ma & Rasmussen (99) that Equation 5.4 together with the conditions $\partial E/\partial x_i = 0$ lead to an energy $E(J)$ expressed in terms of a "generalized stretching variable" t:

$$E(J) = \frac{J(J+1)}{2\mathscr{I}(t)} + \tfrac{1}{2}C't^2, \qquad 5.5.$$

subject to the minimization condition

$$\partial E(J)/\partial t = 0. \qquad 5.6.$$

Equations 5.5 and 5.6 are the starting point for a unified treatment of most existing phenomenological models due to Mantri & Sood (101). These authors write $\mathscr{I}(t)$ in the form

$$\mathscr{I}(t) = \mathscr{I}_0 f(t), \qquad 5.7.$$

where $\mathscr{I}_0$ is the ground-state moment of inertia. Physically acceptable choices for $f(t)$ exhibit the properties: (*a*) $f(0) = 1$ and (*b*) $f(t)$ is an increasing function of t. Various models that have been advanced for the description of ground-state bands can now be obtained by particular choices of $f(t)$. Suppose we start from a Taylor series

$$f(t) = (1 + c_1 t + c_2 t^2 + c_3 t^3 + \cdots). \qquad 5.8.$$

If we make the simplest assumption beyond having a constant moment of inertia, and keep only the term linear in t, we have $f(t) = 1 + t$ and hence

$$t = (\mathscr{I} - \mathscr{I}_0)/\mathscr{I}_0. \qquad 5.9.$$

Substituting Equation 5.9 in Equation 5.5, we obtain the VMI or Harris model. Note that we can take $c_1 = 1$ in Equation 5.8 in full generality, since Equations 5.5 and 5.6 are invariant in form under a scale transformation $c_1 t \to t$. The VMI model

is a special case ($n = 1$) of a more general class of two-parameter models (101), where

$$f(t) = (1+t)^n. \qquad 5.10.$$

The choice $n = 2$ yields the centrifugal stretching model (70, 102, 103). The choice $n \to \infty$ leads to the Draper model (104) if we scale t by $1/n$, i.e. the choice (104)

$$f(t) = \exp(t). \qquad 5.11.$$

All of these formulas are equivalent in the region of low t, i.e. when $\mathscr{I}$ is permitted only small excursions from $\mathscr{I}_0$. However, they can differ appreciably in their predictions for high-spin states. In the case where t refers to the "pairing-stretch" degree of freedom, Ma & Rasmussen (105) have provided a microscopic justification of the ansatz (Equation 5.11); see Section 7.

A detailed comparison of formulas like (5.10) for various n can be found in (104, 106, 107). One way to exhibit the differences between these models is to look at the $\mathscr{I}$ vs ω^2 plot. Defining $r = \mathscr{I}/\mathscr{I}_0$, we may write

$$\begin{aligned} r &= 1+\omega^2/\omega_0^2 && (n = 1), \\ r &= (1-\omega^2/2\omega_0^2)^{-2} && (n = 2), \\ \ln r &= \omega^2/\omega_0^2 && (n = \infty), \end{aligned} \qquad 5.12.$$

where ω_0 is a constant. For $\omega^2/\omega_0^2 \ll 1$, the three formulas in Equation 5.12 are equivalent. For larger values of ω^2/ω_0^2, the VMI curve ($n = 1$) remains linear in ω^2, while the cases $n = 2$ (70, 103, 106) and $n = \infty$ (104) correspond to curves r that are concave upward for increasing ω^2.

The comparison of models like Equation 5.10 can also proceed via a study of the Mallmann curves (58) for R_J vs R_4, where $R_J = E(J)/E(2)$. Such a study has been carried out by Wood & Fink (107). For $2.4 < R_4 < 3.0$, i.e. the "quasi-rotational" region, they find that $n = \frac{1}{2}$ gives a better fit to R_6/R_4 than $n = 1$, 2, or ∞. For $R_4 > 3.25$, i.e. the rotational region, the best model value for n is about 1 for low J, and increases to ∞ for J approaching 16 or so. Their general conclusion (107), also supported by Stockmann & Zelevinsky (106), is that none of the models (5.10) with different n is clearly superior to the others.

A disadvantage of *all* the two-parameter models discussed above (including the VMI model), is that the energy ratios R_J depend on only one parameter. The other parameter of the theory merely fixes the energy scale and drops out of R_J. Hence the plots of R_J vs R_4 are smooth curves, i.e. one cannot account for nuclei that have essentially the same R_4 values but different R_J values. As seen in Section 2, there is some scatter in the Mallmann plots around the smooth curve predicted by the VMI model. To account for this, one would have to introduce at least a third parameter into the theory. This could be done by including more terms in the series (Equation 5.8), where c_2, c_3, etc are taken to be independent parameters. One could also add an anharmonic term proportional to t^3 to the potential term in Equation 5.5.

Most other phenomenological models for the description of ground-state rota-

tional bands can also be derived (101) within the unified framework of Equations 5.5–5.7. These include the Bohr-Mottelson formula discussed in Section 2, as well as the work of Das, Dreizler & Klein (83), Ejiri (82), Gupta (108), Holmberg & Lipas (109), Sood (110), Bose & Varshni (111), and Warke & Khadkikar (112). The Ejiri formula (81), which in addition to a rotational term includes a contribution proportional to J, also emerges from the exactly soluble model of Arima & Iachello (113).

As shown earlier (see Section 2), the VMI model is equivalent to the angular velocity expansion of Harris (71)

$$E(J) = \alpha\omega^2 + \beta\omega^4 + \gamma\omega^6 + \delta\omega^8 + \cdots,$$
$$\mathcal{I} = 2\alpha + \tfrac{4}{3}\beta\omega^2 + \tfrac{6}{5}\gamma\omega^4 + \tfrac{8}{7}\delta\omega^6 + \cdots, \qquad 5.13.$$

if we truncate the expansion at terms of order ω^4 in $E(J)$ or ω^2 in $\mathcal{I}$. An extensive phenomenological analysis for deformed nuclei based on Equation 5.13 has been conducted by Saethre et al (81), keeping terms to order ω^8 in $E(J)$. We compare their results with the VMI model in Section 7.

The angular velocity expansion (Equation 5.13) gives very good fits with four parameters to the energies of deformed nuclei all the way up to the start of the backbending region. Of course, no expansion such as Equation 5.13, even if carried to arbitrarily high order in ω^2, can account for backbending. However, for the low- and moderate-spin region the ω^2 expansion is clearly preferable (81) to an expansion in powers of $J(J+1)$.

6 *Phenomenological Band Mixing Models for the VMI and Backbending Regions*

In Section 5, we examined a variety of phenomenological approaches that focus attention primarily on the low-spin region. We now consider a class of models capable of dealing simultaneously with the low-spin (VMI) and backbending regimes. In these models the backbending phenomenon results from some sort of band mixing or hybridization. This class of models is still primarily phenomenological in nature, but at least tempered with a certain amount of theoretical motivation.

Before discussing any of the more quantitative calculations that have been performed, it is pedagogically useful to consider the simplest prototype of a band mixing calculation, in which two rotational bands are allowed to interact via a spin-independent interaction. This skeletal model is characterized by two constant moments of inertia $\mathcal{I}_1$ and $\mathcal{I}_2$ for the unperturbed bands, the energy separation E_0 of the bands at zero spin, and the strength V of the band coupling. At least four parameters are needed to describe the low-spin and backbending regions simultaneously. Two parameters are needed for the VMI region and two additional parameters are required to describe the two critical values of $\mathcal{I}$ for which $d\omega^2/d\mathcal{I} = 0$. Additional parameters are in general required to describe the *shape* of the $\mathcal{I}$ vs ω^2 curve near backbending and the behavior of $\mathcal{I}$ above the backbending region, i.e. the possibility of downbending. The present model corresponds to the minimal complexity necessary to deal with even the qualitative features of the low- and high-spin regions simultaneously.

We start with two unperturbed rotational bands with energies $E_{1,2}(J)$ given by

$$\begin{aligned} E_1(J) &= J(J+1)/2\mathscr{I}_1, \\ E_2(J) &= E_0 + J(J+1)/2\mathscr{I}_2. \end{aligned} \tag{6.1.}$$

The energy $E(J)$ of the lowest-lying mixed band is given by

$$\begin{aligned} E(J) &= \tfrac{1}{2}\{E_0 + \alpha J(J+1) - [(E_0 - \beta J(J+1))^2 + 4V^2]^{1/2}\}, \\ \alpha &= \tfrac{1}{2}(1/\mathscr{I}_1 + 1/\mathscr{I}_2), \\ \beta &= \tfrac{1}{2}(1/\mathscr{I}_1 - 1/\mathscr{I}_2). \end{aligned} \tag{6.2.}$$

Note that $E(J)$ contains terms to *all* orders when expanded in terms of $J(J+1)$.

The moment of inertia $\mathscr{I}$ of the lowest coupled band can be obtained using Equation 5.2 as

$$\begin{aligned} \mathscr{I}^{-1} &= \alpha + \beta[E_2(J) - E_1(J)]/\xi(J), \\ \xi(J) &= \{[E_2(J) - E_1(J)]^2 + 4V^2\}^{1/2}. \end{aligned} \tag{6.3}$$

Equation 6.3 can now be used to write Equation 6.2 in the form

$$E(J) = \frac{J(J+1)}{2\mathscr{I}} + f(\mathscr{I}), \tag{6.4.}$$

where $f(\mathscr{I})$ is the "potential" term given by

$$\begin{aligned} f(\mathscr{I}) &= E_0(1-\gamma)/2 - V(1-\gamma^2)^{1/2}, \\ \gamma &= (\mathscr{I}^{-1} - \alpha)/\beta. \end{aligned} \tag{6.5.}$$

The form of Equation 6.4 may now be used to extract the VMI parameters $\mathscr{I}_0$ and C:

$$\begin{aligned} \mathscr{I}_0^{-1} &= \alpha + \beta\gamma_m, \\ C^{-1} &= \beta^2 \mathscr{I}_0^4 (1-\gamma_m^2)^{3/2}/V, \\ \gamma_m &= E_0/(E_0^2 + 4V^2)^{1/2}. \end{aligned} \tag{6.6.}$$

The parameters of the two-band model can always be chosen so as to match any empirical VMI description of the low-spin states, as per Equation 6.6. We now investigate under what conditions the model also yields backbending. To do this, we first express $\mathscr{I}$ in terms of ω. We obtain

$$\begin{aligned} \omega^2 &= \frac{2V}{\beta\mathscr{I}^2}[g(\mathscr{I}_0) - g(\mathscr{I})], \\ g(\mathscr{I}) &= \left[\frac{(\beta\mathscr{I})^2}{(1-\alpha\mathscr{I})^2} - 1\right]^{-1/2}. \end{aligned} \tag{6.7.}$$

Note that this model gives ω^2 as a single-valued function of $\mathscr{I}$. This is in contrast to perturbation theory, i.e. the higher-order cranking formula (71), which would give $\mathscr{I}$ as a Taylor series in ω^2, and hence never yield backbending. If we expand the right-hand side of Equation 6.7 in a Taylor series in $(\mathscr{I} - \mathscr{I}_0)$ of the form

$$\omega^2 = \sum_{n=1}^{\infty} C_n(\mathscr{I} \rightarrow \mathscr{I}_0)^n \qquad 6.8.$$

and keep only terms up to $n = 3$, we recover the model of Das & Banerjee (114). It is then clear that we must have $C_1 > 0$, $C_2 < 0$, and $C_3 > 0$ to achieve backbending. In principle, Equation 6.7 can be inverted to yield $\mathscr{I}$ as a function of ω^2, but this will yield a multi-valued function in general. The condition that Equation 6.7 correspond to a backbending situation is that the first derivative of $[g(\mathscr{I}_0) - g(\mathscr{I})]/\mathscr{I}^2$ with respect to $\mathscr{I}$ have two zeroes in the physical region of $\mathscr{I}$. A simple analysis shows that for $\mathscr{I}_2 < \mathscr{I}_1$, i.e. no crossing of the unperturbed bands, the backbending phenomenon cannot occur. For $\mathscr{I}_2 > \mathscr{I}_1$, the unperturbed bands cross, and backbending will occur only if the condition

$$V/E_0 < \frac{\mathscr{I}_2 - \mathscr{I}_1}{\mathscr{I}_2 + \mathscr{I}_1} \qquad 6.9.$$

is satisfied; thus backbending arises if V is sufficiently *weak*.

We have developed this simple model in some detail, since it displays in an analytic way some of the essential features of more detailed studies. However, a quantitative comparison with data requires a less schematic approach. We now review some of the more sophisticated band mixing calculations that have been performed.

The recent work of Goodman & Goswami (115) is based on a two-band model as outlined above, except that the "unperturbed" bands are not pure rotational bands. Instead of Equation 6.1, we have

$$\begin{aligned} E_1(J) &= E_{\mathrm{VMI}}(J), \\ E_2(J) &= E_{\mathrm{VMI}}(J) + E_{\mathrm{exc}}(J), \end{aligned} \qquad 6.10.$$

where $E_{\mathrm{VMI}}(J)$ is the VMI energy and $E_{\mathrm{exc}}(J)$ is a four-quasiparticle intrinsic excitation energy parameterized by

$$\begin{aligned} E_{\mathrm{exc}}(J) &= E_0\left[1 + \exp\left(\frac{x - x_0}{\delta}\right)\right]^{-1}, \\ x &= [J(J+1)]^{1/2}. \end{aligned} \qquad 6.11.$$

In general, this model has six parameters, the VMI parameters $\mathscr{I}_0$ and C; the parameters E_0, x_0, and δ describing the excited band; and the mixing strength V. The proccdurc used (115) was to fix $\mathscr{I}_0$ and C to the low-spin data alone, choose $E_0 = 4$ MeV and $V = 0.9$ MeV as average values over a range of nuclei, and determine x_0 and δ by a final least-squares fit to all the data, including the backbending region. Very nice fits to both the low- and high-spin data can be obtained in this manner. The model is also capable of producing backbending followed by "downbending," i.e. cases where, for large ω^2, $\mathscr{I}$ decreases after the backbending. In this case, ω^2 is not a single-valued function of $\mathscr{I}$, as per Equation 6.7, so the simplest two-band model of Equation 6.1 cannot explain this effect. In this sense, the Goodman-Goswami model (115) is equivalent to a three (or more) interacting band model.

Some two- and three-band models like Equation 6.1 were first investigated in detail by Molinari & Regge (116). They first used a two-band model, but with a spin-dependent coupling term V. A fair fit to the spectrum of ^{162}Er was obtained. A three-band model (116) with interacting $K = 0$, 2, and 3 bands improved the situation somewhat for ^{162}Er, but suggested that a still more complicated dynamical situation prevails.

Multiband calculations were subsequently carried out by Broglia, Molinari, Pollarolo & Regge (117, 118) for the cases of ^{154}Gd (117) and ^{156}Dy (118). These authors diagonalize a model Hamiltonian $\mathscr{H}$ of the form

$$\mathscr{H} = \mathscr{H}_0 + \mathscr{H}_c \qquad 6.12.$$

in an n-dimensional vector space (n bands with various K quantum numbers). They take as unperturbed Hamiltonian

$$\mathscr{H}_0 = A(K)\vec{J}^2 + \mathscr{H}_{\text{int}}(K) \qquad 6.13.$$

with eigenvalues $E = A(K)J(J+1) + B(K)$, where $B(K)$ is the eigenvalue of the intrinsic Hamilton $\mathscr{H}_{\text{int}}(K)$. The coupling term $\mathscr{H}_c$ is chosen to be

$$\mathscr{H}_c = h_0(J_1^2 + J_2^2) + h_1(J_+ + J_-) + h_2(J_+^2 + J_-^2). \qquad 6.14.$$

The three terms in Equation 6.14 correspond to the centrifugal, Coriolis, and asymmetry interactions, respectively. The procedure is now to treat the intrinsic matrix elements of $\mathscr{H}_c$ as well as $A(K)$ and $B(K)$ as free parameters to be determined by a least-squares search on all ground-state and excited-band data.

The application of this approach to ^{154}Gd (117) and ^{156}Dy (118) leads to some interesting results. For ^{154}Gd (117), at least three bands were required to give a good fit to the existing data. The two so far observed $K = 0$ bands (ground-state and β-vibrational bands) display considerably different rates of change of $\mathscr{I}$ in the backbending region of the $\mathscr{I}$ vs ω^2 plot. These rates of change are controlled by the positions of the poles of the energy $E(J)$ in the complex J plane (117, 118). For the two-band model of Equations 6.1–6.9, the backbending behavior of both bands is governed by a single pole. It is clear that at least one additional band (pole) is necessary in order to reproduce two distinct types of backbending curve, as well as the phenomenon of downbending.

The experimental situation for ^{156}Dy is even more complete. Here, the ground-state ($K = 0$), beta ($K = 0$), gamma ($K = 2$), and a $K = 1$ band are known experimentally (119). Using the framework of Equations 6.12–6.14, a multiband calculation is reported in (117). Five bands are needed to obtain a good fit to the high-spin region, while a four-band model is sufficient to fit the low-spin region alone. For ^{156}Dy, even the low-spin VMI region cannot be fitted without the mixing of $K \neq 0$ bands; in particular, the mixing of the γ band ($K = 2$) is important for low spins.

The fact that no acceptable fit can be found for either ^{154}Gd or ^{156}Dy using only $K = 0$ bands suggests that a Mottelson-Valatin (46) type of phase transition (uniform breakdown of pairing) is unlikely for cases where backbending is observed (117, 118). Even if such a fit could be obtained, this type of phase transition

would not account for the downbending phenomenon. On the other hand, the high-lying $K = 1$ (or $K = 3$) bands which appear in these calculations (117, 118) have rather large moments of inertia. They thus have a natural interpretation in terms of pairs of high-spin particles decoupling from the rotating core, i.e. as *two-quasiparticle* bands. Nilsson orbitals with large spin are indeed available in this mass region, and can give the large moment of inertia required. The Stephens-Simon model (120) and subsequent similar treatments (121, 122) of the backbending phenomenon are a particular realization of the two-quasiparticle band hypothesis, in which a pair of $i_{13/2}$ neutrons are involved. The evidence of this model is treated in detail in (120–122), so we will not repeat it here. The main point here is that the band mixing calculations (117, 118) are consistent with the idea of decoupling pairs of particles, and hence provide support for the general ideas of Stephens & Simon (120). A study of the competition between the Coriolis antipairing (46) and pair decoupling (120) mechanisms as a function of mass number has been given by Sheline (123). As we see in Section 8, the decoupled-pair idea also emerges from self-consistent HFB calculations in cases where backbending is predicted. Thus there is a certain consistency in the physical content of these various approaches, even though they may appear to be quite different.

The band mixing model also enables one to predict the $B(E2)$ transition probabilities for interband and intraband transitions (117). Rather little experimental information is available. However, the $B(E2)$ values would provide an even more stringent test of the model than the energy levels themselves.

In summary, the band mixing approach is largely phenomenological, but the form of Equations 6.12–6.14 of the Hamiltonian has some physical basis. The number of data that are fitted (4 bands for ^{156}Dy) considerably exceeds the number of adjustable parameters. Also, the model makes a number of additional predictions regarding transition rates and the energy levels of higher bands that in principle can be tested experimentally. The disadvantage of such models is that there is as yet no firm connection between the parameters of the phenomenological Hamiltonian and the underlying microscopic theory.

A number of other phenomenological approaches, closely related to the band mixing idea, have been advanced to unify the description of the high-spin and VMI regions. Several authors (124–128) have argued that symmetric rotating nuclei must be unstable with respect to asymmetric deformations for high spins, i.e. the γ degree of freedom becomes "unfrozen." Smith & Volkov (128) have shown from a rather general variational approach how to generalize the VMI model to include the backbending region. They arrive at an energy formula

$$E(J) = \frac{R(\gamma)}{2\mathscr{I}} + \tfrac{1}{2}C_0(\mathscr{I} - \mathscr{I}_0)^2 + C_1\gamma(\mathscr{I} - \mathscr{I}_0) + \tfrac{1}{2}C_2\gamma^2 \qquad 6.15.$$

subject to the variational conditions $\partial E/\partial \mathscr{I} = 0$ and $\partial E/\partial \gamma = 0$. Here $R(\gamma)$ is obtained by diagonalizing the operator

$$R = \frac{3}{4}\sum_{\nu=1}^{3} \frac{J_\nu^2}{\sin^2(\gamma - 2\pi\nu/3)}. \qquad 6.16.$$

For many cases, the condition $\partial E/\partial\gamma = 0$ affords two solutions for each spin, one corresponding to $\gamma \approx 0$ (VMI band, no backbending) and another to nonzero values of γ. Above some critical value $J = J_c$, the latter solution lies lower in energy and becomes part of the ground-state band, which then exhibits backbending in this region of J. A very similar phenomenological model was proposed somewhat earlier by Das, Dreizler & Klein (127) for the simultaneous analysis of ground-state and β or γ bands. A formula identical in form to Equation 6.15 was obtained, except that $R(\gamma)$ is replaced by

$$R(\gamma) \approx J(J+1)+n\gamma, \qquad 6.17.$$

where $n = 0$ or 1.

Another method for dealing with the backbending region is that of Wahlborn & Gupta (129) who express $\mathscr{I}$ as a ratio of polynomials in $J(J+1)$. This enables one to reproduce the VMI behavior at low spins and also ensure that $\mathscr{I}$ approaches the proper limit for large J.

Various three-parameter models (125, 126) have been proposed for fitting the low-spin properties of the ground-state and γ bands simultaneously. These models replace the $J(J+1)$ term in the VMI model of Equation 2.11 by various forms of the energies of an asymmetric rotor. No backbending behavior is predicted, however. Note that the usual VMI model of Equation 2.11 was also applied to γ bands in (73).

7 *Microscopic Calculations of the VMI Parameters $\mathscr{I}_0$ and C*

In this section we review several attempts to calculate the VMI parameters $\mathscr{I}_0$ and C, which characterize the low-spin properties of the ground-state band. We first outline the theoretical basis for these calculations. We then examine the question of whether the values of $\mathscr{I}_0$ and C determined empirically by a VMI-model fit can be sensibly compared to the theoretical values, or whether they represent only phenomenological *effective* parameters. In cases where the comparison of theoretical and empirical VMI parameters is appropriate, we evaluate the extent to which the microscopic theory provides a quantitative account of the data.

A considerable amount of theoretical effort has gone into trying to understand the deviations of rotational energy spectra from the rigid-rotor formula. One general type of approach has been based on the cranking model of Inglis (40). Some early calculations (130–134) take into account only the centrifugal stretching and Coriolis antipairing effect (46). More complete calculations, which include the important fourth-order corrections to the cranking model, have been carried out by Marshalek (135), Ma & Rasmussen (99), and Ma & Tsang (100). We focus our attention on these latter calculations here.

We first outline the essential features of the microscopic cranking formalism, following Ma & Rasmussen (99). We consider a Hamiltonian $\mathscr{H}(\lambda_i^{(0)})$ describing the nucleons moving in some average nonrotating deformed potential [a Nilsson potential (25), for example] and interacting through some specified residual interaction. The quantities $\lambda_i^{(0)}$ $(i = 1, N)$ label collective degrees of freedom (the shape of the deformed potential) as well as characteristics of the residual interaction (pairing strengths, etc). The Schrödinger equation describing this nonrotating

system is

$$\mathscr{H}(\lambda_i^{(0)})\Psi^{(0)}(\lambda_i^{(0)}) = E^{(0)}(\lambda_i^{(0)})\Psi^{(0)}(\lambda_i^{(0)}). \tag{7.1.}$$

Now consider the situation where the deformed potential is made to rotate around the x axis with frequency ω, through the action of an external force. The Schrödinger equation for this rotating system in the intrinsic frame is

$$[\mathscr{H}(\lambda_i^{(\omega)}) - \omega J_x]\Psi^{(\omega)}(\lambda_i^{(\omega)}) = E^{(\omega)}(\lambda_i^{(\omega)})\Psi^{(\omega)}(\lambda_i^{(\omega)}), \tag{7.2.}$$

where the quantities $\lambda_i^{(\omega)}$ assume different values from the $\lambda_i^{(0)}$ of Equation 7.1. Note that the potential is time-dependent when expressed in laboratory coordinates. In transforming the Schrödinger equation to the intrinsic frame (body-fixed axes) to obtain a time-independent potential, we must consider the Coriolis and centrifugal inertial forces that exist in a rotating reference frame. These forces give rise to the term $-\omega J_x$ in Equation 7.2. Using the semi-classical relationship

$$\langle\Psi^{(\omega)}(\lambda_i^{(\omega)}) | J_x | \Psi^{(\omega)}(\lambda_i^{(\omega)})\rangle = [J(J+1)]^{1/2}. \tag{7.3.}$$

We can evaluate the energy difference $E(J)$ between the rotational state of spin J and the ground state as

$$E(J) = \langle\Psi^{(\omega)}(\lambda_i^{(\omega)})|\mathscr{H}(\lambda_i^{(\omega)})|\Psi^{(\omega)}(\lambda_i^{(\omega)})\rangle - \langle\Psi^{(0)}(\lambda_i^{(0)})|\mathscr{H}(\lambda_i^{(0)})|\Psi^{(0)}(\lambda_i^{(0)})\rangle. \tag{7.4.}$$

We can make further progress by decomposing $E(J)$ as follows:

$$\begin{aligned} E(J) &= E_1(J) + E_2(J), \\ E_1(J) &= \langle\Psi^{(\omega)}(\lambda_i^{(\omega)})|\mathscr{H}(\lambda_i^{(\omega)})|\Psi^{(\omega)}(\lambda_i^{(\omega)})\rangle - \langle\Psi^{(0)}(\lambda_i^{(\omega)})|\mathscr{H}(\lambda_i^{(\omega)})|\Psi^{(0)}(\lambda_i^{(\omega)})\rangle, \\ E_2(J) &= \langle\Psi^{(0)}(\lambda_i^{(\omega)})|\mathscr{H}(\lambda_i^{(\omega)})|\Psi^{(0)}(\lambda_i^{(\omega)})\rangle - \langle\Psi^{(0)}(\lambda_i^{(0)})|\mathscr{H}(\lambda_i^{(0)})|\Psi^{(0)}(\lambda_i^{(0)})\rangle, \end{aligned} \tag{7.5.}$$

where the wave functions $\Psi^{(0)}(\lambda_i^{(\omega)})$ are defined by

$$\mathscr{H}(\lambda_i^{(\omega)})\Psi^{(0)}(\lambda_i^{(\omega)}) = E^{(0)}(\lambda_i^{(\omega)})\Psi^{(0)}(\lambda_i^{(\omega)}). \tag{7.6.}$$

In Equation 7.5, $E_1(J)$ is the energy difference between the rotating and static systems when the parameters $\lambda_i^{(\omega)}$ are held fixed at the values appropriate to frequency ω. $E_2(J)$ is the contribution arising solely from changes in the parameters λ_i, without the external cranking term.

We now proceed to evaluate $E_1(J)$ and $E_2(J)$. Treating ωJ_x as a perturbation, one can evaluate $E_1(J)$ by a method similar to that of Harris (71). Keeping only second- and fourth-order terms in perturbation theory, we find (99)

$$E_1(J) = J(J+1)/2\mathscr{I}(x_i) + \tfrac{1}{2}C_\eta\eta^2, \tag{7.7.}$$

where $\eta \equiv \omega^2$ and $x_i \equiv \{\eta, \lambda_i^{(\omega)}\}$. The moment of inertia $\mathscr{I}(x_i)$ is given by

$$\mathscr{I}(x_i) = \mathscr{I}_0 + 2C_\eta\eta. \tag{7.8.}$$

In Equation 7.8, $\mathscr{I}_0$ is given by the second-order cranking formula of Inglis (40) and Belyaev (136)

$$\mathscr{I}_0 = 2\sum_{m\neq 0}\frac{|\langle 0|J_x|m\rangle|^2}{E_m - E_0}, \tag{7.9.}$$

where $|m\rangle = |\Psi_m^{(0)}(\lambda_i^{(\omega)})\rangle$ is a two-quasiparticle state and $E_m = E_m^{(0)}(\lambda_i^{(\omega)})$ is the corresponding energy. The constant C_η is given in fourth-order perturbation theory by (99, 100)

$$C_\eta = 2 \sum_{i,j,k \neq 0} \frac{\langle 0|J_x|i\rangle\langle i|J_x\ k\rangle\langle k|J_x|j\rangle\langle j|J_x|0\rangle}{(E_i - E_0)(E_j - E_0)(E_k - E_0)} - 2 \sum_{i,j \neq 0} \frac{|\langle i|J_x|0\rangle|^2 |\langle j|J_x|0\rangle|^2}{(E_i - E_0)^2(E_j - E_0)}, \quad 7.10.$$

where $|0\rangle$ is the quasiparticle vacuum, $|i\rangle$ and $|j\rangle$ are two-quasiparticle states, and $|k\rangle$ is a two- or four-quasiparticle state; E_0, E_i, E_j, and E_k are the corresponding energies.

We now turn to the evaluation of $E_2(J)$ of Equation 7.5. Physically, $E_2(J)$ registers changes in energy due to changes in the variables λ_i. The λ_i represent collective degrees of freedom, such as quadrupole (β_2), hexadecapole (β_4), and triaxial (γ) deformations, the number-displacement degree of freedom (137) (changes of moment of inertia induced by shifting nucleons between orbits of opposite parity); and parameters ν_p and ν_n characterizing the proton and neutron pairing strengths, for instance. The simplest approximation is to assume that these various modes are uncoupled, and that the $\lambda_i^{(\omega)}$ do not deviate strongly from their equilibrium values $\lambda_i^{(0)}$. In this harmonic approximation we would write

$$E_2(J) = \tfrac{1}{2} \sum_i C_i (\lambda_i^{(\omega)} - \lambda_i^{(0)})^2, \quad 7.11.$$

where the spring constants C_i correspond to the stiffness of the system with respect to the various kinds of deformation.

Combining Equations 7.7 and 7.11, we find the total energy

$$E(J) = \sum_i \tfrac{1}{2} C_i (x_i - x_{i0})^2 + \frac{J(J+1)}{2\mathscr{I}(x_i)} \quad 7.12.$$

subject to the equilibrium conditions

$$[\partial E(J)/\partial x_i]_J = 0. \quad 7.13.$$

The application of Equation 7.13 to Equation 7.12 yields

$$x_i - x_{i0} = \frac{\omega^2}{2C_i} \left(\frac{\partial \mathscr{I}}{\partial x_i} \right)_{x_{i0}}. \quad 7.14.$$

We can now identify the VMI constant C of Equation 2.21 by expanding $\mathscr{I}$ to first order in $x_i - x_{i0}$ and using Equation 7.14. We find

$$C^{-1} = \sum_i (C_i)^{-1} (\partial \mathscr{I}/\partial x_i)^2_{x_{i0}}. \quad 7.15.$$

Equations 7.9 and 7.15 form the basis for a comparison of the microscopic theory with the VMI model.

It should be noted that the small amplitude approximation in Equation 7.11 is not expected to be generally valid. In fact, for well-deformed nuclei far from

closed shells, Ma & Rasmussen (105) have shown that the dependence of $\mathcal{I}$ on the pairing correlation parameter ν is nearly exponential, i.e. $\mathcal{I} = \mathcal{I}_0 \exp(-\gamma\nu)$ for $0.3\Delta \leqq \nu \leqq \Delta$, where Δ is the pairing-gap parameter. This provides a partial microscopic justification for the Draper model of Equation 5.11.

Before discussing the detailed comparison of microscopic and empirical values of $\mathcal{I}_0$ and C^{-1}, we must first establish the conditions under which this comparison is meaningful. An important step in this direction is to assess the stability of the VMI parameters $\mathcal{I}_0$ and C to the addition of further terms in the expansion of the energy powers of ω. This has been done by Saethre et al (81), who start from the generalized Harris expansion (71)

$$E(J)/E_{\text{rot}}(J) = 1 + \gamma_J + \varepsilon_1\gamma_J^2 + \varepsilon_2\gamma_J^3, \qquad 7.16.$$

where $E_{\text{rot}}(J) = J(J+1)/2\mathcal{I}_0$ and $\gamma_J = 3\omega^2/4\mathcal{I}_0 C$. Saethre et al (81) have determined the parameters $\mathcal{I}_0$, C, ε_1, and ε_2 by a least-squares fit to the experimental $E2$ transition energies for ground state-bands in the mass region from Ce to Pt. For most cases, the lowest five transition energies are included in the four-parameter fits; thus the emphasis is on the low- to moderate-spin region ($J \leqq 10$) below the onset of backbending.

The critical question in appraising the significance of the parameters $\mathcal{I}_0$ and C is whether or not the higher-order corrections ($\varepsilon_1, \varepsilon_2$) in Equation 7.16 are small. The size of the corrections is dependent on the spin J, and increases monotonically with increasing J. From the work of Saethre et al (81), we are able to calculate these corrections, which are displayed in Table 2 for $J = 4$. If these corrections were small for $J = 4$ then the parameters $\mathcal{I}_0$ and C^{-1} obtained by fitting only $E(2)$ and $E(4)$ could be more meaningfully compared with the microscopic expressions 7.9 and 7.15 than the values of $\mathcal{I}_0$ and C^{-1} resulting from fitting all data up to $J = 10$, say. However, from Table 2, we see that the higher-order corrections $\varepsilon_1\gamma_J$ and $\varepsilon_2\gamma_J^2$ relative to the second term are significant in almost all cases, even for $J = 4$. Only for very few nuclei (^{162}Dy, ^{164}Er, ^{168}Er, ^{166}Yb, ^{174}W, ^{178}Os) are the corrections from *both* third- and fourth-order terms less than 20% in magnitude. Since the third- and fourth-order terms are almost always opposite in sign, they tend to cancel. However, their combined contribution for $J = 4$ is still greater than 20% of the second-order term for half of the nuclei listed in Table 2.

In Equation 7.16 the value of γ_J registers the deviation of the energy spectrum from the rigid-rotor limit $E_{\text{rot}}(J)$. In general, the third- and fourth-order corrections are larger for "soft" nuclei for which γ_J is large. Thus a VMI description, which sets $\varepsilon_1 = \varepsilon_2 = 0$ in Equation 7.16, is most appropriate for very good rotors (small γ_J). For a typical nucleus, the value of ω^2 for $J = 10$ is about 2–3 times that for $J = 4$. Hence, for many nuclei in Table 2, the expansion 7.16 is already slowly convergent, if not divergent, for $J = 10$. If we thus fit the transition energies with a *truncated* Taylor series in ω^2, as per Equation 7.16, the resulting parameters will in general only have significance as *effective* parameters.

The extent to which the above considerations represent a real difficulty can be assessed by determining the VMI parameters $\mathcal{I}_0$ and C^{-1} by several different

methods, and observing whether or not the same values emerge. We consider three methods here:

1. The two-parameter VMI fit of Mariscotti, Scharff-Goldhaber & Buck (73), giving $\mathscr{I}_0^{\rm VMI}$ and $C_{\rm VMI}^{-1}$.
2. The four-parameter fit of Saethre et al (81), giving $\mathscr{I}_0^s$, C_s^{-1}.
3. A two-parameter VMI fit to $E(2)$ and R_4 only, giving $\mathscr{I}_0$ (2, 4) and C^{-1} (2, 4).

In method 3, we used the experimental $E(2)$ and $E(4)$ values of Saethre et al (81). For $\mathscr{I}_0$, the agreement between the methods 1–3 is excellent, indicating that the value of $\mathscr{I}_0$ is stable to variations in the method used to extract it from the data. For good rotors, the values of $\mathscr{I}_0$ vary by 1% or less. Even for soft nuclei such as the Ce isotopes the variation in $\mathscr{I}_0$ is less than 20%.

The situation is somewhat different for C^{-1}. In Table 3, we show the values of C^{-1} determined by methods 1–3. For about one half of the nuclei in Table 3, significant differences (>20%) exist between the three determinations of C^{-1}, often a discrepancy of a factor of two or three. These correspond to the relatively "soft"

Table 2 Higher-order terms in the angular velocity expansion Equation 7.16 for $J = 4$ (81)

Nucleus	γ_4	$\varepsilon_1\gamma_4$	$\varepsilon_2\gamma_4^2$	Nucleus	γ_4	$\varepsilon_1\gamma_4$	$\varepsilon_2\gamma_4^2$
^{128}Ce	1.24	−0.59	0.14	^{176}Yb	0.04	−0.21	1.45
^{130}Ce	2.14	−0.64	0.09	^{166}Hf	0.96	−0.53	0.18
^{132}Ce	3.90	−0.66	0.05	^{168}Hf	0.41	−0.29	0.19
^{134}Ce	5.38	−0.59	0.03	^{170}Hf	0.19	−0.06	0.22
^{152}Sm	0.70	−0.34	0.09	^{172}Hf	0.12	−0.09	0.23
^{154}Gd	0.71	−0.38	0.11	^{174}Hf	0.09	−0.07	0.35
^{156}Gd	0.14	−0.15	0.23	^{176}Hf	0.07	−0.05	0.24
^{158}Gd	0.08	−0.38	1.94	^{178}Hf	0.06	−0.06	0.50
^{156}Dy	0.99	−0.40	0.09	^{180}Hf	0.04	−0.09	0.37
^{158}Dy	0.20	−0.20	0.24	^{172}W	0.45	−0.21	0.24
^{160}Dy	0.09	−0.09	0.28	^{174}W	0.23	−0.08	0.17
^{162}Dy	0.05	−0.03	0.13	^{176}W	0.20	−0.23	0.38
^{158}Er	2.43	−0.58	0.07	^{178}W	0.15	−0.15	0.32
^{160}Er	0.46	−0.34	0.19	^{180}W	0.11	−0.19	0.65
^{162}Er	0.15	−0.15	0.25	^{182}W	0.06	−0.12	0.28
^{164}Er	0.08	−0.03	0.12	^{178}Os	0.52	−0.13	0.11
^{166}Er	0.06	+0.02	0.33	^{180}Os	0.53	−0.55	0.42
^{168}Er	0.03	−0.02	0.10	^{182}Os	0.45	−0.67	0.52
^{160}Yb	4.30	−0.65	0.05	^{184}Os	0.24	−0.36	0.31
^{162}Yb	1.33	−0.65	0.16	^{186}Os	0.35	−0.44	0.29
^{164}Yb	0.34	−0.26	0.23	^{188}Os	0.56	−0.47	0.20
^{166}Yb	0.15	−0.12	0.19	^{182}Pt	3.34	−0.67	0.05
^{168}Yb	0.09	−0.06	0.37	^{184}Pt	3.53	−0.63	0.05
^{170}Yb	0.05	−0.04	0.20	^{186}Pt	6.00	−0.60	0.02
^{172}Yb	0.04	−0.08	0.60	^{188}Pt	6.49	−0.56	0.02
^{174}Yb	0.03	+0.11	−1.87				

Table 3 Empirical values of C^{-1} determined by different methods (in units of 10^2 MeV^{-3})

Nucleus	C^{-1}_{VMI}	C_s^{-1}	$C^{-1}_{(2,4)}$	Nucleus	C^{-1}_{VMI}	C_s^{-1}	$C^{-1}_{(2,4)}$
^{128}Ce	1.84	3.61	2.89	^{176}Yb	1.28	1.20	1.10
^{130}Ce	1.72	3.59	2.08	^{166}Hf	3.97	6.24	4.15
^{132}Ce	1.64	3.15	1.86	^{168}Hf	3.85	4.94	3.95
^{134}Ce	1.07	2.06	1.23	^{170}Hf	4.72	3.91	3.77
^{152}Sm	5.95	9.84	7.45	^{172}Hf	2.84	2.78	3.00
^{154}Gd	5.44	9.52	7.03	^{174}Hf	2.16	2.30	2.23
^{156}Gd	3.38	4.05	3.64	^{176}Hf	1.70	1.85	1.80
^{158}Gd	2.45	2.85	2.24	^{178}Hf	1.35	1.36	1.31
^{156}Dy	6.25	10.04	7.36	^{180}Hf	0.73	0.85	0.79
^{158}Dy	3.79	4.34	3.78	^{172}W	6.10	5.99	5.35
^{160}Dy	2.19	2.65	2.50	^{174}W	3.79	3.64	3.52
^{162}Dy	1.95	1.90	1.87	^{176}W	3.09	3.31	2.86
^{158}Er	4.90	9.66	5.94	^{178}W	2.23	2.49	2.29
^{160}Er	3.68	5.37	4.11	^{180}W	1.88	1.96	1.74
^{162}Er	2.55	2.95	2.72	^{182}W	0.98	1.16	1.06
^{164}Er	1.97	1.91	1.89	^{178}Os	5.68	5.86	5.54
^{166}Er	2.40	2.09	2.13	^{180}Os	4.39	5.43	3.76
^{168}Er	1.10	1.16	1.14	^{182}Os	2.94	4.75	2.74
^{160}Yb	4.03	8.14	4.62	^{184}Os	1.80	2.92	2.19
^{162}Yb	3.85	7.50	4.37	^{186}Os	1.62	2.90	2.05
^{164}Yb	3.33	4.19	3.64	^{188}Os	1.95	3.53	2.43
^{166}Yb	2.55	2.90	2.67	^{182}Pt	9.62	24.66	13.40
^{168}Yb	2.58	2.66	2.58	^{184}Pt	9.26	22.54	12.59
^{170}Yb	1.60	1.66	1.73	^{186}Pt	8.93	21.40	12.12
^{172}Yb	2.14	1.47	1.39	^{188}Pt	4.72	8.57	5.18
^{174}Yb	1.08	1.21	1.27				

nuclei for which $\sigma_s > 0.01$. On the other hand, the nuclei for which the three C^{-1} values are the same to within 20% correspond in most cases to relatively "hard" nuclei (good rotors) for which $\sigma_s \leqq 0.01$. For these nuclei, the VMI correction to the rigid-rotor energy formula is also small at low spins, i.e. $\gamma_4 \leqq 0.2$ in Table 2. The four nuclei ^{164}Yb, ^{172}W, ^{174}W, and ^{178}Os are borderline cases; they have C^{-1} differences of only 5–20%, but fairly large σ_s values in the range 0.01–0.03.

A rather general conclusion is now clear: nuclei that have small VMI corrections $\gamma_4 \leqq 0.2$ to the rigid-rotor energy formula also tend to have small higher-order corrections *relative* to γ_4, and hence C^{-1} values that are relatively stable (to 20%) to the method used to extract them from the data. For these nuclei, one can make a sensible comparison of the microscopic expression 7.15 with the empirical value of C^{-1}. For soft nuclei, however, such a comparison does not seem meaningful; this includes most nuclei for which $\sigma_s > 0.01$. For these nuclei, the VMI model remains a valid phenomenological procedure for fitting the data, as shown in Sections 2–4. However, for these nuclei, the parameters $\mathcal{I}_0$ and C^{-1} are to be

interpreted as *effective* parameters that cannot be identified with $\mathcal{I}_0$ and C^{-1} as given by the microscopic cranking formalism outlined here.

We now proceed with a comparison of the VMI parameters with the microscopic theory for those nuclei where this comparison is reasonable. We restrict our attention to the results of Marshalek (135) and Ma & Tsang (100), which are the most complete.

In (100) the following procedure was used to calculate $\mathcal{I}_0$ and C^{-1}. One first generates a deformed single-particle basis using the deformed oscillator potential of Nilsson et al (138). The residual interaction is taken to be a pairing force of strength G given by

$$G = \left[g_0 - \tau_z g_1 \left(\frac{N-Z}{A} \right) \right] \Big/ A, \qquad 7.17.$$

where $\tau_z = +1$ for neutron and -1 for proton pairing, $g_0 = 19.2$ MeV and $g_1 = 7.4$ MeV. Using Equation 7.17, one now solves the BCS equations numerically (100) to obtain the usual occupation probabilities U_k and V_k and the quasiparticle energies E_k. The pairing correlation parameter ν is now defined by

$$\left.\begin{matrix} U_k^2 \\ V_k^2 \end{matrix}\right\} = \frac{1}{2} \left\{ 1 \pm \frac{(\varepsilon_k - \lambda)}{\left[(\varepsilon_k - \lambda)^2 + \nu^2 \right]^{1/2}} \right\}, \qquad 7.18.$$

where ε_k is the Nilsson single-particle energy and λ is the chemical potential.

In evaluating C^{-1} from Equation 7.15, we need to know both the spring constants C_i and the derivatives $\partial \mathcal{I}/\partial x_i$. In (100) the parameters x_i are taken to be the neutron and proton pairing parameters ν_n and ν_p, the quadrupole and hexadecapole deformation parameters ε_2 and ε_4, and the cranking parameter η. Triaxial deformation and number displacement degrees of freedom (137) among other possibilities, are not considered in (100). Note that the inclusion of such additional degrees of freedom can only *increase* the theoretical value of C^{-1} as per Equation 7.15. For the case at hand, Equation 7.15 can be written more explicitly as

$$C^{-1} = 4C_\eta + \frac{1}{C_{\nu_n}} \left(\frac{\partial \mathcal{I}_0}{\partial \nu_n} \right)^2_{\nu_n^{(0)}} + \frac{1}{C_{\nu_p}} \left(\frac{\partial \mathcal{I}_0}{\partial \nu_p} \right)^2_{\nu_p^{(0)}} + \frac{1}{C_{22}} \left(\frac{\partial \mathcal{I}_0}{\partial \varepsilon_2} \right)^2_{\varepsilon_2^{(0)}} + \frac{1}{C_{44}} \left(\frac{\partial \mathcal{I}_0}{\partial \varepsilon_4} \right)^2_{\varepsilon_4^{(0)}} \qquad 7.19.$$

The derivatives of $\mathcal{I}_0$ with respect to ν_n and ν_p are evaluated for fixed G and particle number $n = \sum_{k>0} 2V_k^2$. The spring constants $C_i = \{C_{\nu_n}, C_{\nu_p}, C_{22}, C_{44}\}$ are obtained from the ground-state energy ε_0 via

$$C_i = (\partial^2 \varepsilon_0 / \partial x_i^2)_{n,G}. \qquad 7.20.$$

The calculations of Marshalek (135) are very similar in spirit to the method of Tsang & Ma (100) outlined above. Outside of the details of the choice of deformed-potential and residual-interaction parameters, the main difference is that Marshalek (135) neglects some corrections due to particle-number conservation and considers the triaxial degree of freedom γ, and not ε_4. The γ degree of freedom was found to be of minor importance in most cases (135).

The results of the theoretical calculations of $\mathcal{I}_0$ and C^{-1} are shown in Tables 4 and 5. The empirical values $\mathcal{I}_0^s$ of Table 4 and C_s^{-1} of Table 3 are from the analysis

Table 4 Comparison of empirical and theoretical values of $\mathcal{I}_0$ (in units of MeV^{-1})

Nucleus	$\mathcal{I}_0^s$	$\mathcal{I}_0^{TM}$ (ref. 100)	$\mathcal{I}_0^M$ (ref. 135)
^{152}Sm	22.6	20.2	18.2
^{154}Gd	22.3	19.1	17.3
^{156}Gd	33.2	25.4	25.9
^{158}Gd	37.5	26.6	30.7
^{160}Dy	34.2	24.8	26.3
^{162}Dy	37.0	26.7	29.9
^{162}Er	28.9	22.6	
^{164}Er	32.6	25.1	28.8
^{166}Er	37.0	27.0	31.9
^{168}Er	37.5	28.3	32.8
^{160}Yb	7.3	29.6	
^{166}Yb	28.9	23.0	
^{168}Yb	33.9	25.1	—
^{170}Yb	35.4	26.8	32.1
^{172}Yb	38.0	28.7	34.8
^{174}Yb	39.1	29.7	35.9
^{176}Yb	36.4	29.1	34.7
^{174}Hf	32.7	25.9	
^{176}Hf	33.7	28.1	34.3
^{178}Hf	32.0	27.4	31.5
^{180}Hf	32.0	29.0	28.0
^{180}W	28.6	25.0	
^{182}W	29.8	26.6	28.6
^{184}Os	24.4	24.3	
^{186}Os	21.1	21.6	—
^{188}Os	18.2	18.8	

of Saethre et al (81), based on Equation 7.16. In Table 5, we have included only those nuclei for which the empirical value of C^{-1} is empirically determined to 20% or better (see earlier discussion). If one decomposes the theoretical value of C^{-1} into contributions from the various mechanisms, one finds:

1. The fourth-order cranking contribution C_η and the neutron Coriolis antipairing contribution are comparable in size and generally represent the largest contributions to C^{-1}.
2. The proton antipairing term usually contributes only 10–20% of the total C^{-1}.
3. The contributions of quadrupole and hexadecapole stretching to C^{-1} are comparable but usually small, except for nuclei with $N = 90$ or 92 (among those calculated).

From Table 4, we see that the trends of $\mathcal{I}_0$ with N and Z are well reproduced, but the calculated magnitudes of $\mathcal{I}_0$ are too small (except for ^{160}Yb), generally

by 10-40%. This level of disagreement is not very serious relative to the situation for C^{-1} values. We note that $C_M^{-1} > C_{TM}^{-1}$ except for ^{156}Gd and ^{160}Dy. This is mostly due (99) to the sizable reduction in the Coriolis antipairing effect ($C_{\nu_{n,p}}^{-1}$) due to the inclusion of number conservation corrections to the BCS energy, which were included by Ma & Tsang (100) and omitted by Marshalek (135). We also note that C_{TM}^{-1} is neither systematically larger nor smaller than the empirical values C_s^{-1} (80). For only a few nuclei (^{160}Dy, ^{164}Er, ^{168}Yb, ^{170}Yb, ^{178}Hf) is the agreement between C_{TM}^{-1} and C_s^{-1} better than 20%; in several cases the discrepancy is of the order of a factor of two.

It is clear that the calculations done thus far with the microscopic cranking perturbation formalism do not seem to provide a very quantitative description of the VMI parameter C^{-1}. However, it should be noted that C^{-1} is much more sensitive than $\mathcal{I}_0$ to the details of the single-particle levels. Preliminary studies (100) indicate that the C^{-1} values can be considerably improved by an adjustment of the neutron single-particle Nilsson levels around $N = 104$ and 108. Of course, these adjustments must be done in such a way as not to disturb the description of other nuclear properties. It is still not clear whether the discrepancies in Table 5 reflect the inadequacies of the cranking formalism or an inappropriate choice of a single-particle basis and residual interaction. These questions deserve further study.

Table 5 Theoretical values of C^{-1} (in units of 10^2 MeV^{-3})

Nucleus	C_{TM}^{-1} (ref. 100)	C_M^{-1} (ref. 135)
^{156}Gd	2.88	2.31
^{158}Gd	2.18	2.64
^{160}Dy	2.49	2.21
^{162}Dy	2.35	2.86
^{162}Er	1.68	—
^{164}Er	1.94	2.82
^{166}Er	2.54	3.27
^{168}Er	1.74	2.89
^{166}Yb	1.79	—
^{168}Yb	2.36	—
^{170}Yb	1.79	3.18
^{172}Yb	2.28	3.94
^{174}Yb	2.63	4.26
^{176}Yb	1.63	3.46
^{174}Hf	1.78	—
^{176}Hf	2.77	4.59
^{178}Hf	1.59	3.55
^{180}Hf	1.97	2.27
^{180}W	1.49	—
^{182}W	1.80	2.82

8 *The Hartree-Fock-Bogoliubov Approach to the VMI Region and Backbending*

8.1 INTRODUCTION In previous sections, we have considered phenomenological models for the low-spin region and also approaches that can account for the backbending behavior observed at high spins. The microscopic cranking model developed in Section 7 provides a method of calculating the VMI parameters $\mathcal{I}_0$ and C^{-1}, which characterize the low-spin behavior of the nucleus. However, neither the cranking model in perturbation theory nor the VMI model can account for the properties of all nuclei at high spins. We thus need a microscopic model capable of dealing simultaneously with the VMI and backbending regions. The Hartree-Fock-Bogoliubov (HFB) method is one such microscopic model. We devote the present section to an evaluation of its successes and limitations.

We first derive the HFB equations in a compact fashion. A more extensive discussion is given in (139–141). We note that the HFB method includes all of the physical effects considered in the cranking-model formalisms of Ma & Rasmussen (99) and Marshalek (135), treated in Section 7. However, the HFB method is not restricted to small oscillations of each collective variable around its equilibrium value. Since the HFB equations represent a nonlinear system that is solved self-consistently, they are capable of describing large oscillations, coupling between normal modes of the system, and phase transitions. We show that the HFB method includes the important physical mechanisms of (*a*) Coriolis antipairing of neutrons and protons, (*b*) axially symmetric as well as nonaxial deformations, (*c*) pair realignment effect, and (*d*) possibility of shape transitions. The HFB equations are sufficiently flexible to allow the nuclear dynamics to choose which of these mechanisms will dominate in a given situation.

8.2 DERIVATION OF HFB EQUATIONS We start from the many-body Hamiltonian

$$H_\omega = H - \omega J_x,$$
$$H = \sum_{ij} T_{ij} C_i^\dagger C_j + \tfrac{1}{4} \sum_{ijkl} v_{ijkl} C_i^\dagger C_j^\dagger C_l C_k, \qquad 8.1.$$

where ωJ_x is the external cranking potential (see Equation 7.2), $\langle J_x \rangle$ is given by Equation 7.3, $C_i^\dagger$ and C_i are particle creation and destruction operators, T is the kinetic energy, and v is an effective nucleon-nucleon interaction. If an inert core is assumed, then T includes the spherical single-particle potential which describes the effect of the core on a valence particle.

It is impractical to diagonalize H_ω when many active nucleons are present. Consequently we seek a canonical transformation such that the transformed quasiparticles are approximately noninteracting. When the quasiparticle interactions are neglected, the resulting Hamiltonian may not conserve particle number. Consequently H_ω must be replaced by

$$H' = H_\omega - \lambda N, \qquad 8.2.$$

where $N = \sum_i C_i^\dagger C_i$ is the number operator and the Fermi energy λ is chosen so that N has the correct expectation value.

The goal is to express H' as

$$H' = H'_0 + \sum_i E_i a_i^\dagger a_i + H_{\text{int}}, \tag{8.3.}$$

where $H'_0 + \lambda\langle N\rangle + \omega\langle J_x\rangle$ is the energy of the quasi-particle vacuum $|\Phi_0\rangle$, the E_i are the quasi-particle energies, and H_{int} is the neglected quasi-particle interaction. H' is a function of ω, so the quasi-particle states, energies, and vacuum are ω-dependent.

The HFB quasi-particle creation operators $a_i^\dagger$ are obtained from the unitary transformation

$$a_i^\dagger = \sum_j (U_{ij}C_j^\dagger + V_{ij}C_j), \tag{8.4.}$$

subject to the constraints

$$UU^\dagger + VV^\dagger = I, \quad U\tilde{V} + V\tilde{U} = 0. \tag{8.5.}$$

Equation 8.5 also follows from the requirement that the quasi-particle operators obey Fermion commutation rules. The quasi-particle vacuum $|\Phi_0\rangle$ is defined by $a_i|\Phi_0\rangle = 0$. Since the quasi-particles are fermions, a solution is $|\Phi_0\rangle = \Pi_i a_i|0\rangle$.

The HFB equations may be derived by choosing the quasi-particle transformations (Equation 8.4) so that Equation 8.2 is cast into the form of Equation 8.3. The derivation employs Wick's theorem: any product of operators can be expressed as a sum of normal products $:\mathcal{O}:$ containing all possible contractions $\langle\mathcal{O}\rangle$. For example,

$$\begin{aligned}
C_i^\dagger C_j &= \langle C_i^\dagger C_j\rangle + :C_i^\dagger C_j: \\
C_i^\dagger C_j^\dagger C_l C_k &= \langle C_i^\dagger C_k\rangle\langle C_j^\dagger C_l\rangle - \langle C_i^\dagger C_l\rangle\langle C_j^\dagger C_k\rangle + \langle C_i^\dagger C_j^\dagger\rangle\langle C_l C_k\rangle + \langle C_i^\dagger C_k\rangle :C_j^\dagger C_l: \\
&\quad + \langle C_j^\dagger C_l\rangle :C_i^\dagger C_k: - \langle C_i^\dagger C_l\rangle :C_j^\dagger C_k: - \langle C_j^\dagger C_k\rangle :C_i^\dagger C_l: \\
&\quad + \langle C_l C_k\rangle :C_i^\dagger C_j^\dagger: + \langle C_i^\dagger C_j^\dagger\rangle :C_l C_k: + :C_i^\dagger C_j^\dagger C_l C_k:.
\end{aligned} \tag{8.6.}$$

The expectation values $\langle\mathcal{O}\rangle$ are with respect to the quasi-particle vacuum. The density matrix ρ and the pairing tensor t are defined by

$$\rho_{ij} = \rho_{ji}^* = \langle\Phi_0|C_j^\dagger C_i|\Phi_0\rangle = (V^\dagger V)_{ij}, \tag{8.7.}$$

$$t_{ij} = -t_{ji} = \langle\Phi_0|C_j C_i|\Phi_\bullet\rangle = (V^\dagger U)_{ij}, \tag{8.8.}$$

where the expectation values are evaluated by inverting Equation 8.4 and applying $a_i|\Phi_0\rangle = 0$ and the fermion commutation relations. The Hamiltonian H' may be re-expressed by substituting Equation 8.6 into 8.2, so that

$$H' = H'_0 + H'_2 + H'_4, \tag{8.9.}$$

where the subscripts denote the number of uncontracted operators, and

$$H'_0 = \sum_{ij} (T - \lambda - \omega J_x + \tfrac{1}{2}\Gamma)_{ij}\rho_{ji} + \tfrac{1}{2}\sum_{ij}\Delta_{ij}t_{ji}^\dagger, \tag{8.10.}$$

$$H'_2 = \sum_{ij}(H-\lambda-\omega J_x)_{ij}:C_i^\dagger C_j: + \tfrac{1}{2}\sum_{ij}\Delta_{ij}:C_i^\dagger C_j^\dagger: + \tfrac{1}{2}\sum_{ij}\Delta_{ij}^\dagger:C_iC_j:, \quad 8.11.$$

$$H'_4 = \tfrac{1}{4}\sum_{ijkl} v_{ijkl}:C_i^\dagger C_j^\dagger C_l C_k:. \quad 8.12.$$

The HF Hamiltonian H, the HF potential Γ, and the pair potential Δ are defined by

$$H = H^\dagger = T+\Gamma, \quad \Gamma_{ij} = \Gamma_{ij}^\dagger = \sum_{kl} v_{ikjl}\rho_{lk}, \quad \Delta_{ij} = -\Delta_{ji} = \tfrac{1}{2}\sum_{kl} v_{ijkl}t_{kl}. \quad 8.13.$$

Expectation values of Wick normal products $:\mathcal{O}:$ with respect to $|\Phi_0\rangle$ vanish by construction. Consequently the vacuum energy $\langle\Phi_0|H'|\Phi_0\rangle$ is H'_0. The first sum in Equation 8.10 is the HF energy, whereas the second sum is the pairing energy. The neglected quasi-particle interactions are described by H'_4.

The Hamiltonian (Equation 8.9) assumes the desired form (Equation 8.3) if H'_2 is an independent quasi-particle Hamiltonian

$$H'_2 = \sum_i E_i a_i^\dagger a_i. \quad 8.14.$$

The commutator $[H'_2, a_i^\dagger]$ may be evaluated with Equation 8.14:

$$[H'_2, a_i^\dagger] = E_i a_i^\dagger = E_i\sum_j (U_{ij}C_j^\dagger + V_{ij}C_j), \quad 8.15.$$

or with Equation 8.11:

$$[H'_2, a_i^\dagger] = \sum_{jk}[H-\lambda-\omega J_x)_{jk}U_{ik} + \Delta_{jk}V_{ik}]C_j^\dagger + \sum_{jk}[-\Delta_{jk}^* U_{ik} - (H-\lambda-\omega J_x)_{jk}^* V_{ik}]C_j. \quad 8.16.$$

Equating the coefficients of $C_j^\dagger$ and C_j in Equations 8.15 and 8.16, we obtain the HFB eigenvalue equations

$$\begin{pmatrix}(H-\lambda-\omega J_x) & \Delta \\ -\Delta^* & -(H-\lambda-\omega J_x)^*\end{pmatrix}\begin{pmatrix}U_i \\ V_i\end{pmatrix} = E_i\begin{pmatrix}U_i \\ V_i\end{pmatrix}. \quad 8.17.$$

This energy matrix ($\boldsymbol{\kappa}$) is hermitian, so the quasi-particle energies E_i are real.

The HFB equations are nonlinear, and solutions are obtained by an iterative procedure. A guess is made for the quasi-particle transformations (Equation 8.4), subject to the constraints of Equation 8.5. The wave function (ρ, t) is calculated from Equations 8.7 and 8.8. Then the potentials (Γ, Δ) are constructed from Equation 8.13. The HFB energy matrix (Equation 8.17) is diagonalized to obtain a new set of quasi-particles. This procedure is repeated until the same wave function is obtained on successive iterations. At each iteration λ and ω are adjusted to satisfy the number constraint and the cranking constraint (Equation 7.3).

8.3 PHYSICAL EFFECTS INCLUDED IN HFB-CRANKING THEORY In order to explain both the low- and high-spin behavior of the moment of inertia, a microscopic theory must be general enough to encompass a great variety of physical effects, of which the HFB method includes the following:

8.3.1 *Deformations* The nuclear shape may be characterized by the multipole moments (Q_{LM}) of the quasi-particle vacuum. If j_{max} is the largest single-particle angular momentum in the model space, then Q_{LM} can be nonzero for $L = 0, 2, \ldots, 2j_{max}$ and $M = 0, 2, \ldots, L$. (For the realistic calculations described below, $j_{max} = \frac{13}{2}$.) The quadrupole (β_2), the hexadecapole (β_4), and the nonaxial (γ) deformation parameters are only a few of the degrees of freedom that the nuclear shapes are permitted to have. All deformations result from the nucleon-nucleon effective interaction.

8.3.2 *Pairing field* In HFB theory Δ is a matrix constructed from the same two-body interaction as is the HF field. (The BCS approximation retains only the diagonal elements of Δ and neglects self-consistent rearrangements in the HF single-particle basis due to the presence of pairing correlations.) The pair field is level-dependent, since each pair of orbits $|ab\rangle$ has a potential Δ_{ab}, in contrast to simpler models where a single order parameter Δ is assumed to represent all pairs of levels.

8.3.3 *Inertial forces* The Coriolis and centrifugal forces are described by $-\omega J_x$ and are treated exactly in HFB, as opposed to perturbation methods, which treat them only in lowest orders. At high spins these inertial forces are strong, and perturbation techniques are not appropriate.

8.3.4 *Self-consistency* The HF field, the pair field, and the inertial forces are all treated simultaneously, on an equal footing, and self-consistently. That is, any change in one of these three potentials results in rearrangements in the other two. Consequently, all deformation parameters and pairing gaps are J-dependent. Self-consistency of these various effects is ensured since the potentials (Γ, Δ) are determined by the wave function (ρ, t) and vice versa.

8.3.5 *VMI law* At low spins $\mathcal{I}_{exp}$ is approximately linear in ω^2, and depends upon both deformation and pairing properties. Since HFB treats the response of these properties to the inertial forces, it is of considerable interest to see whether this linearity can be reproduced and explained.

8.3.6 *Coriolis antipairing effect* In 1960 Mottelson & Valatin (46) observed that the Coriolis force acts in opposite directions on each member of a time-reversed pair and therefore tends to decouple the correlated pair. They predicted that the pairing gap Δ would decrease with increasing angular velocity ω. At a critical value of angular momentum J_c, the nucleus would suddenly become normal with $\Delta = 0$ for all pairs, and $\mathcal{I}$ would rise to $\mathcal{I}_{rigid}$. The HFB theory is suitable for investigating this effect.

8.3.7 *Realignment effect* Stephens & Simon (120) have proposed that the effect of the Coriolis force may be to decouple a single neutron or proton pair from the pairing field with subsequent alignment of this pair along the rotation axis. Consequently the nucleus would not be axially symmetric at high spins. The realigned pair should be in a high-j orbital, where the Coriolis force is the strongest.

Since HFB theory permits a state-dependent pair gap as well as nonaxial deformations, it includes the possibility of such a realignment effect.

8.3.8 *Shape transitions* Two rotational bands with different moments of inertia and deformations (such as spherical and deformed, prolate and oblate, or axial and nonaxial) could cross at a high spin (116, 118, 142, 143). At the J corresponding to the band intersection, $\mathcal{I}$ would suddenly rise, producing a backbending curve. Similarly, an axially symmetric rotating nucleus may become unstable with respect to asymmetric deformations at some critical angular momentum (128, 144). HFB predicts not only absolute minima (ground-state intrinsic bands) but also relative minima (excited intrinsic bands). At each J several shapes may be produced. Therefore a band crossing of different shapes or a sudden transition from axial to nonaxial shape could result from an HFB calculation.

8.3.9 *Gapless superconductivity* The order parameter (Δ) and the energy gap of the excitations (quasi-particle energy $E_{\rm qp}$) are distinct. Goswami, Lin & Struble (145) showed that the Coriolis force could cause the smallest $E_{\rm qp}$ to vanish, even though Δ is nonzero. Such gapless excitations may be connected with backbending (146, 147) and they are permitted by HFB.

8.3.10 *Negative quasi-particle energies* The eigenvalues of the HFB equations ($E_{\rm qp}$) occur in pairs ($+E_i, -E_i$). In conventional applications of HFB theory the positive eigenvalues ($+E_i > 0$) are selected as quasi-particle energies. As was noted above in Section 8.3.9, at a critical angular velocity ω_a the lowest quasi-particle energy E_1 can go to zero. Banerjee, Ring & Mang (148) have proven that if the positive branch is chosen for $\omega > \omega_a$, then the quasi-particle vacuum changes from even to odd number parity. A wave function has even (odd) number parity if all components have an even (odd) number of particles. To preserve the number parity for $\omega > \omega_a$, the negative branch of E_1 must be followed. If $E_1 + E_2 = 0$ at $\omega_b > \omega_a$, then the signs of both quasi-particles can be changed at ω_b, and number parity will be conserved. This prescription guarantees that a two-quasi-particle excitation (which is the lowest noncollective excited state of an even nucleus) will never have lower energy than the quasi-particle vacuum.

8.3.11 *Symmetries in a rotating frame* The symmetries of the Hamiltonian H are extremely useful in simplifying ground-state ($\omega = 0$) HFB calculations. Unfortunately the inertial forces, $-\omega J_x$, violate most of these symmetries, such as time-reversal, rotations about the y and z axes, and reflections through the xy and xz planes. Consequently, cranked wave functions contain neither time-reversal, nor axial or triaxial symmetry, and they are therefore difficult to calculate.

Goodman (149) has used the one remaining reflection symmetry σ_x (reflection through the yz plane) to reduce the dimension of the cranked HFB equations, and hence make a realistic calculation possible. The σ_x basis is shown (149) to block diagonalize J_x, $\mathcal{H}$, Δ, and consequently κ. Also, the HFB quasi-particle vacuum $|\Phi_0\rangle$ is reduced to canonical form. For all ω, we have

$$|\Phi_0\rangle = \prod_{\alpha} C_{\alpha}^{\dagger} \prod_{\beta \neq \alpha} (u_{\beta} + v_{\beta} C_{\beta}^{\dagger} C_{\hat{\beta}}^{\dagger}) |0\rangle, \qquad 8.18$$

where $|\alpha\rangle$, $|\beta\rangle$ and $|\hat{\beta}\rangle$ are eigenvectors of σ_x with eigenvalues, respectively, of $\pm i$, $-i$ and $+i$. $|\hat{\beta}\rangle = T|\beta\rangle$ only when $\omega = 0$. The orbits $|\beta\hat{\beta}\rangle$ are pair-correlated, whereas the orbits $|\alpha\rangle$ are decoupled from the pair field.

8.4 HFB-CRANKING CALCULATIONS

8.4.1 *Exact tests of HFB in soluble models* How well does the HFB method approximate the exact eigenstates of the cranking Hamiltonian H_{ω}, of Equation 8.1? Chu et al (150) studied this question by applying HFB to the exactly soluble two-level $R(8)$ model of Krumlinde & Szymanski (151). This model consists of 2 Ω identical fermions interacting through a pairing force, and populating two single-particle levels ($m = \frac{1}{2}, \frac{3}{2}$), which are 2 Ω-fold degenerate, separated in energy, and coupled to an external rotor with fixed $\mathscr{I}$. The Hamiltonian can be exactly diagonalized by group theoretical methods.

Self-consistent cranking (HFB) is extremely accurate below and above the transition region (which encompasses only two or three yrast states). HFB is more accurate when sharp backbending occurs than when there is no backbending. The relative lack of accuracy of HFB in the transition region is largely caused by the vanishing of Δ when only one pair of particles has their spins aligned. This behavior is intrinsic to the two-level model and would not occur in a realistic calculation. It is concluded that the many-body techniques (HFB) will be even more accurate for studies with a larger number of particles in a more realistic model space.

Although backbending is often accompanied by gapless superconductivity and one negative quasi-particle energy, the correspondence is not one to one. The existence of a negative E_{qp} is due entirely to the matrix element $\langle m = \frac{1}{2}|J_x|m = -\frac{1}{2}\rangle$. In the two-dimensional $R(5)$ model (152), this matrix element is omitted, so that negative quasi-particle energies cannot occur. Nevertheless, sharp backbending is produced in the $R(5)$ model. Finally, it is argued that backbending does not necessarily imply instability in the HFB equations.

8.4.2 *Reid interaction* Goodman & Vary (153, 154) have attempted a realistic description of the spectra of rare-earth nuclei. The Brueckner **G** matrix (ladder-series summation) was calculated (155) using the Reid soft-core nucleon-nucleon potential (156). The valence space contains essentially one major shell of each parity for both neutrons and protons and can accommodate 52 protons and 66 neutrons. The spherical single-particle energies (T_i) of the inert core (40 protons and 70 neutrons) are fixed by equating average spherical HF single-particle energies with spherical Nilsson energies. The HF potential and the pair potential are both determined by the **G** matrix, and include matrix elements of **G** between two particle states $|j_1 j_2 JT\rangle$ of all permissible couplings.

The experimental and HFB spectra of ^{168,170,172}Yb and ^{174}Hf are presented in Figures 26a and 26b. The essential characteristics of the experimental spectra are (*a*) slow variations in $\mathscr{I}$ at low spins, (*b*) rapid increase in $\mathscr{I}$ at high spins, (*c*) $\mathscr{I}(\omega^2)$ remains single-valued for ^{168}Yb and ^{174}Hf, and (*d*) $\mathscr{I}(\omega^2)$ is triple-valued (back-

bends) for ^{170}Yb. All of these features are reproduced by the HFB moment of inertia.

The low-spin behavior of $\mathcal{I}$ is governed by the VMI rule Equation 2.9. The

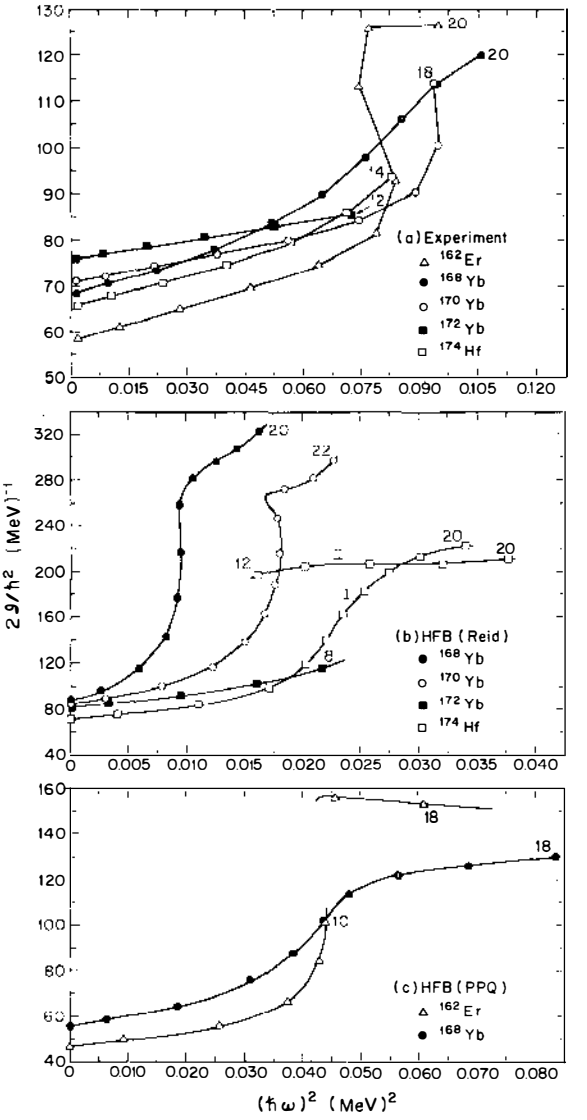

Figure 26 $\mathcal{I}$ vs ω^2 curves for (*a*) experiment (66), (*b*) HFB with **G** matrix derived from Reid potential (153, 154), and (*c*) HFB with pairing-plus-quadrupole interaction (157). Note that the scales differ.

HFB values $\mathcal{I}_0$ of $\mathcal{I}$ at $\omega \to 0$ (Table 6) agree with the VMI values of $\mathcal{I}_0$ (Table 4) to about 20%. However the slopes $1/2C$ of the HFB $\mathcal{I}$ vs ω^2 curves at $\omega \to 0$ (Table 6) are much larger than the VMI slopes of Table 3. Furthermore, the HFB curves deviate from linearity at too small a value of J. These discrepancies are correlated with the magnitudes of the HFB $J = 0$ prolate-oblate energy differences E_{po} (0.49, 1.45, 2.46, and 2.20 MeV), which are too small by several MeV, thereby making these nuclei too soft with regard to nonaxial deformations and increases in $\mathcal{I}$. As E_{po} increases towards more reasonable values (4–5 MeV), the HFB slope decreases, and the extent of the linear region in $\mathcal{I}(\omega^2)$ increases. At high spins $\mathcal{I}_{\text{HFB}}$ rises more rapidly than $\mathcal{I}_{\text{exp}}$. As E_{po} increases towards more physical magnitudes, $\mathcal{I}_{\text{HFB}}$ $(J = 20)$ decreases rapidly towards $\mathcal{I}_{\text{exp}}$ $(J = 20)$.

The triple-valued portion of the ^{170}Yb curve cannot be obtained by performing HFB for fixed ω, since all physical quantities are multivalued in ω, thereby creating apparent instabilities. However, all observables are single-valued in J. Consequently, when J is held fixed (and ω varied) at each iteration, these artifical "instabilities" disappear, and convergence in $\langle H' \rangle$ and ω is rapid.

To decide which of the proposed mechanisms for the rapid rise of $\mathcal{I}$ is operative in each nucleus, a brief analysis of the wave functions is presented in Table 7. The properties of four neutron pairs near the Fermi surface are given for various $\hbar\omega$. These neutrons are primarily in the $i_{13/2}$ shell. In the ground state $(\hbar\omega = 0)$ $\alpha = 1,2,3,4$ corresponds to $m_z = 7/2, 5/2, 3/2, 1/2$.

Consider ^{168}Yb. At $\hbar\omega = 0$ the state-dependent pair gap $\Delta_{\alpha\hat{\alpha}}$ is nearly constant. The members of each pair are related by time-reversal, so that each pair produces a net $\langle J_x \rangle = 0$. The rapid rise in $\mathcal{I}$ begins at $\hbar\omega = 0.095$ MeV and ends at 0.100 MeV. It is apparent that $\Delta_{\alpha\hat{\alpha}}$ decreases to zero over this interval very uniformly for all orbits. The angular momentum is spread over several pairs, and no single pair predominates. The maximum for any one pair is 5.3 units, whereas a fully aligned $i_{13/2}$ pair would have $\langle J_x \rangle = 13/2 + 11/2 = 12$. The nucleus ^{168}Yb therefore presents a clear example of the Mottelson-Valatin Coriolis antipairing effect (46).

Consider ^{170}Yb. At $\hbar\omega = 0.130$ MeV, $\mathcal{I}(\omega^2)$ is triple-valued. For $\langle J_x \rangle = 11$, $\Delta_{\alpha\hat{\alpha}}$ is not very state-dependent. One pair has $\langle J_x \rangle = 6.2$, which is only half the aligned value. The solution at $\langle J_x \rangle = 17.332$ is drastically altered. While the entire nucleus gained 6.3 units of angular momentum, the fourth pair has acquired 9.9 units.

Table 6 HFB values of $\mathcal{I}_0$ and C^{-1}

Nucleus	$\mathcal{I}_0$ (MeV^{-1})	C^{-1} (10^2 MeV^{-3})	Ref.
^{162}Er	24	3.4	157
^{168}Yb	28	3.7	157
	44	34.1	153, 154
^{170}Yb	42	15.8	153, 154
^{172}Yb	41	10.0	153
^{174}Hf	36	9.2	153

Consequently, all of the other nucleons actually "slow down." Furthermore, this pair has decoupled from the pairing field. The average of the state-dependent pairing gap for the first three pairs is 45% of the $\hbar\omega = 0$ strength, while $\Delta_{x\hat{x}}$ is rapidly vanishing for the last pair.

What is the nature of this decoupled pair $|\alpha\hat{\alpha}\rangle$ in ^{170}Yb? Employment of the σ_x basis makes possible a precise identification. The HFB orbital $|\alpha\rangle$ and the J_x eigenstate $|i_{13/2}, m_x = 13/2\rangle$ have a 98% overlap at $\hbar\omega = 0.14$ MeV. The overlap of $|\hat{\alpha}\rangle$ and $|i_{13/2}, m_x = 11/2\rangle$ is 94%. The decoupled pair is therefore aligned along the x axis of rotation. Whereas m_z is a good quantum number in the ground state, for high spins m_x is essentially a good quantum number for this pair. The nucleus

Table 7 HFB with **G** matrix derived from Reid potential (153, 154)[a]

$\hbar\omega$ (MeV)	$\langle J_x \rangle$	α	v_α^2	$\Delta_{\alpha\hat{\alpha}}$ (MeV)	J_z
^{168}Yb					
0	0	1	0.206	0.520	0
		2	0.731	0.522	0
		3	0.907	0.498	0
		4	0.942	0.483	0
0.095	7.961	1	0.078	0.297	−0.231
		2	0.851	0.301	+1.538
		3	0.964	0.305	+1.771
		4	0.987	0.265	+1.156
0.100	13.844	1	0	0.007	0
		2	1	0.008	−1.216
		3	1	0.009	+4.001
		4	1	0.008	+5.291
^{170}Yb					
0	0	1	0.438	0.517	0
		2	0.883	0.483	0
		3	0.955	0.450	0
		4	0.969	0.437	0
0.130	11.000	1	0.245	0.249	−1.076
		2	0.981	0.277	+0.046
		3	0.987	0.212	+6.171
		4	0.993	0.252	+1.232
0.130	17.332	1	0.055	0.225	+0.045
		2	0.984	0.205	−0.622
		3	0.996	0.205	+0.536
		4	1.000	0.045	+11.106

[a] The occupation probabilities v_α^2, the pairing gap $\Delta_{\alpha\hat{\alpha}}$, and the contribution to the angular momentum, $J_z = [(J_x)_{\alpha\alpha} + (J_x)_{\hat{\alpha}\hat{\alpha}}]v_\alpha^2$, are given for four neutron pairs near the Fermi surface for various angular velocities ω. The single-particle basis α diagonalizes the density matrix ρ. At each ω the states α are ordered with increasing v_α^2. The total angular momentum of the nucleus is $\langle J_x \rangle$.

^{170}Yb is therefore a clear illustration of the realignment effect. In the backbending region a single quasi-particle energy goes to zero and becomes negative, evoking the picture of gapless superconductivity.

The richness of HFB is manifested in ^{174}Hf. There are two single-valued bands, one ($0 \leqq J \leqq 20$) resembling the experimental band, and a second ($12 \leqq J \leqq 20$) with a nearly constant $\mathcal{I}$. The first band has Δ_n slowly vanishing, an $i_{13/2}$ neutron pair aligning along the x axis, and one negative quasi-particle energy. The second band has a nearly constant Δ_n, a realigned pair, and one gapless excitation. This clearly demonstrates that there is not a one-to-one correspondence between any particular physical mechanism and the existence (or nonexistence) of backbending.

Finally, we consider the spin dependence of the shapes. For $J = 0$ these nuclei are prolate and axially symmetric ($\gamma = 0°$). At high spins β_2 fluctuates by only 4%. The nonaxial deformation parameter γ rises rapidly in the transition region to about 15° for ^{168,170}Yb and 10° for ^{174}Hf.

8.4.3 *Pairing-plus-quadrupole interaction* Banerjee, Mang & Ring (157) have solved the HFB cranking equations with the phenomenological PPQ force. The model space is identical to that described above for the Reid interaction. The parameters of the PPQ interaction are adjusted to produce reasonable ground-state properties.

The experimental and HFB spectra of ^{162}Er and ^{168}Yb are given in Figure 26a and 26c. The experimental $\mathcal{I}(\omega^2)$ curves vary slowly at low spins, and rise rapidly at high spins. The ^{162}Er curve is multivalued, whereas the ^{168}Yb curve is single-valued. These essential characteristics are reproduced by HFB. However the backbending section of ^{162}Er was not obtained.

The HFB values of $\mathcal{I}_0$ (Table 6) compare favorably with the VMI values of Table 4. The slopes of the HFB curves at $\omega \to 0$ (Table 6) differ from the VMI slopes $(2C)^{-1}$ (Table 3) by about 40%. However, significant deviations from linearity begin at $J = 4$ in the HFB curves. This may be caused by the absence of higher multipoles of the interaction in the construction of Δ.

The primary mechanism for the rapid rise of $\mathcal{I}$ in ^{162}Er is the decoupling of an $i_{13/2}$ neutron pair from the pairing field concurrent with the alignment of this pair along the x rotation axis. This realignment effect is accompanied by one negative quasi-particle energy. The increase in $\mathcal{I}$ in ^{168}Yb is essentially caused by the sudden reduction of the neutron pairing gap. The Reid and the PPQ interactions give very similar explanations for the ^{168}Yb curve.

The HFB-cranking equations have also been solved for the odd-mass nuclei ^{155,159}Dy (158, 159). The agreement with experiment for both negative and positive parity bands is excellent. In particular, the inversion of J levels at high spins in the positive parity bands is reproduced exactly. This level inversion is known to result from the Coriolis force. However, in other theories the Coriolis force must be attenuated by an arbitrary parameter R ($0.4 < R < 0.9$) in order to fit such spectra.

In the HFB-cranking theory no attenuation factor was needed. The reason is as follows: the Coriolis force is included in $-\omega J_x$, where $\omega \sim 1/\mathcal{I}$. In HFB $\mathcal{I}$ is calculated self-consistently and is strongly dependent on J. In particular $\mathcal{I}_{\text{HFB}}$

includes the effect of decoupling the odd particle. For low J this particle is coupled to the core, and it is easy to gain angular momentum in the x direction by decoupling the particle. Consequently $\mathcal{I}_{\text{HFB}}$ is large, and the Coriolis force is strongly "attenuated." At higher spins where this particle is becoming x-aligned, its contribution to $\mathcal{I}_{\text{HFB}}$ is greatly reduced, so that $\mathcal{I}_{\text{HFB}}$ decreases as J increases. Correspondingly, there is less "attenuation" of the Coriolis force.

This self-consistency effect may also be explained by noting that the quasi-particle vacuum $|\Phi_0(J)\rangle$ is a function of angular momentum. Consequently, the one quasi-particle state $a^\dagger_{x(J)}|\Phi_0(J)\rangle$ that describes odd nuclei contains three, five, ... $J=0$ quasi-particle $(a^\dagger_{x(0)})$ admixtures into $|\Phi_0(0)\rangle$. That the HFB-cranking theory explains the "attenuation" of the Coriolis force and the level inversions in odd nuclei without the conventional adjustable parameter is a remarkable achievement.

8.4.4 *Effect of $J \neq 0$ multipoles of the interaction on the pairing field* The PPQ interaction contains only a $J=0$ pairing force. Krumlinde & Szymanski (160) included a quadrupole pairing interaction in their two-dimensional two-level model. The qualitative features of the backbending curves are not altered by this inclusion. However the critical angular momentum of the transition is slightly decreased.

Bhargava & Thouless (161, 162) have used the Sussex interaction in a model calculation containing only the $1h_{11/2}$ shell. The effect of including the $J=2$ and $J=4$ components of the particle-particle (pairing) channel is studied. They find that whereas the effective strength of the $J=0$ pairing force rapidly diminishes at high spins, the higher multipole components retain some strength and considerably alter the shapes of the $\mathcal{I}(\omega^2)$ curves. It should be noted that in the work of Goodman & Vary (154) all components ($0 \leqq J \leqq 12$) of the **G** matrix are included.

8.4.5 *Assessment of HFB-cranking* The HFB-cranking theory (*a*) compares very well with exact solutions in soluble models, (*b*) reproduces the essential qualitative features of $\mathcal{I}_{\text{exp}}(\omega^2)$, (*c*) exhibits the ability to include and clearly differentiate the various mechanisms leading to high-spin anomalies, and (*d*) explains the attenuation of the Coriolis force in odd nuclei.

Quantitative defects of the predicted spectra include deviations from the VMI model at low spins. $\mathcal{I}_0^{\text{HFB}}$ and $\mathcal{I}_0^{\text{VMI}}$ differ by 20%. C^{-1}_{HFB} and C^{-1}_{VMI} differ by 40% for the PPQ interaction and by an order of magnitude more for the Reid **G** matrix. Improvements in the effective interaction may lead to a more quantitative agreement with experiment.

8.5 PROJECTION OF ANGULAR MOMENTUM AND PARTICLE NUMBER Faessler et al (163–165) have minimized the pairing-plus-quadrupole Hamiltonian with respect to the set of projected trial wave functions $|\Delta_p\Delta_n\beta JM\rangle$, which are constructed as follows: given β, axially symmetric Nilsson single-particle states are calculated. Given Δ_p and Δ_n, a BCS state is formed with the Nilsson levels. Angular momentum and partial number projection on these BCS states provide the trial wave functions. There are three variational parameters Δ_p, Δ_n, and β. Kumar (166) has employed the same degrees of freedom, but he used the cranking constraint without any projection.

Since the realignment effect requires the possibility of one pair of particles decoupling from the pair field, Δ must be state-dependent (as in HFB) for realignment to occur. However in this model Δ_n is the same for all neutron Nilsson levels, and similarly for protons. Furthermore, realignment of particles along the rotation axis requires that the nuclear shape be nonaxial. Triaxial degrees of freedom are expected to be significant at high spins (128, 144, 167–170). In this model the nuclear shape is restricted to be axial at all J. Consequently the realignment effect and transitions to triaxial shapes are excluded from the model space. The moment of inertia of the core is a free parameter.

The nuclei investigated include the backbending ^{162}Er, ^{166,170} Yb, ^{168}Hf, and ^{182}Os and the non-backbending ^{158}Dy and ^{168}Yb. The theory predicts backbending only for ^{158}Dy and ^{170}Yb. The cause in ^{158}Dy is a sudden jump in deformation due to level crossings at the Fermi surface. For ^{170}Yb the cause is Coriolis antipairing of the neutrons. In general the high-spin anomalies cannot be reproduced. Partial-number projection considerably alters the unprojected spectra. This is also suggested by the similar model calculations of Dalafi et al (171, 172).

9 *Conclusions*

The VMI-Harris model has replaced the appealing simplicity of the early collective model by an equally succinct and more general description. The collective model distinguished between a "strong coupling region" halfway between the larger closed shells, in which each nucleus was characterized by an intrinsic, deformation-dependent quadrupole moment and moment of inertia, derived from the transition probability and energy of the lowest 2+ state, and a weak coupling region in which nuclei were thought to be spherical and undergoing only vibrational motions related to the values of $B(E2)$ and $E2$. The discovery of the energy gap. as well as the rigid moment of inertia result for the independent particle cranking model, later led to the introduction of the pairing-plus-quadrupole model. While this model is more realistic, some of the intuitive appeal of the early collective model was lost.

In the VMI model, each non-magic nucleus is characterized by two parameters, which can be deduced from the spectrum (E_2, E_4) only: a ground-state moment of inertia $\mathscr{I}_0 = \mathscr{I}_{J=0}$ and a stiffness parameter C. In the case of $\mathscr{I}_0 < 0$, $\mathscr{I}_{J=0}$ vanishes and $(C/2)\mathscr{I}_0^2$ measures the resistance to deformation. In both cases, for $J > 0$ the moment of inertia $\mathscr{I}(J)$ is positive and increases monotonically. Stable, strongly deformed nuclei are nearly perfect rotors—the spectra deviate only slightly from $J(J+1)$. With increasing β-ray instability and with decreasing deformation the softness of the spectra becomes more marked, i.e. the moment of inertia increases more rapidly with angular momentum, producing a quasi-vibrational spectrum.

The VMI model fits ground-state bands up to a limiting value $J = J_c$ for the whole range of non-magic nuclei ($1.82 \leqq R_4 \leqq 3.33$). R_J ratios for ground-state bands in magic nuclei, for which $R_4 \lesssim 1.82$, abruptly become almost degenerate.

The empirical relation of $\mathscr{I}$ to Q is essentially independent of A and Z, but can be divided into two clearly distinguishable domains, which roughly coincide with the previous weak-coupling and strong-coupling regions. For nuclei with one or two extra-shell nucleon pairs of one kind, a linear relationship exists between $\mathscr{I}$ and Q.

described by a dumbbell model. For nuclei with several extra-shell nucleon pairs a quadratic $\mathcal{I}$ vs Q relationship exists, described by a macroscopic two-fluid model. For the heaviest, spontaneously fissioning nuclei $\mathcal{I}$ remains essentially constant while Q increases.

In the region in which the quadratic relationship holds for the $0 \rightarrow 2$ transition, $\mathcal{I}$ increases somewhat faster than Q^2, as J increases. The relationship of $\mathcal{I}$ and Q at higher J for all three groups requires further analysis.

The knowledge of the mode of coupling of other bands to the ground-state band is still at a primitive stage; e.g. an empirical relationship not yet well understood is the coupling of the γ band, with a strength decreasing linearly with increasing R_4, while the ratio of the vibrational to rotational frequency first remains almost constant at ~ 2, and increases steeply by approximately an order of magnitude as the rotational limit is approached.

The onset of deviations from the VMI predictions at the critical angular momentum J_c can be studied best by means of the $\mathcal{I}$ vs ω^2 representation (where ω denotes the angular velocity). In many cases the deviations set in suddenly at J_c, and in a number of cases "backbending" occurs, i.e. the curve becomes triple-valued in ω^2. The process taking place in the nucleus near J_c is frequently referred to as a phase transition. It now appears that several mechanisms, either singly or combined, are involved in this transition, such as decoupling of a nucleon pair with high j, as well as a sudden decrease in pairing.

Numerous authors have attempted to find improvements on the VMI approach, either by somewhat different two-parameter expressions, or by adding higher-order terms in the angular velocity expansion. Attempts have further been made to develop more detailed nuclear theories in order to fit the R_I vs R_4 curves.

In cases where the angular velocity expansion converges, we obtain an identification of the phenomenological VMI parameters $\mathcal{I}_0$ and $(2C)^{-1}$ with corresponding expressions in the microscopic cranking perturbation formalism. This provides a test of the adequacy of our theories of nuclear structure, in particular the correctness of our choice of a deformed single-particle basis and residual interaction. The close connection of the VMI parameterization and the microscopic cranking formalism enables us to predict which physical effects (Coriolis antipairing, fourth-order cranking, centrifugal stretching, etc) contribute to deviations from a constant moment of inertia for a given nucleus.

Even for very good rotors ($\sigma \leqq 0.01$), for which the ω^2 expansion converges, the microscopic perturbative cranking formalism does not give a quantitative account of either $\mathcal{I}_0$ or C^{-1}. The values of $\mathcal{I}_0$ are systematically too low by 10–40%, while the C^{-1} values often suffer a discrepancy of a factor of two. The existing cranking perturbation calculations do not use realistic nucleon-nucleon interactions, are not fully self-consistent, and are of course not capable of dealing with the backbending phenomenon. A promising approach seems to be provided by the HFB-cranking method with realistic residual forces; this method is nonperturbative and self-consistent. The HFB method relates the rotational spectrum directly to the effective nucleon-nucleon interaction (**G** matrix). It is sufficiently flexible to accommodate exactly the physical mechanisms whose effect can only be estimated per-

turbatively in the usual cranking model. The HFB method is thus capable of achieving simultaneously a description of both the low-spin VMI region and the high-spin backbending regions in nuclei. Only relatively few HFB-cranking calculations with either realistic or phenomenological forces have been performed, but the preliminary results are very encouraging. For the few cases studied, the sudden rise in $\mathcal{I}$ in backbending nuclei is caused by the realignment of a single neutron pair along the rotation axis, whereas the rapid increase in $\mathcal{I}$ in non-backbending nuclei results from the sudden disappearance of the neutron pairing gap. Further work employing this method may ultimately provide a quantitative understanding of rotational spectra in nuclei.

ACKNOWLEDGMENTS

G. Scharff-Goldhaber would like to thank many of her colleagues for helpful discussions, and A. S. Goldhaber for his constant interest and understanding support. She further owes particular gratitude to M. McKeown for his resourceful and enthusiastic collaboration during many years of research, and to W. F. Piel, Jr. for his participation in the more recent phases of the work described here. Two of us (G.S.G. and C.B.D.) should like to acknowledge the generous advice and incisive criticism of Joseph Weneser. A. L. Goodman is indebted to R. Sorensen for a critical reading of Section 8.

Literature Cited

1. Pauli, W. 1924. *Naturwissenschaften* 37:741–43
2. Casimir, H. B. G. 1963. On the interaction between atomic nuclei and electrons. San Francisco & London: Freeman. 2nd ed. *Teyler's Tweede Genootschap, Haarlem.* Originally published in 1936.
3. Schüler, H., Schmidt, T. 1935. *Z. Phys.* 94:452; 95:265
4. Heitler, W., London, F. 1927. *Z. Phys.* 44:455–72
5. Gamow, G. 1930. *R. Soc. London Proc. A* 126:632–44
6. Rutherford, E., Chadwick, J., Ellis, C. D. 1930. *Radiations from Radioactive Substances,* p. 530. Cambridge, Engl: Univ. Press
7. von Weizsäcker, C. F. 1935. *Z. Phys.* 96:431–58
8. Bohr, A., Mottelson, B. R. 1969. *Nuclear Structure,* 1:141, 142. New York & Amsterdam: Benjamin
9. Bethe, H. A. 1971. *Ann. Rev. Nucl. Sci.* 21:93–244
10. Clark, J. W., Lam, P. M., ter Louw, W. J. 1975. *Nucl. Phys. A* 255:1–12 and references therein
11. Flowers, B. 1952. *Progress in Nuclear Physics.* 2:235–70. London: Pergamon
12. Thibaud, J. 1930. *CR Acad. Sci. Paris* 191:656–58
13. Teller, E., Wheeler, J. 1938. *Phys. Rev.* 53:778–89
14. Bohr, N. 1936. *Nature* 137:344–48
15. Bohr, N., Wheeler, J. A. 1939. *Phys. Rev.* 56:426–50
16. Frenkel, J. 1939. *Phys. Rev.* 55:987
17. Jensen, J. H. D. 1963. Zur Geschichte der Theorie des Atomkerns, pp. 153–64. *Les Prix Nobel en 1963.* Stockholm: Norstedt
18. Mayer, M. G. 1948. *Phys. Rev.* 74:235–39
19. Feenberg, E. 1949. *Phys. Rev.* 75:320–22; Nordheim, L. W. 1949. *Phys. Rev.* 75:1894–1901
20. Schmidt, T. 1940. *Naturwissenschaften* 28:565
21. Feenberg, E., Hammack, K. 1949. *Phys. Rev.* 75:1877–93; Gordy, W. 1949. *Phys. Rev.* 76:139–40; Hill, R. D. 1949. *Phys. Rev.* 76:998
22. Townes, C. H., Foley, H. W., Low, W. 1949. *Phys. Rev.* 76:1415–16
23. Rainwater, J. 1950. *Phys. Rev.* 79:432–34
24. Bohr, A. 1951. *Phys. Rev.* 81:134–38
25. Nilsson, S. G. 1955. *Kgl. Dan. Vidensk. Selsk. Mat. Fys. Medd.* 29(16):1–68

26. Goldhaber, M., Sunyar, A. W. 1951. *Phys. Rev.* 83:906–18
27. Bohr, A. 1952. *Kgl. Dan. Vidensk. Selsk. Mat. Fys. Medd.* 26:1–40
28. Bohr, A., Mottelson, B. R. 1953. *Phys. Rev.* 89:316–17
29. Bohr, A., Mottelson, B. R. 1953. *Phys. Rev.* 90:717–19
30. Goldhaber, M., Hill, R. D. 1952. *Rev. Mod. Phys.* 24:179
31. Burson, S. B., Blair, K. W., Keller, H. B., Wexler, S. 1951. *Phys. Rev.* 83:62–68
32. Mihelich, J. W., Scharff-Goldhaber, G., McKeown, M. 1953. *Phys. Rev. A* 94: 794
33. Mihelich, J. W., Scharff-Goldhaber, G., McKeown, M. Unpublished
34. Bohr, A. Mottelson, B. R. 1953. *Kgl. Dan. Vidensk. Selsk. Mat. Fys. Medd.* 27(16): 1–174
35. Sunyar, A. W. 1955. *Phys. Rev.* 98:653–57
36. Scharff-Goldhaber, G. 1953. *Phys. Rev.* 90:587–602. Energies of the lowest 2+ states were independently compiled by Preiswerk, P., Stahelin, P. 1952. *Helv. Phys. Acta* 24:623
37. Kurath, D. 1952. *Phys. Rev. A* 87:218; Flowers, B. H. 1952. *Phys. Rev.* 86:254–55
38. Goldhaber, M., Teller, E. 1948. *Phys. Rev.* 74:1046–49
39. Preface to 2nd ed. Ref. 34. 1957, pp. 3–6
40. Inglis, D. R. 1956. *Phys. Rev.* 103:1786–95
41. Sorensen, R. A. 1973. *Rev. Mod. Phys.* 45:353–77
42. Bohr, A., Mottelson, B. R. 1955. *Kgl. Dan. Vidensk. Selsk. Mat. Fys. Medd.* 30(1):1–24
43. Bohr, A., Mottelson, B. R., Pines, D. 1958. *Phys. Rev.* 110:936–38
44. Griffin, J. J., Rich, M. 1960. *Phys. Rev.* 118:850–54
45. Nilsson, S. G., Prior, D. 1961. *Kgl. Dan. Vidensk. Selsk. Mat. Fys. Medd.* 32(16): 1–61
46. Mottelson, B. R., Valatin, J. G. 1960. *Phys. Rev. Lett.* 5:511–12
47. Scharff-Goldhaber, G., Weneser, J. 1955. *Phys. Rev.* 98:212–14
48. Mottelson. B. R., Nilsson, S. G. 1955. *Phys. Rev.* 99:1615–17
49. Scharff-Goldhaber, G. 1956. *Phys. Rev.* 103:837–38
50. Wilets, L., Jean, M. 1956. *Phys. Rev.* 102:788–96
51. Hadermann, J., Rester, A. C. 1974. *Nucl. Phys. A* 231:120
52. Scharff-Goldhaber, G. 1957. *Proc. Pittsburgh Conf.*, ed. S. Meshkov, pp. 447–79
53. Scharff-Goldhaber, G., Alburger, D. E., Harbottle, G., McKeown, M. 1958. *Phys. Rev.* 111:913–19
54. Kane, W. R., Emery, G. T., Scharff-Goldhaber, G., McKeown, M. 1960. *Phys. Rev.* 119:1953–69
55. Emery, G. T., Kane, W. R., McKeown, M., Perlman, M. L., Scharff-Goldhaber, G. 1963. *Phys. Rev.* 129:2597–2621
56. Diamond, R. M., Hollander, J. M., Horen, D. J., Naumann, R. A. 1961. *Nucl. Phys.* 25:248–58
57. Sakai, M. 1975. *At. Data Nucl. Data Tables* 15:513–42
58. Mallmann C. 1959. *Phys. Rev. Lett.* 2:507–9
59. Davydov, A. S., Filippov, G. F. 1958. *Nucl. Phys.* 8:237–49
60. Davydov, A. S., Chaban, A. A. 1960. *Nucl. Phys.* 20:499–508
61. Baranger, M. 1961. *Phys. Rev.* 122:992–96
62. Kumar, K., Baranger, M. 1968. *Nucl. Phys. A* 110:490–528, 529–54
63. de Boer, J., Eichler, J. 1968. *Adv. Nucl. Phys.* 1:1–65 and references therein. See also Kleinfeld, A. M., Mäggi, G., Werdecker, D. 1975. *Nucl Phys. A* 248: 342–55
64. Christy, A., Häusser, O. 1972. *At. Nucl. Data Tables* 11:281–98
65. Morinaga, H., Gugelot, P. C. 1963. *Nucl. Phys.* 46:210–24
66. Sayer, R. O., Smith, J. S. III, Milner, W. T. 1975. *At. Nucl. Data Tables* 15: 85–110
67. Cheifetz, E., Jared, J. C., Thompson, S. G., Wilhelmy, J. B. 1970. *Phys. Rev. Lett.* 25:38–43; Wilhelmy, J. B., Thompson, S. G., Jared, J. C., Cheifetz, E. 1970. *Phys. Rev. Lett.* 25:1122–25
68. Grosse, E., de Boer, J., Diamond, R. M., Stephens, F. S., Tjøm, P. 1975. *Phys. Rev. Lett.* 35:562
69. Morinaga, H. 1966. *Nucl. Phys.* 75:385–95
70. Diamond, R. M., Stephens, F. S., Swiatecki, W. J. 1964. *Phys. Rev. Lett.* 11:315–18
71. Harris, S. H. 1965. *Phys. Rev. B* 138: 509–13
72. Scharff-Goldhaber, G. 1967. *Proc. Int. Conf. Nucl. Struct., Tokyo, 1967*, pp. 150–59
73. Mariscotti, M. A. J., Scharff-Goldhaber, G., Buck, B. 1969. *Phys. Rev.* 178:1864–87
74. Proetel, D., Diamond, R. M., Stephens, F. S. 1974. *Phys. Lett. B* 48:102–4; Lieder, R. M., Beuscher, H., Davidson,

W. F., Neskakis, A., Mayer-Böricke, C. 1975. *Nucl. Phys. A* 248:317–41
75. Garrett, J. D., Scharff-Goldhaber, G., Vary, J. P. 1974. *Bull. Am. Phys. Soc.* 19:59
76. Scharff-Goldhaber, G., Goldhaber, A. S. 1970. *Phys. Rev. Lett.* 24:1349–53
77. Mariscotti, M. A. J. 1970. *Phys. Rev. Lett.* 24:1242–45; Gorfinkiel, J. I., Mariscotti, M. A. J., Pomar, C. 1974. *Phys. Rev. C* 9:1243–52
78. Thieberger, P. 1970. *Phys. Rev. Lett.* 25: 1664–66
79. Scharff-Goldhaber, G. 1974. *J. Phys. A: Math. Nucl. Gen.* 7:L212–14
80. Scharff-Goldhaber, G., Takahashi, K. 1967. *Bull. Acad. Sci. USSR Phys. Ser.* 31:42
81. Saethre, Ø., Hjorth, S.-A., Johnson, A., Jagare, S., Ryde, H., Szymanski, Z. 1973. *Nucl. Phys. A* 207:486–512
82. Ejiri, H., Ishihara, M., Sakai, M., Katori, K., Inamura, T. 1968. *J. Phys. Soc. Jpn.* 24:1189
83. Das, T. K., Dreizler, R. M., Klein, A. 1970. *Phys. Rev. C* 2:632–38
84. Grodzins, L. 1962. *Phys. Lett.* 2:88–91
85. Scharff-Goldhaber, G., Goldhaber, A. S. 1974. *Proc. Int. Conf. Nucl. Struct. Spectrosc., Amsterdam, The Netherlands.* 2:182–85
86. Goldhaber, A. S., Scharff-Goldhaber, G. To be published
87. Ford, J. L. C. Jr., Stelson, P. H., Bemis, C. E. Jr., McGowan, F. K., Robinson, R. L., Milner, W. T. 1971. *Phys. Rev. Lett.* 27:1232–34
88. Griffin, R. E., Jackson, A. D., Volkov, A. B. 1971. *Phys. Lett. B* 36:281–86
89. Van Rij, W. I., Kahana, S. H. 1972. *Phys. Rev. Lett.* 28:50–54
90. Thieberger, P., Sunyar, A. W., Rogers, P. C., Lark, N., Kistner, O. C., der Mateosian, E., Cochavi, S., Auerbach, E. H. 1972. *Phys. Rev. Lett.* 28:972–74
91. Cochavi, S., Kistner, O., McKeown, M., Scharff-Goldhaber, G. 1972. *J. Phys. France* 33:102
92. Scharff-Goldhaber, G., McKeown, M., Lumpkin, A. H., Piel, W. F. Jr., 1973. *Phys. Lett. B* 44:416–20; Piel, W. F. Jr., Scharff-Goldhaber, G., Lumpkin, A. To be published
93. Arima, A., Iachello, F. 1975. *Phys. Lett. B* 57:34–43
Iachello, F. 1974. *Proc. Int. Conf. Nucl. Struct. Spectrosc., Amsterdam, Sept. 1974.* 2:163–81
94. Krien, K., Naumann, R. A., Rasmussen, J. O., Rezanka, I. 1973. *Nucl. Phys. A* 209:572–88
Wisshak, K., Klewe-Nebenius, H., Habs, D., Faust, H., Nowicki, G. Rebel, H. 1974. *Nucl. Phys. A* 247 59–73
95. Toki, H., Faessler, A. 1975. *Nucl. Phys A* 253:231–52
96. Klein, A., Dreizler, R. M., Das, T. K 1970. *Phys. Lett. B* 31:333–35
97. Draper, J. E. 1970. *Phys. Lett. B* 32 581–82
98. Thieberger, P. 1970. *Phys. Lett. B* 45 417–20
99. Ma, C. W., Rasmussen, J. 1970. *Phys Rev. C* 2:798–819
100. Ma, C., Tsang, C. F. 1975. *Phys. Rev. C* 11:213–27
101. Mantri, A. N., Sood, P. C. 1973. *Phys. Rev. C* 7:1294–1305
102. Moszkowski, S. A. 1966. *Proc. Conf. Nucl. Spin Parity Assignments, Gatlinburg, Tenn., 1965.* ed. H. B. Gove, R. L. Robinson. New York: Academic
103. Sood, P. C. 1968. *Can. J. Phys.* 46: 1419–23; 1969. *J. Phys. Soc. Jpn.* 26: 1059
104. Draper, J. E. 1972. *Phys. Lett. B* 41: 105–9
105. Ma, C. W., Rasmussen, J. O. 1974. *Phys. Rev. C* 9:1083–90
106. Stockmann, M. I., Zelevinsky, V. G. 1972. *Phys. Lett. B* 41:19–22
107. Wood, J. L., Fink, R. W. 1974. *Nucl. Phys. A* 224:589–95
108. Gupta, R. K. 1971. *Phys. Lett. B* 36: 173–78
109. Holmberg, P., Lipas, P. O. 1968. *Nucl. Phys. A* 117:552–60
110. Sood, P. C. 1967. *Phys. Rev.* 161:1063–70
111. Varshni, Y. P., Bose, S. 1972. *Phys. Rev. C* 6:1770–80; Varshni, Y. P. 1974. *J. Phys. Soc. Jpn.* 36:317–25
112. Warke, C. S., Khadkikar, S. B. 1968. *Phys. Rev.* 170:1041–46
113. Iachello, F., Arima, A. 1974. *Phys. Lett. B* 53:309–12
114. Das, T. K., Banerjee, B. 1973. *Phys. Rev. C* 7:2590–92
115. Goodman, A., Goswami, A. 1974. *Phys. Rev. C* 9:1948–53
116. Molinari, A., Regge, T. 1972. *Phys. Lett. B* 41:93–96
117. Broglia, R. A., Molinari, A., Pollarolo, G., Regge, T. 1974. *Phys. Lett. B* 50: 295–98
118. Broglia, R. A., Molinari, A., Pollarolo, G., Regge, T. 1975. *Phys. Lett. B* 57: 113–16
119. Lieder, R. M. et al 1974. *Phys. Lett. B* 49:161–64
120. Stephens, F. S., Simon, R. S. 1972.

Nucl. Phys. A 183:257–84
121. Stephens, F. S., Kleinheinz, P., Sheline, R. K., Simon, R. S. 1974. *Nucl. Phys. A* 222:235–51; Grosse, E., Stephens, F. S., Diamond, R. M. 1973. *Phys. Rev. Lett.* 31:840–43; 1974. 32:74–77
122. Stephens, F. S. 1975. *Rev. Mod. Phys.* 47:43–65
123. Sheline, R. K. 1972. *Nucl. Phys. A* 195: 321–32; 1973. *Phys. Lett. B* 45:459–62
124. Mottelson, B. R. *Proc. Nucl. Struct. Symp. Thousand Lakes, Joutsa, 1970,* Pt. II, pp. 148–65 (Univ. Jyväskylä Res. Rep. 4/1971)
125. Abecasis, S. M., Hernandez, E. S. 1972. *Nucl. Phys. A* 180:485–96; Abecasis, S. M. 1973. *Nucl. Phys. A* 205:475–80
126. Gupta, R. 1973. *Phys. Rev. C* 7:2476–83; 1972. 6:26–35
Trainor, L. E. H., Gupta, R. 1971. *Can. J. Phys.* 49:133
127. Das, T. K., Dreizler, R. M., Klein, A. 1970. *Phys. Rev. Lett.* 25:1626–28
128. Smith, B. C., Volkov, A. B. 1973. *Phys. Lett. B* 47:193–96
129. Wahlborn, S., Gupta, R. K. 1972. *Phys. Lett. B* 40:27–31
130. Udagawa, T., Sheline, R. K. 1966. *Phys. Rev.* 147:671–84
131. Chan, K. Y., Valatin, J. G. 1966. *Nucl. Phys.* 82:222–40
132. Chan, K. Y. 1966. *Nucl. Phys.* 85:261–72
133. Bes, D. R., Landowne, S., Mariscotti, M. A. J. 1968. *Phys. Rev.* 166:1045–51
134. Krumlinde, J. 1968. *Nucl. Phys. A* 121: 306–28
135. Marshalek, E. R. 1965. *Phys. Rev. B* 139:770–89; 1967. *Phys. Rev.* 158:993–1000
136. Belyaev, S. T. 1959. *Kgl. Danske Videnskab Selskab, Mat. Fys. Medd.* 31(11):1–54
137. Rasmussen, J. O., Ma, C. W. 1973. *Phys. Rev. Lett.* 31:317–19
138. Nilsson, S. G., Tsang, C. F., Sobiczewski, A., Szymanski, Z., Wycech, S., Gustafson, C., Lamm, I. L., Moller, P., Nilsson, B. 1969. *Nucl. Phys. A* 131: 1–66
139. Mang, H. J. 1975. *Phys. Rep.* 18(6): 325–68
140. Ring, P., Beck, R., Mang, H. J. 1970. *Z. Phys.* 231:10–25
141. Beck, R., Mang, H. J., Ring, P. 1970. *Z. Phys.* 231:26–47
142. Pavlichenkov, I. M. 1974. *Phys. Lett. B* 53:35–38
143. Perazzo, R. P. J., Reich, S. L. 1975. *Phys. Lett. B* 55:354–56
144. Turner, R. J., Kishimoto, T. 1973. *Nucl. Phys. A* 217:317–41
145. Goswami, A., Lin, L., Struble, G. L. 1967. *Phys. Lett. B* 25:451–54
146. Grin, Y. T. 1974. *Phys. Lett. B* 52:135–37
147. Goswami, A. To be published
148. Banerjee, B., Ring, P., Mang, H. J. 1974. *Nucl. Phys. A* 221:564–72
149. Goodman, A. L. 1974. *Nucl. Phys. A* 230:466–76
150. Chu, S. Y., Marshalek, E. R., Ring, P., Krumlinde, J., Rasmussen, J. O. 1975. *Phys. Rev. C* 12:1017–35
151. Krumlinde, J., Szymanski, Z. 1973. *Ann. Phys. NY* 79:201–49
152. Bose, S., Krumlinde, J., Marshalek, E. R. 1974. *Phys. Lett. B* 53:136–40
153. Goodman, A. L. 1976. *Nucl. Phys.* 113–41
154. Goodman, A. L., Vary, J. P. 1975. *Phys. Rev. Lett.* 35:504–7
155. Goodman, A. L., Vary, J. P., Sorensen, R. A. 1976. *Phys. Rev. C* 13:1674
156. Reid, R. V. 1968. *Ann. Phys.* 50:411
157. Banerjee, B., Mang, H. J., Ring, P. 1973. *Nucl. Phys. A* 215:366–82
158. Ring, P., Mang, H. J., Banerjee, B. 1974. *Nucl. Phys. A* 225:141–56
159. Ring, P., Mang, H. J. 1974. *Phys. Rev. Lett.* 33:1174–77
160. Krumlinde, J., Szymanski, Z. 1974. *Phys. Lett. B* 53:322–24
161. Bhargava, P. C. 1973. *Nucl. Phys. A* 207:258–72
162. Bhargava, P. C., Thouless, D. J. 1973. *Nucl. Phys. A* 215:515–24
163. Faessler, A., Lin, L., Wittmann, F. 1973. *Phys. Lett. B* 44:127–30
164. Faessler, A., Grümmer, F., Lin, L., Urbano, J. 1974. *Phys. Lett. B* 48:87–90
165. Gruemmer, F., Schmid, K. W., Faessler, A. 1975. *Nucl. Phys. A* 239:289–300
166. Kumar, K. 1973. *Phys. Rev. Lett.* 30: 1227–30
167. Sugawara-Tanabe, K., Tanabe, K. 1973. *Nucl. Phys. A* 208:317–32
168. Meyer ter Vehn, J. 1975. *Phys. Lett. B* 55:273–76
169. Meyer ter Vehn, J. 1975. *Nucl. Phys. A* 249:111–40
170. Meyer ter Vehn, J. 1975. *Nucl. Phys. A* 249:141–65
171. Dalafi, H. R., Banerjee, B., Mang, H. J., Ring, P. 1973. *Phys. Lett. B* 44:327–29
172. Dalafi, H. R., Mang, H. J., Ring, P. 1975. *Z. Phys. A* 273:47–55